NASA/TM-2000-210316

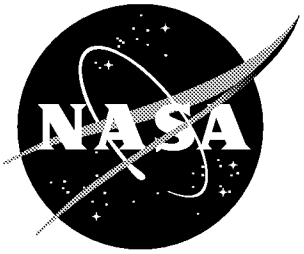

Forced Boundary-Layer Transition on X-43 (Hyper-X) in NASA LaRC 20-Inch Mach 6 Air Tunnel

Scott A. Berry, Michael DiFulvio, and Matthew K. Kowalkowski
Langley Research Center, Hampton, Virginia

August 2000

The NASA STI Program Office ... in Profile

Since its founding, NASA has been dedicated to the advancement of aeronautics and space science. The NASA Scientific and Technical Information (STI) Program Office plays a key part in helping NASA maintain this important role.

The NASA STI Program Office is operated by Langley Research Center, the lead center for NASA's scientific and technical information. The NASA STI Program Office provides access to the NASA STI Database, the largest collection of aeronautical and space science STI in the world. The Program Office is also NASA's institutional mechanism for disseminating the results of its research and development activities. These results are published by NASA in the NASA STI Report Series, which includes the following report types:

- TECHNICAL PUBLICATION. Reports of completed research or a major significant phase of research that present the results of NASA programs and include extensive data or theoretical analysis. Includes compilations of significant scientific and technical data and information deemed to be of continuing reference value. NASA counterpart of peer-reviewed formal professional papers, but having less stringent limitations on manuscript length and extent of graphic presentations.

- TECHNICAL MEMORANDUM. Scientific and technical findings that are preliminary or of specialized interest, e.g., quick release reports, working papers, and bibliographies that contain minimal annotation. Does not contain extensive analysis.

- CONTRACTOR REPORT. Scientific and technical findings by NASA-sponsored contractors and grantees.

- CONFERENCE PUBLICATION. Collected papers from scientific and technical conferences, symposia, seminars, or other meetings sponsored or co-sponsored by NASA.

- SPECIAL PUBLICATION. Scientific, technical, or historical information from NASA programs, projects, and missions, often concerned with subjects having substantial public interest.

- TECHNICAL TRANSLATION. English-language translations of foreign scientific and technical material pertinent to NASA's mission.

Specialized services that complement the STI Program Office's diverse offerings include creating custom thesauri, building customized databases, organizing and publishing research results ... even providing videos.

For more information about the NASA STI Program Office, see the following:

- Access the NASA STI Program Home Page at ***http://www.sti.nasa.gov***

- E-mail your question via the Internet to help@sti.nasa.gov

- Fax your question to the NASA STI Help Desk at (301) 621-0134

- Phone the NASA STI Help Desk at (301) 621-0390

- Write to:
  NASA STI Help Desk
  NASA Center for AeroSpace Information
  7121 Standard Drive
  Hanover, MD 21076-1320

NASA/TM-2000-210316

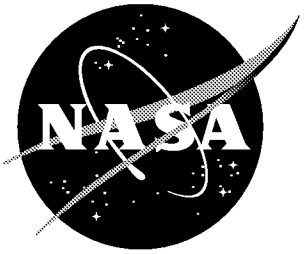

Forced Boundary-Layer Transition on X-43 (Hyper-X) in NASA LaRC 20-Inch Mach 6 Air Tunnel

Scott A. Berry, Michael DiFulvio, and Matthew K. Kowalkowski
Langley Research Center, Hampton, Virginia

National Aeronautics and
Space Administration

Langley Research Center
Hampton, Virginia 23681-2199

August 2000

Available from:

NASA Center for AeroSpace Information (CASI)
7121 Standard Drive
Hanover, MD 21076-1320
(301) 621-0390

National Technical Information Service (NTIS)
5285 Port Royal Road
Springfield, VA 22161-2171
(703) 605-6000

Contents

Abstract

Aeroheating and boundary layer transition characteristics for the X-43 (Hyper-X) configuration have been experimentally examined in the Langley 20-Inch Mach 6 Air Tunnel. Global surface heat transfer distributions, and surface streamline patterns were measured on a 0.333-scale model of the Hyper-X forebody. Parametric variations include angles-of-attack of 0-deg, 2-deg, and 4-deg; Reynolds numbers based on model length of 1.2 to 15.4 million; and inlet cowl door both open and closed. The effects of discrete roughness elements on the forebody boundary layer, which included variations in trip configuration and height, were investigated. This document is intended to serve as a release of preliminary data to the Hyper-X program; analysis is limited to observations of the experimental trends in order to expedite dissemination.

Introduction

NASA's X-43 (Hyper-X) program will culminate in flight tests of an operational airframe-integrated scramjet propulsion system at hypersonic conditions, which includes two flights at Mach 7 and one at Mach 10. Details about the flight and wind tunnel test program can be found in Rausch, et al. (1997a, 1997b) and McClinton, et al. (1998). A simulated launch sequence is shown in Fig. 1, while Fig. 2 shows the sequence of events during the nominal Mach-7 flight trajectory. This program will provide the first opportunity to obtain flight data on a hypersonic airbreathing propulsion system that is fully integrated with the vehicle airframe, and will validate/calibrate the experimental, numerical, and analytical methods used in the design and for prediction of flight performance of these vehicles. In an effort to reduce the uncertainties associated with this cutting-edge technology maturation program prior to the first flight, a systematic and combined experimental and numerical approach has been utilized. This includes (but is not limited to) development of aerodynamic performance and aeroheating databases, verification of performance and operability of the propulsion-airframe integration, and establishment of a method for boundary layer control. For instance, in order to provide the most robust scramjet propulsion system, a turbulent boundary layer at the inlet interface is required. Ingestion of a turbulent boundary layer into the inlet enhances the performance and operability of the engine through improved fuel mixing and reduced susceptibility to (drag-enhancing) internal flow separations. Based on the current knowledge of boundary layer transition at hypersonic flight conditions, an estimation of the location of natural transition on the Hyper-X forebody suggests that boundary layer trip devices are necessary to ensure a turbulent boundary layer at the inlet for both Mach 7 and 10 flight conditions. Figure 3 shows a sketch of the full-scale flight vehicle having a forebody length of approximately 6-ft. An estimate (based on boundary-layer transition criteria developed during the National Aero-Space Plane program) of the distance required for natural transition to occur at these hypersonic slender-body conditions is, at best, over 50% beyond this forebody length. A wind tunnel test program has been initiated to develop potential boundary layer trip configurations for the Hyper-X flight vehicle, and has resulted in a selection of a baseline trip configuration. The testing sequence that has been completed to date is listed in Table 1.

This report presents the preliminary results of several wind tunnel tests conducted in the NASA Langley Research Center (LaRC) 20-Inch Mach 6 Air Tunnel. The primary purpose of these tests was to investigate the aeroheating characteristics of the Hyper-X forebody and to examine the effect of discrete roughness elements on the windward surface boundary layer. Based on preliminary trajectory information, the flight forebody length Reynolds number (Re_L), for a forebody length of 6-ft, is approximately 5.5 million at a freestream Mach number of 7. These conditions can be approximated in the LaRC 20-Inch Mach 6 Air Tunnel, which has a Re_L range of 1.2 to 18.4 million for a model length of 28-in (2.3-ft). Test techniques utilized during these tests include thermographic phosphors which provides global surface heating images, schlieren which provide detailed shock shapes, and oil-flow which provides surface streamline information. Parametrics included in these tests, on both inlet cowl door open and closed, were the effect of angle of attack (α of 0-deg, 2-deg, and 4-deg), unit Reynolds number (Re between 0.5 and 6.7 million per foot), and both

discrete and distributed roughness' (including configuration and height). The discrete roughness effects were included in these tests to provide information to develop an efficient trip device for the Hyper-X flight vehicle. Similar preliminary results from the LaRC 31-Inch Mach 10 Tunnel has been presented in Berry, et al. (2000).

Nomenclature

M	Mach number
Re	unit Reynolds number (1/ft.)
Re_L	Reynolds number based on body length
α	model angle of attack (deg)
β	model sideslip angle (deg)
p	pressure (psi)
T	temperature (deg-R)
x	longitudinal distance from the nose (in)
y	lateral distance from the centerline (in)
z	height above the waterline (in)
L	reference length of vehicle at the model scale (48.00 in)
h	heat transfer coefficient (lbm/ft^2-sec), $=q/(H_{aw} - H_w)$ where $H_{aw} = H_{t2}$
h_{ref}	reference coefficient using Fay-Ridell calculation to stagnation point of a sphere
q	heat transfer rate (BTU/ft^2-sec)
H	enthalpy (BTU/lbm)
k	roughness element height (in)
Subscripts	
∞	freestream static conditions
t1	reservoir conditions
t2	stagnation conditions behind normal shock
aw	adiabatic wall
e	conditions at edge of the boundary layer
w	model surface
θ	momentum thickness

Test Facility

The Hyper-X forebody model has been tested in both the 20-Inch Mach 6 Air and the 31-Inch Mach 10 Air Tunnels of the LaRC Aerothermodynamic Facilities Complex (see Fig. 4). Miller (1990) and Micol (1998) provide detailed descriptions of these facilities and related instrumentation. Both are blowdown facilities that utilize dried, heated, and filtered air as the test gas.

The present tests were conducted in the 20-Inch Mach 6 tunnel. Typical operating conditions for the 20-Inch Mach 6 Air tunnel are stagnation pressures ranging from 30 to 500 psia, stagnation temperatures from 410 to 500-degF, and free stream unit Reynolds numbers from 0.5 to 8 million per foot. A two-dimensional, contoured nozzle is used to provide freestream Mach numbers from 5.8 to 6.1. The test section is 20.5 by 20 inches. A bottom-mounted model injection system can insert models from a sheltered position to the tunnel centerline in less than 0.5-sec. Run times up to 15 minutes are possible with this facility, although for most heat transfer and flow visualization tests, run times are only a few seconds. Optical access to the model for both thermographic phosphors and oil-flow is viewed through a high-quality window on the top of the tunnel.

Test Techniques

Surface Heating

The rapid advances in image processing technology which have occurred in recent years have made digital optical measurement techniques practical in the wind tunnel. One such optical acquisition method is two-color relative-intensity phosphor thermography (a diagram is shown in Fig. 5), which is currently being applied to aeroheating tests in the hypersonic wind tunnels of NASA Langley Research Center. Buck (1989, 1991) and Merski (1998) provide details about the phosphor thermography technique and Horvath (1990), Berry, et al. (1997, 1998a, 1998b), and Thompson, et al. (1998) provide additional recent examples of the application of this technique. With this technique, ceramic wind tunnel models are fabricated and coated with phosphors that fluoresce in two regions of the visible spectrum when illuminated with ultraviolet light. The fluorescence intensity is dependent upon the amount of incident ultraviolet light and the local surface temperature of the phosphors. By acquiring fluorescence intensity images with a color video camera of an illuminated phosphor model exposed to flow in a wind tunnel, surface temperature mappings can be calculated on the portions of the model that are in the field of view of the camera. A temperature calibration of the system conducted prior to the study provides the look-up tables that are used to convert the ratio of the green and red intensity images to global temperature mappings. With temperature images acquired at different times in a wind tunnel run, global heat transfer images are computed assuming one-dimensional heat conduction. The primary advantage of this technique is the global resolution of the quantitative heat transfer data. Such data can be used to identify the heating footprint of complex, three-dimensional flow phenomena (e.g., transition fronts, turbulent wedges, boundary layer vortices, etc.) that are extremely difficult to resolve by discrete measurement techniques. Phosphor thermography is routinely used in Langley's hypersonic facilities because models can be fabricated more quickly and economically than other more "conventional" techniques and the method provides quantitative global information. Comparisons of heat transfer measurements obtained from phosphor thermography to conventional thin-film resistance gauges measurements (Micol 1995) and to CFD predictions (Thompson, et al. 1998, Berry, et al. 1998b, Loomis, et al. 1997, Hamilton, et al. 1998) have shown good agreement.

Flow Visualization

Flow visualization techniques, in the form of schlieren and oil-flow, were used to complement the surface heating tests. The LaRC 20-Inch Mach 6 Tunnel is equipped with a pulsed white-light, Z-pattern, single-pass schlieren system with a field of view encompassing the entire 20-in test core. Images were recorded with a high-resolution digital camera. Surface streamline patterns were obtained using the oil-flow technique. The model with metal inserts was spray-painted black to enhance contrast with the white pigmented oils used to trace streamline movement. A thin basecoat of clear silicon oil was first applied to the surface, and then a mist of small pigmented-oil droplets was applied to the surface. After the model surface was prepared, the model was injected into the airstream and the development of the surface streamlines was recorded with a conventional video camera. The model was retracted immediately following flow establishment and formation of streamline patterns, and post-run digital photographs were recorded with a high-resolution digital camera.

Model Description

A sketch of the 33% scale Hyper-X forebody model is shown in Fig. 6. This slender-body configuration is characterized by a thin leading edge and 3 flat ramps that provide discrete compression and processing of the flow prior to the scramjet inlet. Outboard of the flat ramps are the chines, which are designed to minimize three-dimensional effects and flow spillage. The chines of the forebody model were laterally truncated aft of the first ramp-corner, as shown in Fig. 6, in order to minimize tunnel blockage and to isolate the model within the tunnel test core. A numerically controlled milling machine was used to build the forebody model with a detachable stainless-steel leading edge and interchangeable measurement surface inserts as well as various stainless-steel trip and inlet configurations. Although a majority of the forebody (the strongback) was constructed from aluminum to save weight, the leading edge (detachable to allow replacement if damaged) was

machined from stainless steel with a nose radius of 0.010-in. In order to provide for adequate thickness for attachment to the strongback, the length of the detachable leading edge piece was selected to be 5-in. The location of the trips was placed another 2.418-in aft of the leading edge attachment point (for a total length from the model leading edge of 7.418-in). For the flight vehicle, this location represents a compromise between maximizing the running length behind the trips and minimizing the thermal environment around the trip. The interchangeable trip configurations were consequently designed and sized based on the local flow properties at this forebody station. The remaining flat ramp sections were designed to accommodate both a Macor and aluminum set of inserts. Macor is a machinable glass ceramic and is a registered trademark of Corning Incorporated. The engine inlet side-walls were made of stainless steel and were designed to accommodate both open and closed engine cowl door configurations. The open configuration represents the forebody at test point with the engine cowl door in the operating position, although for the model the cowl is removed to provide optical access to the internal flat ramp surface. The closed configuration represents the forebody prior to test point with the engine cowl door down in the blocked inlet position and was tested to investigate the heating effect of the trips on the closed cowl. Figure 7 is a photograph of the Hyper-X forebody model with the Macor inserts for the phosphor thermography testing in the open-cowl configuration. Figure 8 is a photograph of the Hyper-X forebody model with the aluminum inserts for flow visualization testing in the closed-cowl configuration.

In order to obtain accurate heat transfer data using the one-dimensional heat conduction equation, models need to be made of a material with low thermal diffusivity and well-defined, uniform, isotropic thermal properties. Also, the models must be durable for repeated use in the wind tunnel and not deform when thermally cycled. Normally a cast ceramic process, which can provide accurate replication of complex three-dimensional configurations, is used to build phosphor thermography models. In this case, cast models could not be utilized because of the need to interchange the various complex trip configurations. As the ramp sections behind the trip location were flat across most of the span, 0.25-in thick flat sheets of Macor were used for the phosphor substrate. The Macor substrates were then coated with a mixture of phosphors suspended in a silica-based colloidal binder. This coating consisted of a 5:1 mixture of lanthanum oxysulfide (La_2O_2S) doped with trivalent europium and zinc cadmium sulfide (ZnCdS) doped with silver and nickel in a proprietary ratio. The coatings typically do not require refurbishment between runs in the wind tunnel and are approximately 0.001 inches thick. Typically, the final step in the fabrication process is to apply fiducial marks along the body to assist in determining spatial locations accurately. The fiducial marks used for the present study were the joints between the Macor inserts, which correspond to the location of the ramp angle changes shown in the sketch in Fig. 6 and listed in Table 2.

There were four trip configurations originally developed for this study, designated as Trips 1, 2a, 2b, and 3, and these are shown in Figs. 9 through 12. A fifth configuration, designated as Trip 2c (as it was a modification of Trip 2b), was added midway through testing and is shown in Fig. 13. These five configurations were sized based on flow conditions for the 31-Inch Mach 10 Tunnel with the trip height (k) as the primary variable. Trip 1 (Fig. 9), sometimes referred to as the diamond configuration, is based on prior experience (Berry, et al. 1998a) and is a row of squares rotated 45-deg to the flow with spacing roughly equal to the width of each trip. As shown in the sketch in Fig. 9a, this configuration was designed in two pieces with the trips protruding through holes in the base plate. Various thickness spacers between the parts provide the required variability in trip height. Figure 9b is a photograph of Trip 1 shown with the tallest height (k = 0.120-in) obtained by leaving out all of the spacers. This trip concept had been extensively tested during the NASP, Hyflite, and HySTP programs and was found to be a highly efficient vortex generator and trip. Unfortunately for the Hyper-X program, the diamond configuration has two potentially significant drawbacks. First, the diamond trips generate strong vortices that have a tendency to persist into the turbulent region thus providing a non-uniform flowfield for the inlet. The second is concern over whether this configuration, with sharp edges along the blunt face, could be structurally designed for Mach 7 and 10 flight conditions. The purpose of this experimental program, therefore, was to determine if Trip 1 could be redesigned to remedy these concerns. The remaining configurations, thus, were selected as modifications to this original trip design with the intent of providing a vortex-generating trip as efficient as Trip 1, but without the flow non-uniformity and structural concerns. Trip 2a (Fig. 10) and Trip 2b (Fig. 11) are similar in concept, both ramped tetrahedrons with the sharp apex pointing aft. For these configurations the number of vortices generated per trip was thought to be half that of Trip 1, thus the spacing between the trips was removed, which doubled the number of trips. The

Trip 2a design held the length and width of each trip constrained, so the ramp angle of the trips changed in order to provide the required variability in trip height. The Trip 2b design held the width and ramp angle of each trip constrained, so the length of the trips changed in order to provide the required variability in trip height. Trip 2c is identical to Trip 2b with the exception of a truncated base (Fig. 13), which is hoped to provide a local low-pressure region behind each trip that would enhance vortex generation. Trip 3 is also a ramped tetrahedron with the length and width constrained, but with a flared blunt base facing aft. Because of the blunt base, the spacing for Trip 3 was the same as Trip 1. A two piece tongue-in-groove construction was used for Trips 2a, 2b, 2c and 3 to provide 6 fixed-height trips for each configuration. Also, the tongue-in-groove construction required, for Trips 2a and 2b, an extra 0.010-in spacing between trips to accommodate the tool path. Consequently, in order to maintain the same number of vortices across the span of the model the spacing between trip centers for Trips 1 and 3 was increased to 0.260-in. At the time of the initial entry into the 20-In Mach 6 Tunnel, only the 4 smallest sizes (k = 0.015, 0.030, 0.045, and 0.060-in) of Trips 2a, 2b, 2c, and 3 were available for testing. Based on the expected boundary layer thickness at the trip location for Mach 6 flow, this range was adequate to provide a trip height to boundary-layer thickness (k/δ) up to one.

The model support hardware used for the present test is shown in Fig. 14. There were two previously constructed struts available for use, but only the longer strut allowed placement of the model near the centerline of the tunnel and therefore was used exclusively. An 8-inch I-beam spacer was required to locate the model 1-inch below the tunnel centerline and 5-inches behind the leading edge of the injection floor plate. This location allowed schlieren optical access to nearly the entire 1st ramp of the forebody model and phosphor optical access (from above) of the entire model.

Test Conditions

Nominal reservoir stagnation and corresponding freestream flow conditions for the present tests are presented in Table 3. Flow conditions for the 20-Inch Mach 6 Air Tunnel were based on measured reservoir pressures and temperatures and recent unpublished calibrations of the facility. The flow conditions shown are based on a statistical mean of all the runs at each condition and, for the conditions with a sufficient number of repeat runs, the run-to-run repeatability reflects a 95% uncertainty interval.

Data Reduction

Heating rates were calculated from the global surface temperature measurements using the one-dimensional semi-infinite solid heat-conduction equations, as discussed in detail in Buck (1991) and Merski (1998). Based on Merski (1998), phosphor system measurement error is typically quoted as ±8 to 10% for the 20-Inch Mach 6 Air Tunnel, with overall experimental uncertainty of ±15%. However, due to the relatively low surface temperature increase (as compared to the 31-Inch Mach 10 Tunnel) during a typical run, the actual phosphor system precision error may be slightly higher. The scatter in the heating images shown in the Appendices exemplify this increased precision error. Global heating images are presented in terms of the ratio of heat-transfer coefficients h/h_{ref}, where h_{ref} corresponds to the Fay and Ridell (1958) stagnation-point heating to a sphere with radius 4.0-in (a 1-ft radius sphere scaled to the model size). Repeatability of centerline heat transfer distributions (on the average) was generally found to be better than ±4%.

Results

Surface Heating

The phosphor thermography data was acquired in September of 1997, during Test 6755 and in August/September of 1999, during Tests 6791 and 6793. The earlier test compared the orignal 4 trip configurations, while the later tests investigated the proposed modification to Trip 2b and the effect of distributed roughness at the leading edge. The run logs, which lists the parametrics that were investigated during a total of 82 aeroheating runs, are presented in Table 4 for Test 6755, Table 5 for Test 6791, and Table 6 for Test 6793, and the resulting global heating images are shown in chronological order by run number in

Appendices A, B, and C, respectively. The primary purpose of these wind tunnel entries was to acquire roughness transition data and to compare tripping efficiency. Therefore, most of the run matrix was set-up to investigate the effect of different trip configurations and height for a range of angles of attack and Reynolds numbers. A few baseline (no trip) cases were run and repeated to provide data that could be compared to each other and to predictions in order to check data quality. The trip effectiveness run matrix is shown in Table 7 and provides a handy cross-reference of the run numbers that provide trends and repeatability. General observations based on the baseline-heating images are provided and followed by a discussion of roughness trends. Note that the images shown in Appendices A, B, and C represent the heating on the three ramped Macor surfaces directly behind the trip strip location only, as shown in Fig. 15, and not the entire Hyper-X windward surface. The h/h_{ref} color-bar scale of 0 to 1.0 was selected for all the heating images as this scale provided the best sensitivity to observe the trip effectiveness. Based on this scale, for the sake of discussion in the following sections, the location of the onset of transition in the images of Appendices A, B, and C is qualitatively identified by the change in color from blue to green. Ideally the onset of transition would be identified by comparison of the heating profiles extracted from the images for a series of runs to computational predictions, which is beyond the scope of this data-release document. Also, please note that the heating images that are referred to by run number will be from Appendix A unless specifically identified otherwise.

The baseline (no trip) data includes the effect of Reynolds number, angle of attack, and engine cowl door open and closed. In the Mach 6 tunnel, as the unit Reynolds number is increased to 2.2 million per foot (to match the Re_L of 5.5 million for flight) for the baseline angle of attack of 2-deg, the onset of transition is established just inside the inlet. This is illustrated by comparing Run 4 ($Re = 0.5x10^6$/ft), Run 3 ($Re = 1.1x10^6$/ft), and Run 2 ($Re = 2.2x10^6$/ft). For the flight vehicle, the ideal location for the onset of transition would be just slightly ahead of the inlet. Thus, even in the noisy environment of a conventional-type hypersonic wind tunnel, enhancement to the location of transition by a tripping device would be required for α = 2-deg to provide the desired level of inlet efficiency. Doubling the unit Reynolds number to $Re = 4.4x10^6$/ft moves the onset of transition to the beginning of Ramp 3 (see Run 5). Tripling the unit Reynolds number to $Re = 6.7x10^6$/ft moves the onset of transition to midway on Ramp 2 (see Run 61). Increasing the angle of attack also strongly affected the location of transition onset. For instance, for a freestream unit Reynolds number of 2.2 million per foot, Runs 37, 2, and 41 (α = 0, 2, and 4-deg, respectively) show a steady forward movement of transition on the last ramp as the angle of attack is increased. Only a limited number of runs were completed with the inlet door in the closed position as the closed-cowl Macor piece had been previously cracked on one side during the Mach 10 entry. Also, the heating was still severe enough to exceed the temperature limit of the phosphor thermography system (the phosphor system temperature range is typically 50 to 380-degF) within the first couple of data frames. While the closed-cowl images show the heating to be above the selected scale of 0 to 1, quantitative data can still be extracted (for the most part) from these images.

For Trip 1 at the baseline condition (α = 2-deg and $Re = 2.2x10^6$/ft) the effect of varying the trip height (k) provides a steady forward movement of the onset of transition from just inside the inlet to the beginning of the Macor inserts. The first trip height that just begins to affect the location of transition, the so-called *incipient*[1] trip height is k = 0.015-in. For example, compare Run 6 (k = 0.015-in) to Run 2 (no trip baseline). By k = 0.030-in, a significant forward movement of the transition front (the *critical* value) on ramp 3 is evident in the image of Run 7. Increasing the trip height further, the vortices begin to appear on Ramp 2 and by the largest trip height, k = 0.120-in (Run 1), transition onset is at the beginning of the Macor insert (an *effective* trip). Note in Runs 1, 9, and 10 the relative consistency of the vortices across the span of Ramps 1 and 2 and that the streaks appear to persist through the turbulent regions of Ramps 2 and 3.

For Trips 2a, 2b, 2c and 3, the effect of varying k provided similar results as with Trip 1 but with one important difference. All trips provided roughly the same *incipient* and *critical* values of k as Trip 1 (*effective* values were not identified due to the k = 0.060-in limitation), but Trips 2a, 2b, and 2c did so without evidence of strong vortices in either the laminar or turbulent regions. As the largest trip height is reached (k = 0.060-in),

[1] Note that the terminology used here is similar to the definitions of Bertin, et al. (1982). *Incipient* identifies the maximum roughness height that had no effect on the transition location. *Critical* identifies the roughness height that first begins to move transition rapidly towards the nose. *Effective* identifies the minimum roughness height that established transition just downstream of the roughness element.

the onset of transition for Trips 2a (Run 15), 2b (Run 20), and 2c (Run 5 of Appendix B) is qualitatively the same as the results shown for Trip 1 (Run 9 or Run 4 of Appendix B), but without the vortex streaks that persist into the turbulent region. The results from Trip 3 (Run 24) closely resembled Trip 1 in both effectiveness and strength of vortices. Based on the images alone, the Trip 2 series would appear to provide an adequate amount of transition enhancement, but without the persistent vortices that plagued Trip 1.

Test 6793 was initiated to determine if distributed roughness on or near the leading edge might cause premature transition on the X-43 leeward side. While the windward side is intended to be transitional or turbulent due to the trips, the lee-side has been assumed to be laminar. The as-built condition of the first flight vehicle was identified to have an inherent surface roughness on the leading edge equivalent to a non-polished machined finish, which was slightly rougher than specified. Concern over whether this roughness might initiate premature transition on the leeward side (that would provide more skin friction drag than expected) led to a short tunnel entry detailed in the run matrix shown in Table 6. As the windward side of the model is the only side that is instrumented, the lee-side was simulated by placing the angle of attack at –0.5-deg (the 2.5-deg windward wedge angle becomes 2-deg, which is the lee-side wedge angle when the vehicle is flying at α = 2-deg). The distributed roughness, using both coarse and medium grain sizes, was applied to the first 1.33-in. (the entire 4-in Carbon-Carbon nose-tip at the model scale) of the stainless-steel leading edge and an overcoat of clear high-temperature Krylon paint was used to affix the grit to the surface. The two largest grain sizes (24 and 46 grit) had a noticeable effect on the downstream flow at the nominal Re of 2.2 x 10^6/ft (compare Runs 2, 4, and 5 of Appendix C), but are much rougher than a non-polished machined surface. The smallest grain size (60 grit) is probably on the order of the full-scale surface finish, but on a 1/3-scale model is 3 times larger than would be flight, and barely had an effect on the downstream flow (compare Runs 2 and 8 of Appendix C). The final parametric that was examined was a 0.010-in forward-facing step (0.030-in on the full-scale vehicle) at the Carbon-Carbon/Tungsten-ballast interface. For nominal conditions the forward facing step had no effect (compare Runs 2, 3, 10, and 11 of Appendix C).

Flow Visualization

The schlieren data were acquired simultaneously with the phosphor data during Test 6755. However, the images from the first 15 runs were lost due to a malfunction of the digital camera prior to downloading and saving of the data. Appendix D shows the saved schlieren images in chronological order by run number. The primary result that is observable in the schlieren data is that even the smallest trip height (k = 0.015-in), which based on the heating results had very little effect on the onset of transition, generates a noticable shock.

The oil-flow data was acquired in April of 1998, during Test 6768. The run log, which lists the parametrics that were investigated during the 22 flow visualization runs of Test 6768, are presented in Table 8 and the resulting oil-flow images are shown in chronological order by run number in Appendix E. The digital images utilized in this report were all acquired post-test with the camera approximately perpendicular to the model windward surface. All the oil-flow images were acquired with the model at zero sideslip (β = 0-deg). General observations that can be made based on the baseline oil-flow images are provided and followed by a discussion of results with trips. The oil-flow runs were completed using both the standard technique of a random pattern of small drops of white pigmented oil sprayed onto the black model surface and a relatively new approach of completely covering the model surface using a large paint brush to apply the white-pigmented oil. The standard technique of oil-dots was especially useful for tracing the surface streamline directions, but was not useful for visualizing the vortices that were being generated by the trips. This new approach of painted oil-flow is similar in concept to the sublimating chemical technique. The entire model is coated with, in this case, pigmented-oil and during the run the higher energy flow removes or scrubs away the oil to reveal the footprint of complex flow features. This second technique provided clear indications of the vortices, regions of separations, and lines of reattachments, and was used for the remainder of the tests. When viewing these images, note that oil accumulation lines identify both the lateral (vertical in the image) lines of separation at the end of the ramps and the axial (horizontal) lines between pairs of counter-rotating vortices. The paint brush marks (which tend to be small white lines running in a lateral direction) identify the regions of low shear or separated flow.

The oil-flow images of the runs without trips shows a complex three-dimensional flow pattern that is

dominated by the separated regions at the end of Ramp 1 and 2. These separated regions, which appear relatively two-dimensional over the width of the flat ramps, merge with a separated or low shear area, which run the length of the chines, to generate a chine vortex emanating from the compression ramp corners. The images of Runs 1 and 14 provide the best evidence of these chine vortices. The surface streamlines, as provided by Run 1, indicate flow spillage off the flat ramps. Perhaps as little as a third of the surface streamlines on the end of the first flat ramp appear to be captured by the inlet.

The addition of trips to the forebody provides the added complexity of streamwise vortices within the boundary layer that tend to diminish the separated regions at the end of the compression ramps. As the flow separations are removed, the surface streamlines indicate reduced spillage off the flat ramps (implying improved mass capture), as indicated by the image of Run 13. The previous observation regarding the inlet capture of only a third of the surface streamlines on the end of the first flat ramp without trips appears to be improved to about a half with trips. One must keep in mind that these streamlines only indicate the flow direction at the surface. The painted-oil images with trips clearly indicate that the inlet ingests all the vortices, with the exception of those generated by the two outboard trips (see Run 2). (Thus the surface streamlines as generated by the oil-flow method are not necessarily a good indication of the mass capture of the inlet.) The effect of trip height on the forward extent of separation at the compression ramp corners is in agreement with the heating results.

Conclusions

An experimental investigation of the boundary layer trip effectiveness and the effect of the trips on the aeroheating characteristics for a 33% scale Hyper-X forebody model has been conducted in the LaRC 20-Inch Mach 6 Air Tunnel. Phosphor thermography was used to provide global heating images of a portion of the windward surface for a range of angles-of-attack and Reynolds numbers. Additionally, the effect of discrete roughness elements was investigated, which included trip configuration and height parametrics. The aeroheating results were complemented with oil-flow images that provided surface streamline information and schlieren that provided shock wave details. As this report was intended to be a data-release of the experimental results for review by the Hyper-X program, the discussion of results was limited to observations of experimental trends.

Acknowledgment

This experimental effort was accomplished with the help of many dedicated individuals. The trip configurations were selected and designed with the assistance of Aaron Auslender of AGDD/HAPB and Doug Dilley of NYMA, Inc. William Kimmel of ETTD/MISB designed the model hardware. Kevin Meidinger of FD/ARES led a team of machinists that constructed the model hardware and helped design the trips. Greg Draughon of FD/MTSS supported the Macor machining and installation. Mike Powers and Mark Griffin of FD/CMFSB sprayed the phosphor coatings on the Macor surfaces. Johnny Ellis, Rhonda Manis, and Grace Gleason of FSSD/ASS, and Bert Senter of CSC provided facility support. And Glenn Bittner of CSC and Ron Merski of AGDD/AB assisted with the phosphor thermography system. The authors greatly appreciate the invaluable assistance of these individuals and the contributions of others not mentioned that assisted behind the scenes.

References

Berry SA, DiFulvio M, and Kowalkowski MK. 2000. Forced Boundary Layer Transition on X-43 (Hyper-X) in NASA Langley 31-Inch Mach 10 Tunnel. *NASA TM-2000-210315*

Berry SA, Bouslog SA, Brauckmann GJ, and Caram JM. 1998a. Shuttle Orbiter Experimental Boundary-Layer Transition Results with Isolated Roughness. *J. Spacecr. Rockets 35(3): 241-248*

Berry SA, Horvath TJ, DiFulvio M, Glass C, and Merski NR. 1998b. X-34 Experimental Aeroheating at Mach 6 and 10. *AIAA Paper 98-0881*

Berry SA, Horvath TJ, Roback VE, and Williams GB. 1997. Results of Aerothermodynamic and Boundary-Layer Transition Testing of 0.0362-Scale X-38 (Rev. 3.1) Vehicle in NASA Langley 20-Inch Mach 6 Tunnel. *NASA TM-112857*

Bertin JJ, Hayden,TE, and Goodrich WD. 1982. Shuttle Boundary-Layer Transition Due to Distributed Roughness and Surface Cooling *J. Spacecr. Rockets 19(5):389-396*

Buck GM. 1989. Automated Thermal Mapping Techniques Using Chromatic Image Analysis. *NASA TM 101554*

Buck GM. 1991. Surface Temperature/Heat Transfer Measurement Using A Quantitative Phosphor Thermography System. *AIAA Paper 91-0064*

Fay JA and Ridell FR. 1958. Theory of Stagnation Point Heat Transfer in Dissociated Air. *J. Aerosp. Sci. 25(2):73-85,121*

Hamilton HH, Berry SA, Horvath TJ, and Weilmuenster KJ. 1998. Computational/ Experimental Aeroheating Predictions for X-33 Phase II Vehicle. *AIAA Paper 98-0869*

Horvath TJ, Rhode MN, and Buck GM. 1990. Aerothermodynamic Measurements on a Proposed Assured Crew Return Vehicle (ACRV) Lifting Body Configuration at Mach 6 and 10 in Air. *AIAA Paper 90-1744*

Loomis MP, Venkatapathy E, Davies CB, Campbell CH, Berry SA, Horvath TJ, and Merski NR. 1997. Aerothermal CFD Validation and Prediction for the X-38 Program. *AIAA Paper 97-2484*

McClinton CR, Holland SD, Rock KE, Englund WC, Voland RT, Huebner LD, and Rogers RC. 1998. Hyper-X Wind Tunnel Program. *AIAA Paper 98-0553*

Merski NR. 1998. Reduction and Analysis of Phosphor Thermography Data with the IHEAT Software Package. *AIAA Paper 98-0712*

Micol JR. 1995. Aerothermodynamic Measurement and Prediction for a Modified Orbiter at Mach 6 and 10 in Air. *J. Spacecr. Rockets 32(5):737-748*

Micol JR. 1998. Langley Aerothermodynamic Facilities Complex: Enhancements and Testing Capabilities. *AIAA Paper 98-0147*

Miller CG. 1990. Langley Hypersonic Aerodynamic/Aerothermodynamic Testing Capabilities - Present and Future. *AIAA Paper 90-1376*

Rausch VL, McClinton CR, and Crawford JL. 1997a. Hyper-X: Flight Validation of Hypersonic Airbreathing Technology. *ISABE Paper 97-7024*

Rausch VL, McClinton CR, and Hicks JW. 1997b. NASA Scramjet flights to Breath New Life into Hypersonics. *Aerospace America 35(7): 40-46*

Thompson RA, Hamilton HH, Berry SA, and Horvath TJ. 1998. Hypersonic Boundary Layer Transition for X-33 Phase II Vehicle. *AIAA Paper 98-0867*

Table 1: Hyper-X Trip Screening Tests in NASA facilities

Year	Tunnel	Test	Occupancy Dates	Runs	Description
1997	31" M10	338	Aug 14 – Aug 29	1-76	Phosphor
1997	**20" M6**	**6755**	**Sept 2 - Sept 5**	**1-61**	**Phosphor and schlieren**
1997	31" M10	338	Sept 30 - Oct 20	77-170	Phosphor and oil-flow
1998	**20" M6**	**6768**	**Mar 30 – Apr 2**	**22**	**Oil-flow**
1998	31" M10	346	Apr 6 - Apr 10	1-20	Oil-flow
1998	31" M10	349	Sept 3 - Sept 8	1-25	Phosphor w/ new trip
1998	31" M10	351	Sept 16 - Sept 18	1-19	Phosphor on closed cowl
1999	Hypulse		Feb 23 – Mar 26	1-28	Thin Film and schlieren
1999	**20" M6**	**6791**	**Aug 10**	**1-10**	**Phosphor w/ new trip**
1999	**20" M6**	**6793**	**Sept 15 - Sept 17**	**1-11**	**Phosphor w/ leading edge roughness**

Table 2: Trip location and fiducial marks.

Location	x (in)	x/L
Trips	7.418	0.1545
Start of Macor	8.166	0.1701
End of 1st Ramp	12.433	0.2590
End of 2nd Ramp	17.767	0.3701
End of Model	28.000	0.5833

L = 48-in (Length of full vehicle at model scale).

Table 3: Nominal flow conditions and run-to-run repeatability for 20-Inch Mach 6 Tunnel.

$Re_\infty(x10^6/ft)$	M_∞	P_{t1} (psi)	T_{t1} (°R)	H_{t1}(BTU/lbm)	P_{t2}(psi)
0.54	5.84	29.8	869.6	209.1	0.99
1.12 ± 5.3%	5.94 ± 1.8%	60.1 ± 3.1%	883.5 ± 0.4%	212.5 ± 0.4%	1.86 ± 8.0%
2.21 ± 2.6%	5.96 ± 0.8%	125.5 ± 1.5%	906.6 ± 0.4%	218.2 ± 0.4%	3.81 ± 3.7%
4.40 ± 2.1%	5.98 ± 0.1%	252.1 ± 1.2%	909.4 ± 1.1%	218.9 ± 1.1%	7.57 ± 1.7%
6.721	6.00	405.1	933.4	224.9	12.02

Table 4: Run log for test 6755 conducted in LaRC 20-Inch Mach 6 Air Tunnel.

Run Number	Model	α (deg)	β (deg)	*Re (x106/ft)*	Trip Type	k (in)	Cowl	*Results*
1	1-L	2	0	2.2	1	0.120	Open	yaw seems ok
2	1-L	2	0	2.2	0	no trip	Open	visual comp to M-10 ok
3	1-L	2	0	1.1	0	no trip	Open	
4	1-L	2	0	0.5	0	no trip	Open	
5	1-L	2	0	4.4	0	no trip	Open	
6	1-L	2	0	2.2	1	0.015	Open	
7	1-L	2	0	2.2	1	0.030	Open	
8	1-L	2	0	2.2	1	0.045	Open	
9	1-L	2	0	2.2	1	0.060	Open	
10	1-L	2	0	2.2	1	0.075	Open	
11	1-L	2	0	2.2	1	0.020	Open	
12	1-L	2	0	2.2	2a	0.015	Open	
13	1-L	2	0	2.2	2a	0.030	Open	**Bad Run** Lost Prerun
14	1-L	2	0	2.2	2a	0.045	Open	
15	1-L	2	0	2.2	2a	0.060	Open	
16	1-L	2	0	2.2	2a	0.030	Open	reran Run 13
17	1-L	2	0	2.2	2b	0.015	Open	
18	1-L	2	0	2.2	2b	0.030	Open	
19	1-L	2	0	2.2	2b	0.045	Open	
20	1-L	2	0	2.2	2b	0.060	Open	
21	1-L	2	0	2.2	3	0.015	Open	
22	1-L	2	0	2.2	3	0.030	Open	
23	1-L	2	0	2.2	3	0.045	Open	
24	1-L	2	0	2.2	3	0.060	Open	
25	1-L	2	0	1.1	1	0.020	Open	
26	1-L	2	0	1.1	1	0.030	Open	
27	1-L	2	0	1.1	1	0.045	Open	
28	1-L	2	0	1.1	1	0.060	Open	
29	1-L	2	0	1.1	1	0.075	Open	
30	1-L	2	0	1.1	1	0.090	Open	
31	1-L	2	0	1.1	1	0.120	Open	
32	1-L	2	0	1.1	2a	0.060	Open	
33	1-L	2	0	1.1	2b	0.060	Open	
34	1-L	2	0	1.1	3	0.060	Open	
35	1-L	0	0	1.1	0	no trip	Open	
36	1-L	0	0	0.5	0	no trip	Open	
37	1-L	0	0	2.2	0	no trip	Open	
38	1-L	0	0	4.4	0	no trip	Open	
39	1-L	4	0	0.5	0	no trip	Open	
40	1-L	4	0	1.1	0	no trip	Open	
41	1-L	4	0	2.2	0	no trip	Open	
42	1-L	4	0	4.4	0	no trip	Open	
43	1-L	4	0	2.2	1	0.015	Open	
44	1-L	4	0	2.2	1	0.030	Open	

45	1-L	4	0	2.2	1	0.045	Open	
46	1-L	4	0	2.2	1	0.020	Open	
47	1-L	4	0	2.2	2a	0.030	Open	
48	1-L	4	0	2.2	2b	0.030	Open	
49	1-L	4	0	2.2	2b	0.030	Open	Ran Trip 2b backwards
50	1-L	4	0	2.2	3	0.030	Open	
51	1-L	4	0	2.2	2a	0.030	Open	Repeat of R47
52	2-L	2	0	1.1	0	no trip	Closed	Used cracked closed-cowl
53	2-L	2	0	2.2	0	no trip	Closed	Used cracked closed-cowl
54	2-L	2	0	4.4	0	no trip	Closed	Used cracked closed-cowl
55	2-L	2	0	2.2	1	0.030	Closed	Used cracked closed-cowl
56	2-L	2	0	2.2	1	0.045	Closed	Used cracked closed-cowl
57	2-L	2	0	2.2	1	0.060	Closed	Used cracked closed-cowl
58	2-L	2	0	2.2	2a	0.060	Closed	Used cracked closed-cowl
59	2-L	2	0	2.2	2b	0.060	Closed	Used cracked closed-cowl
60	2-L	2	0	2.2	3	0.060	Closed	Used cracked closed-cowl
61	1-L	2	0	6.7	0	no trip	Open	

Table 5: Run log for test 6791 conducted in LaRC 20-Inch Mach 6 Air Tunnel.

Run Number	Model	α (deg)	β (deg)	*Re (x106/ft)*	Trip Type	k (in)	Cowl	Results
1	1-L	2	0	1.1	0	no trip	Open	CL disturbance?
2	1-L	2	0	2.2	0	no trip	Open	
3	1-L	2	0	4.4	0	no trip	Open	
4	1-L	2	0	2.2	1	0.060	Open	
5	1-L	2	0	2.2	2c	0.060	Open	
6	1-L	2	0	2.2	2c	0.030	Open	
7	1-L	2	0	2.2	2c	0.015	Open	
8	1-L	2	0	2.2	2b	0.030	Open	
9	1-L	2	0	2.2	1	0.030	Open	
10	1-L	2	0	2.2	1	0.045	Open	

Table 6: Run log for test 6793 conducted in LaRC 20-Inch Mach 6 Air Tunnel.

Run Number	Model	α (deg)	β (deg)	*Re ($x10^6$/ft)*	*Trip Type*	*k (in)*	*Cowl*	*Results*
1	1-L	-0.5	0	1.1	0	no trip	Open	**Bad run**, lost flow conditions
2	1-L	-0.5	0	2.2	0	no trip	Open	
3	1-L	-0.5	0	4.4	0	no trip	Open	
4	1-L	-0.5	0	2.2	24 Grit	0.038	Open	
5	1-L	-0.5	0	2.2	46 Grit	0.016	Open	
6	1-L	-0.5	0	4.4	46 Grit	0.016	Open	
7	1-L	-0.5	0	4.4	60 Grit	0.0115	Open	
8	1-L	-0.5	0	2.2	60 Grit	0.0115	Open	
9	1-L	-0.5	0	6.0	60 Grit	0.0115	Open	
10	1-L	-0.5	0	2.2	Kapton	0.010	Open	
11	1-L	-0.5	0	4.4	Kapton	0.010	Open	

Table 7: Aeroheating test matrix cross-reference of Tests 6755 and 6791 conducted in the LaRC 20-Inch Mach 6 Tunnel.

		Trip 1			Trip 2a			Trip 2b			Trip 2c			Trip 3			Baseline		
	α	0	2	4	0	2	4	0	2	4	0	2	4	0	2	4	0	2	4
k	Re																		
0.000	0.5																A36	A4	A39
	1.1																A35	A3,B1	A40
	2.2																A37	A2,B2	A41
	4.4																A38	A5,B3	A42
	6.7																	A61	
0.015	0.5																		
	1.1																		
	2.2		A6	A43		A12			A17			B7			A21				
0.030	0.5																		
	1.1		A26																
	2.2		A7,B9	A44		A16	A51		A18,B8	A48		B6			A22	A50			
0.045	0.5																		
	1.1		A27																
	2.2		A8,B10	A45		A14			A19						A23				
0.060	0.5																		
	1.1		A28			A32			A33						A34				
	2.2		A9,B4			A15			A20			B5			A24				
0.075	0.5																		
	1.1		A29																
	2.2		A10																
0.090	0.5																		
	1.1		A30																
	2.2																		
0.120	0.5																		
	1.1		A31																
	2.2		A1																

Note: A designates Test 6755, B designates Test 6791

Table 8: Run log for flow visualization portion of test 6768 conducted in the LaRC 20-Inch Mach 6 Tunnel.

Run Number	Model	(deg)	*Re/ft (x10^6)*	Trip Type	k (in)	Cowl	Oil-Flow Type	Oil Flow Results
1	1-L	2	2	0	0	open	Dots	OK
2	1-L	2	2					Insufficient oil flow
3	1-L	2	2	0	0	open	Paint	OK
4	1-L	2	2	0	0	open	Paint	OK
5	1-L	2	2	1	0.06	open	Paint	OK
6	1-L	2	2	2a	0.06	open	Paint	OK
7	1-L	2	2	2b	0.06	open	Paint	OK
8	1-L	2	2					Insufficient oil flow
9	1-L	2	2	3	0.06	open	Paint	OK
10	1-L	2	2	3	0.06	open	Dots	OK
11	1-L	2	2	2b	0.06	open	Dots	OK
12	1-L	2	2	2a	0.06	open	Dots	OK
13	1-L	2	2	1	0.06	open	Dots	OK
14	1-L	2	2	0	0	open	Paint	OK
15	1-L	2	2	1	0.03	open	Paint	OK
16	1-L	2	2	0	0	closed	Paint	OK
17	1-L	2	2	1	0.03	closed	Paint	OK
18	1-L	2	2	3	0.06	closed	Paint	OK
19	1-L	2	2	2a	0.06	closed	Paint	OK
20	1-L	2	2					Insufficient oil flow
21	1-L	2	2	2b	0.06	closed	Paint	OK
22	1-L	2	2	1	0.06	closed	Paint	OK

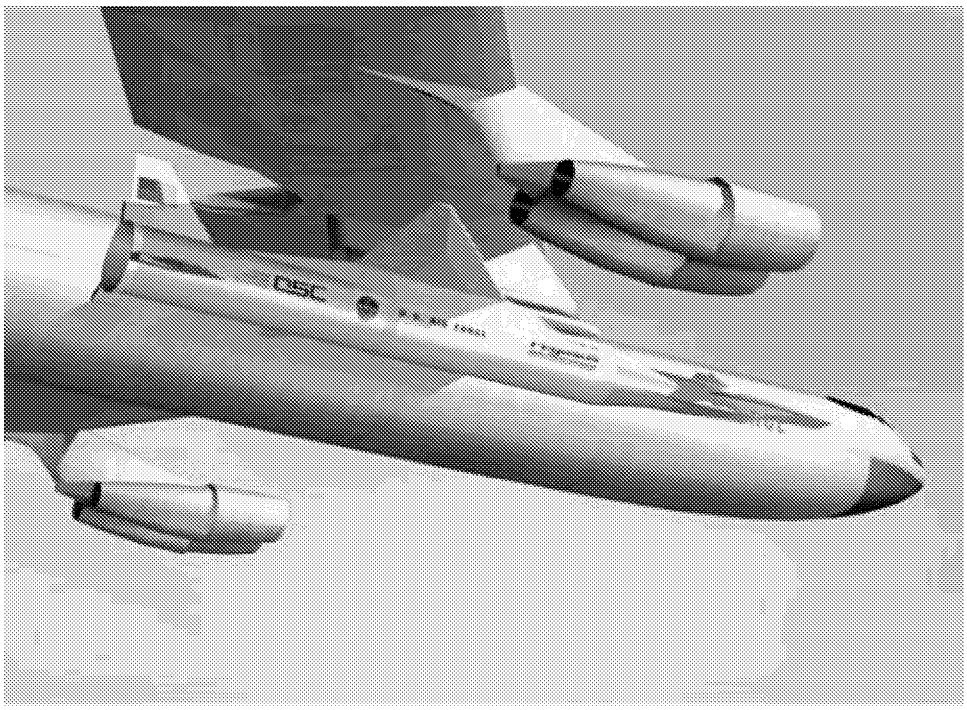

Figure 1a. Hyper-X vehicle mated to Pegasus booster awaiting drop from B-52.

Figure 1b. Hyper-X vehicle lofted to test-point by Pegasus booster.

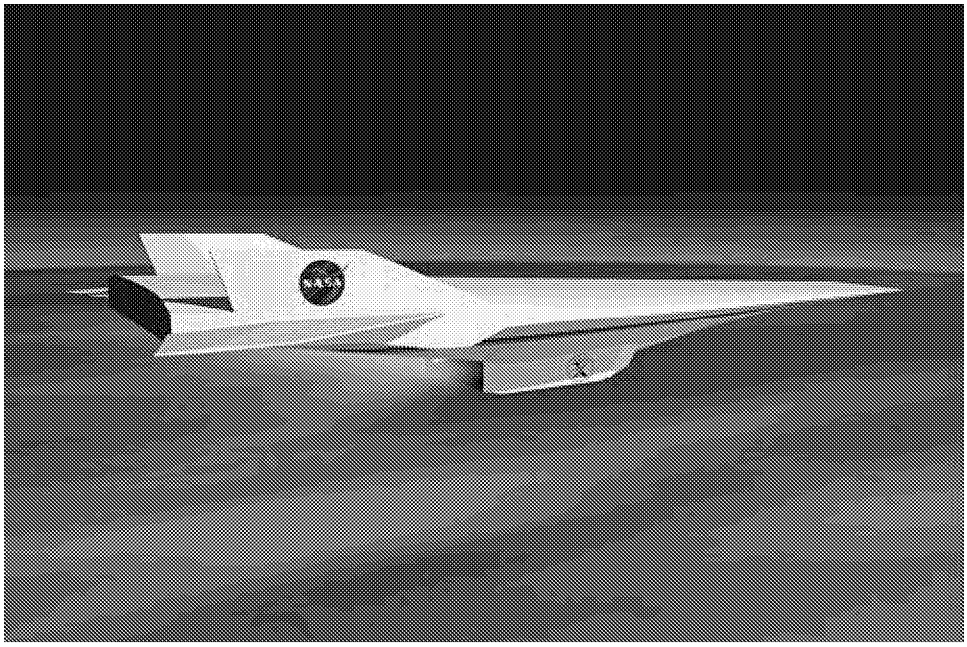

Figure 1c. Hyper-X vehicle flying at test-point.

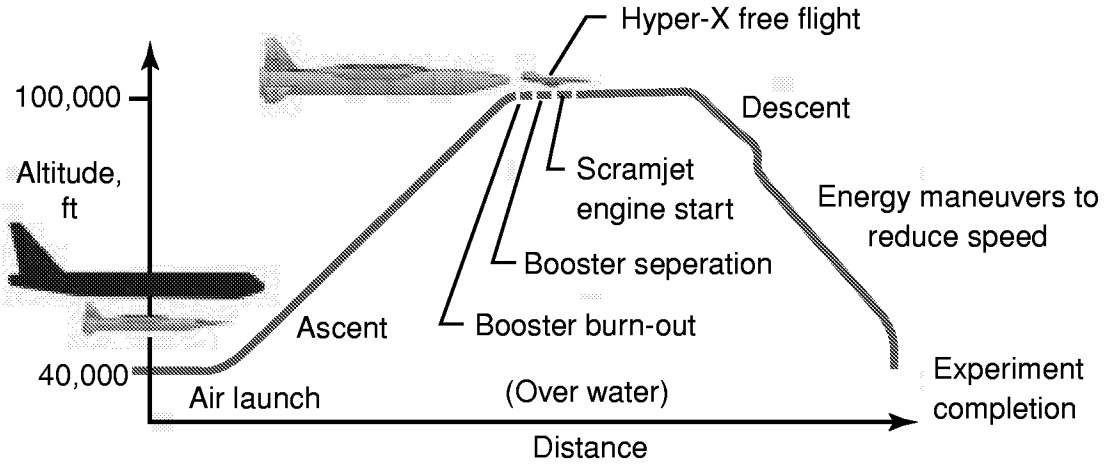

Figure 2. Preliminary Hyper-X trajectory

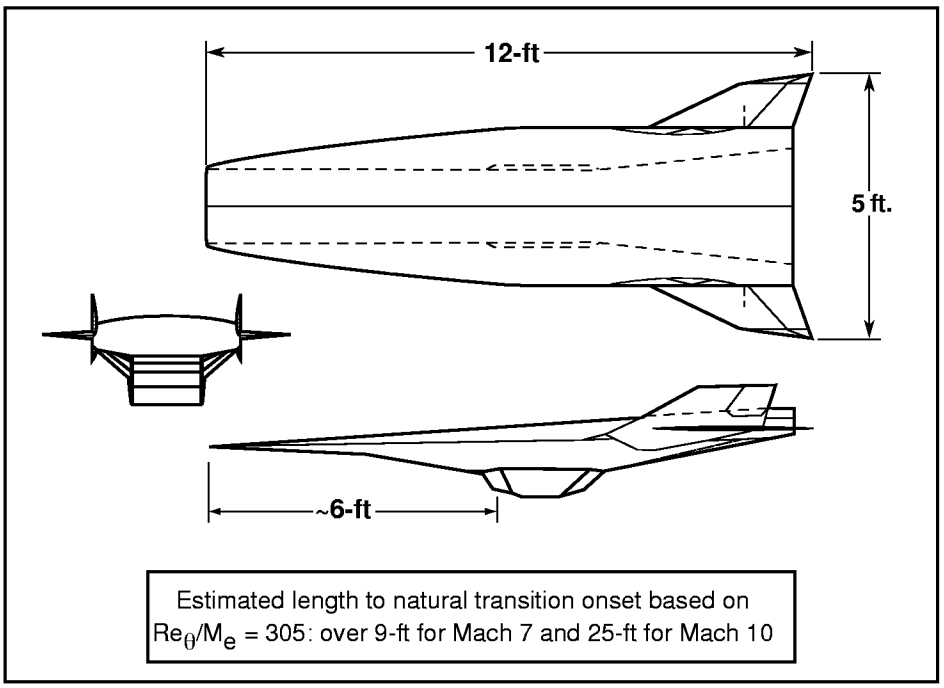

Figure 3. Hyper-X vehicle dimensions.

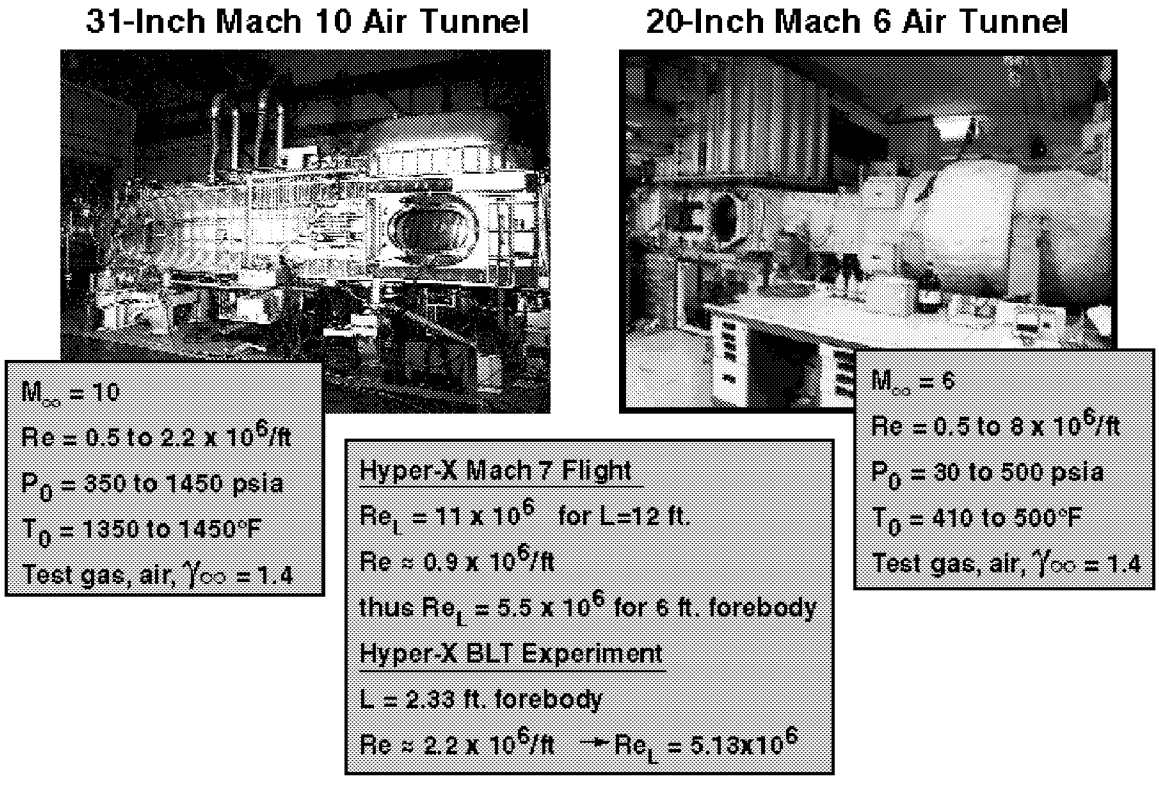

Figure 4. NASA Langley facilities utilized for Hyper-X transition tests.

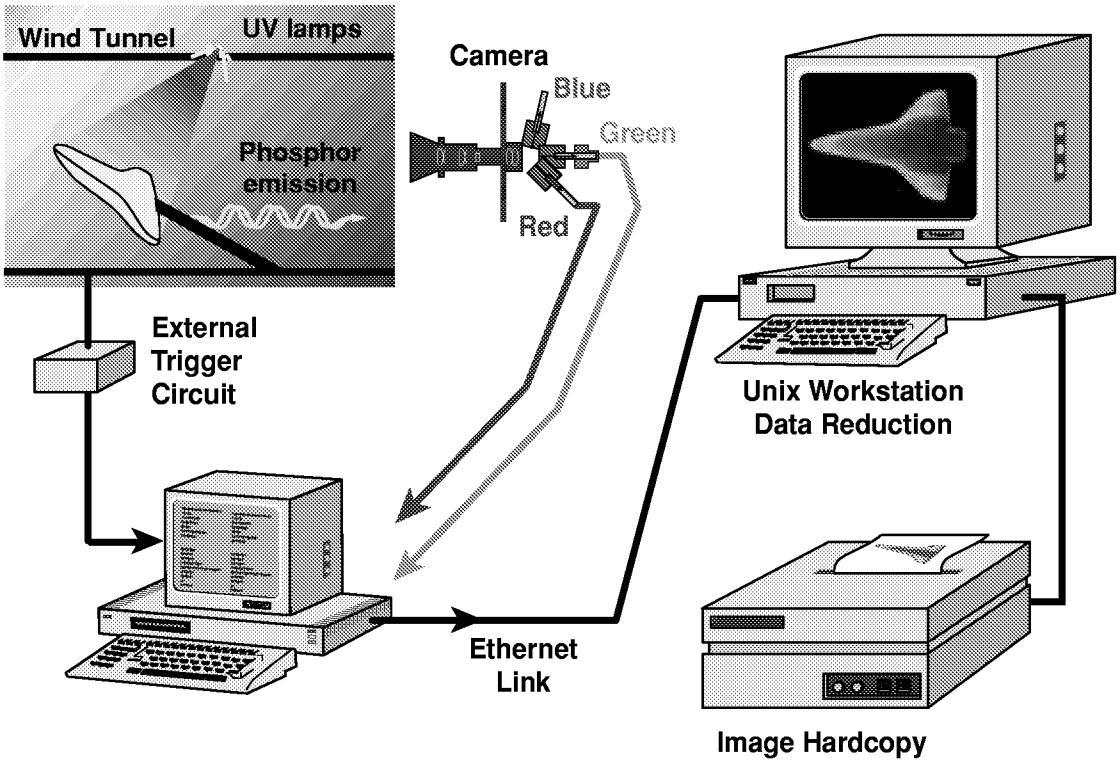

Figure 5. Schematic of phosphor thermography system.

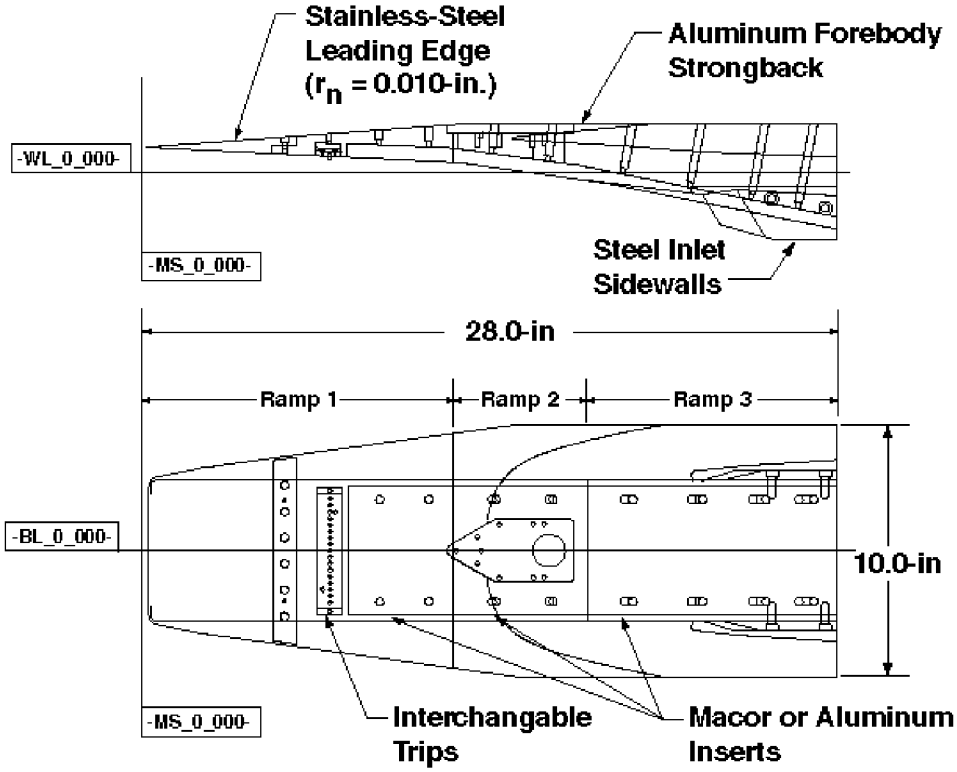

Figure 6. Hyper-X forebody model dimensions.

Figure 7. Photograph of 0.333-scale Hyper-X forebody model in the open-cowl configuration with Macor inserts for phosphor thermography testing.

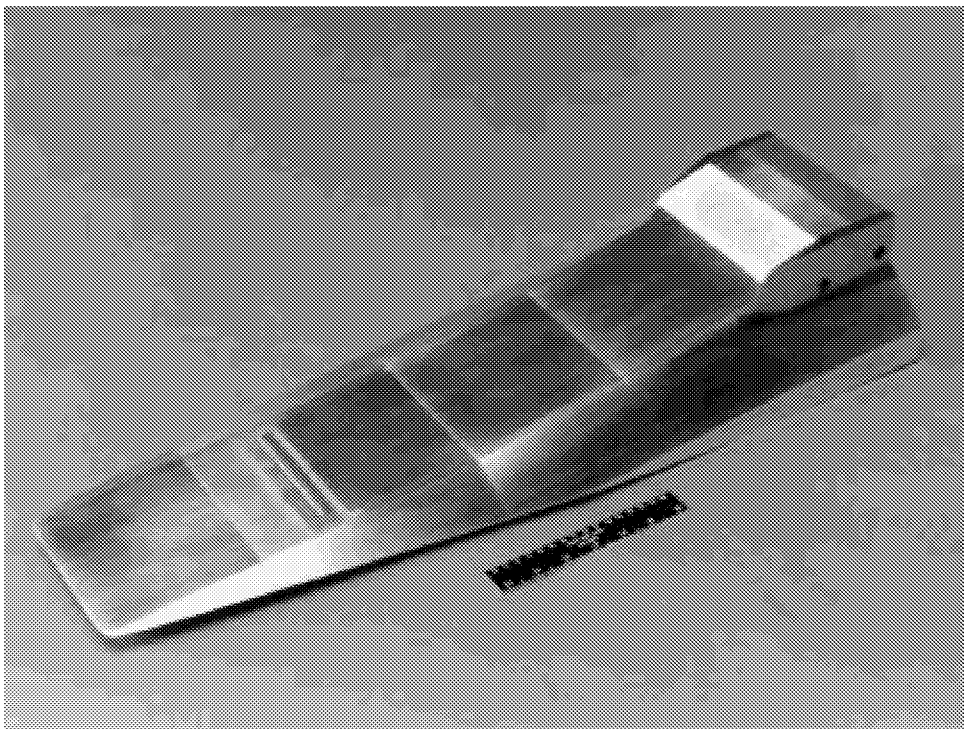

Figure 8. Photograph of 0.333-scale Hyper-X forebody model in the closed-cowl configuration with metal inserts for flow visualization testing.

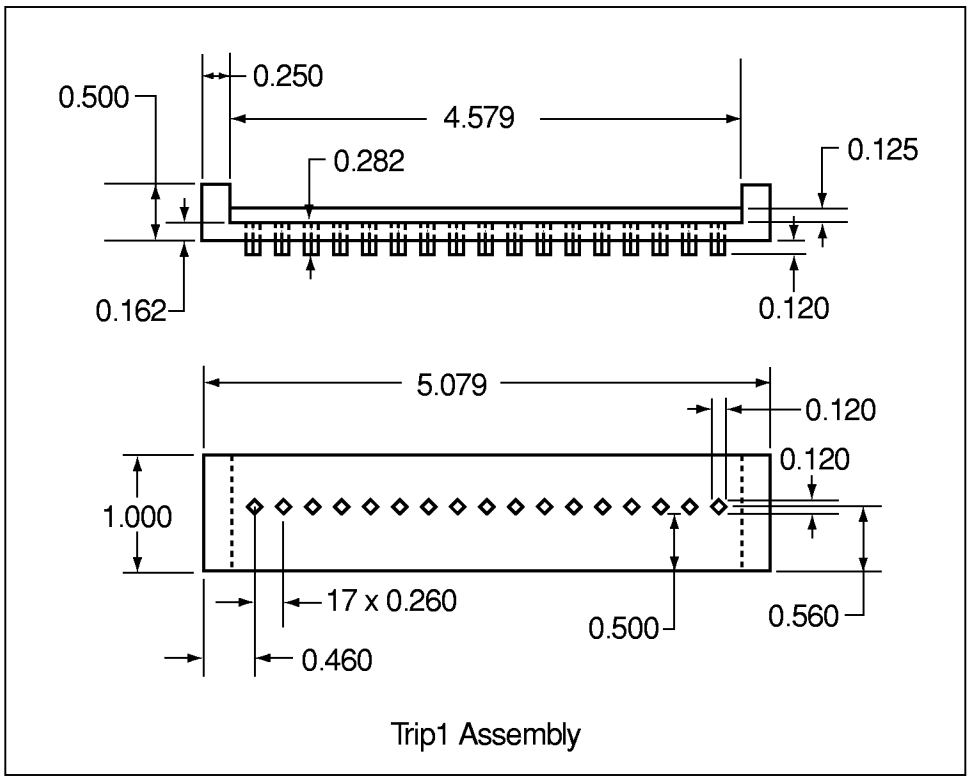

Figure 9a. Detail sketch of Trip Configuration 1.

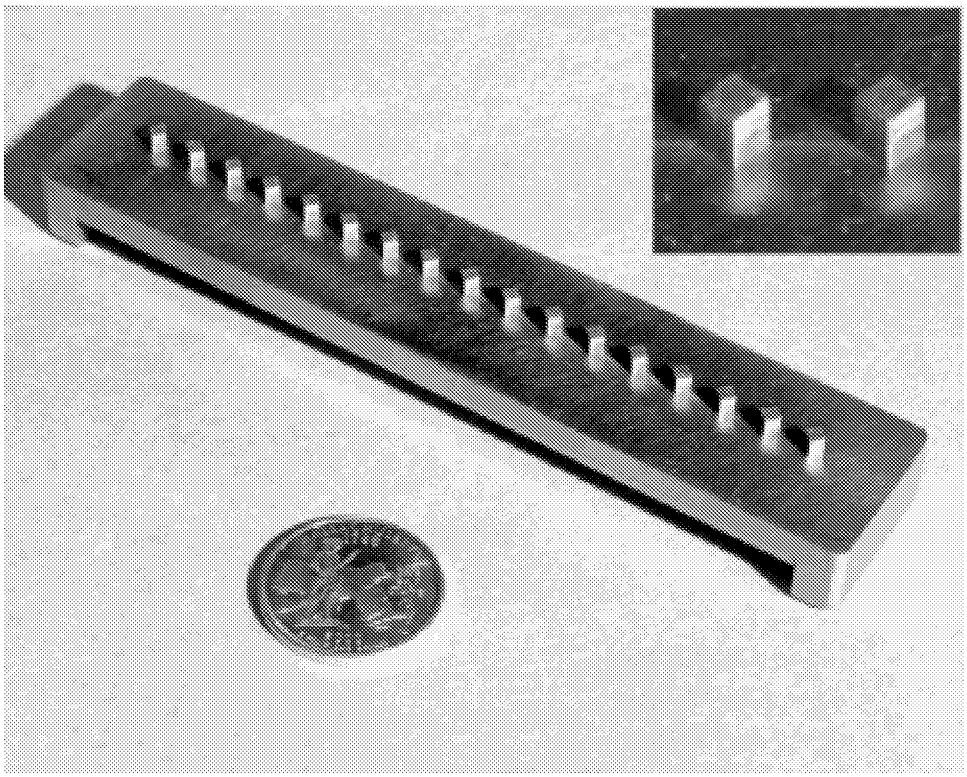

Figure 9b. Photograph of Trip Configuration 1.

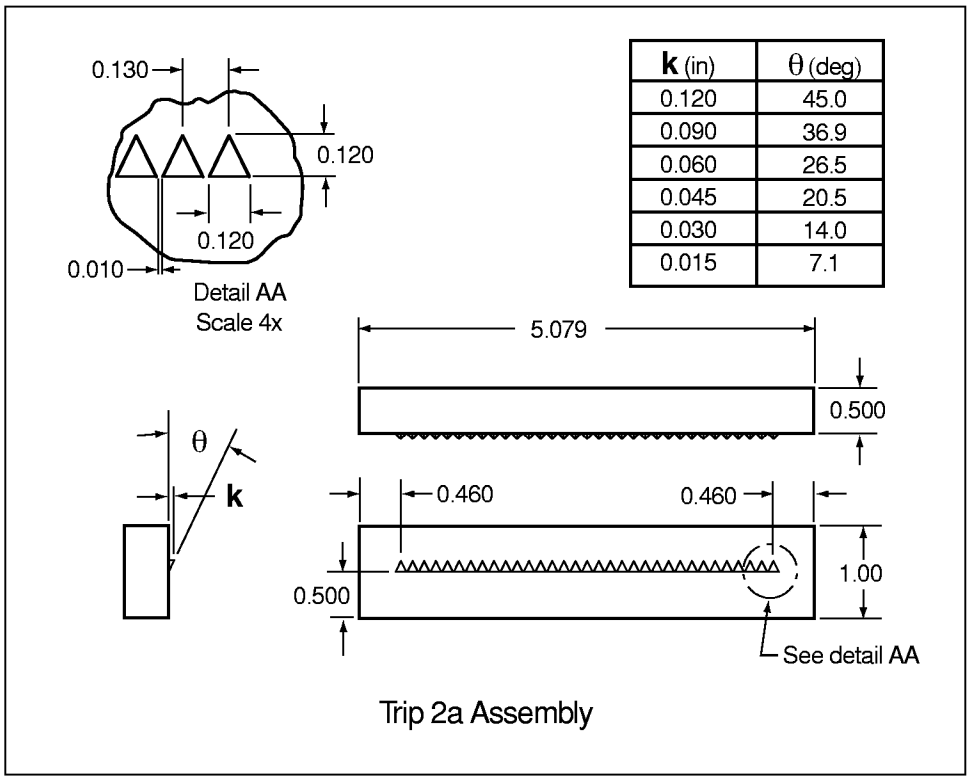

Figure 10a. Detailed sketch of Trip Configuration 2a.

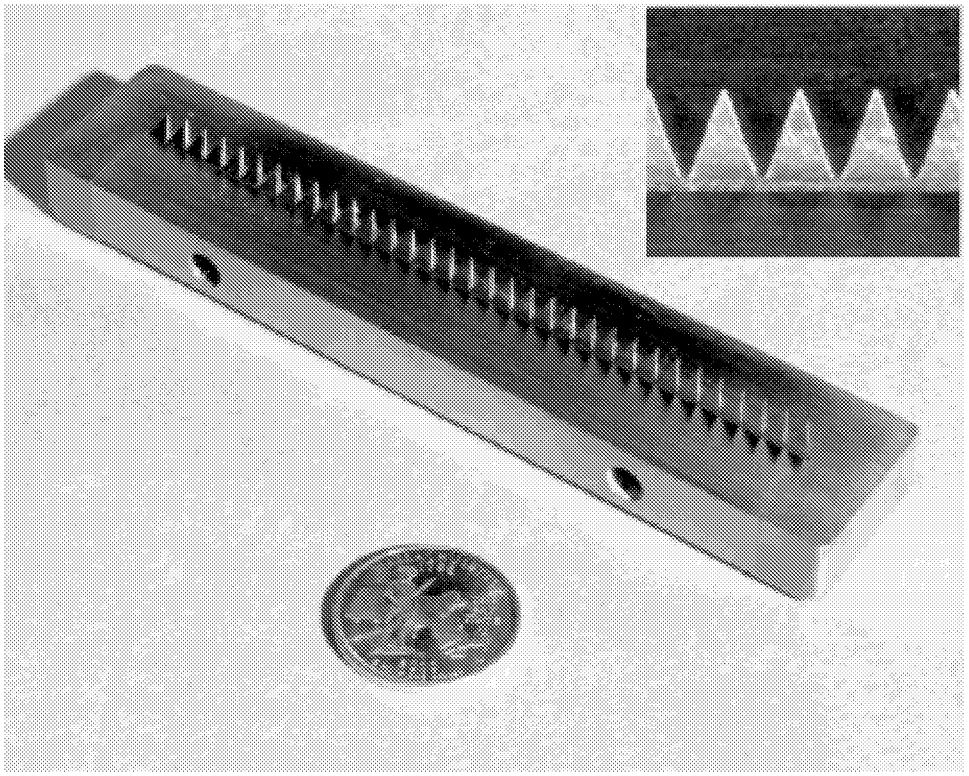

Figure 10b. Photograph of Trip Configuration 2a.

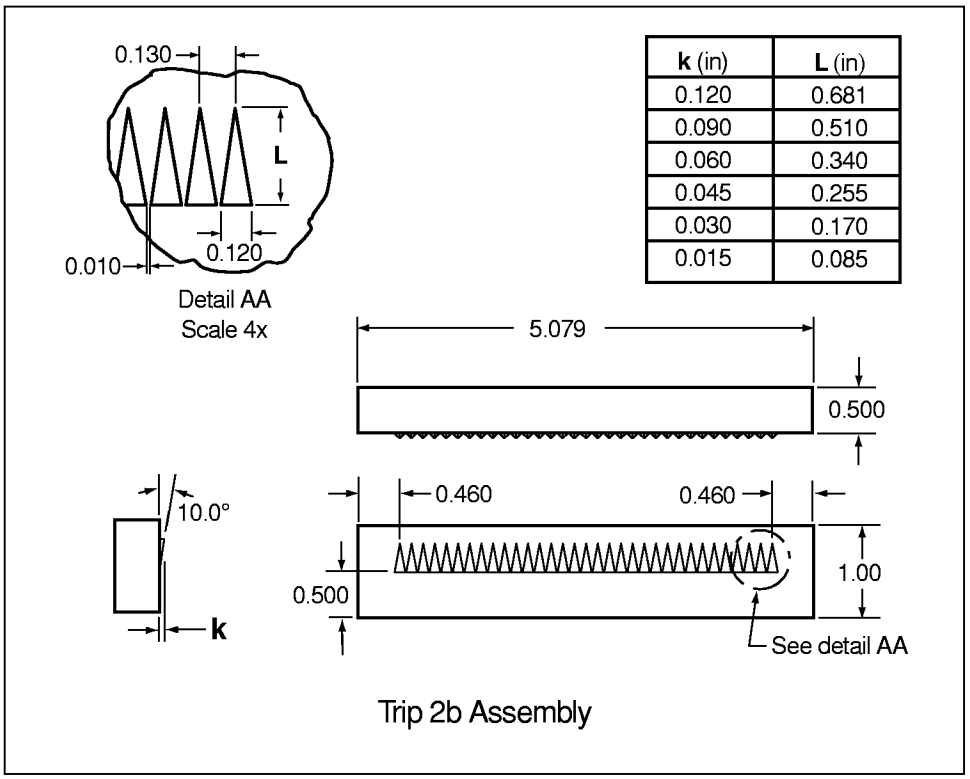

Figure 11a. Detailed sketch of Trip Configuration 2b.

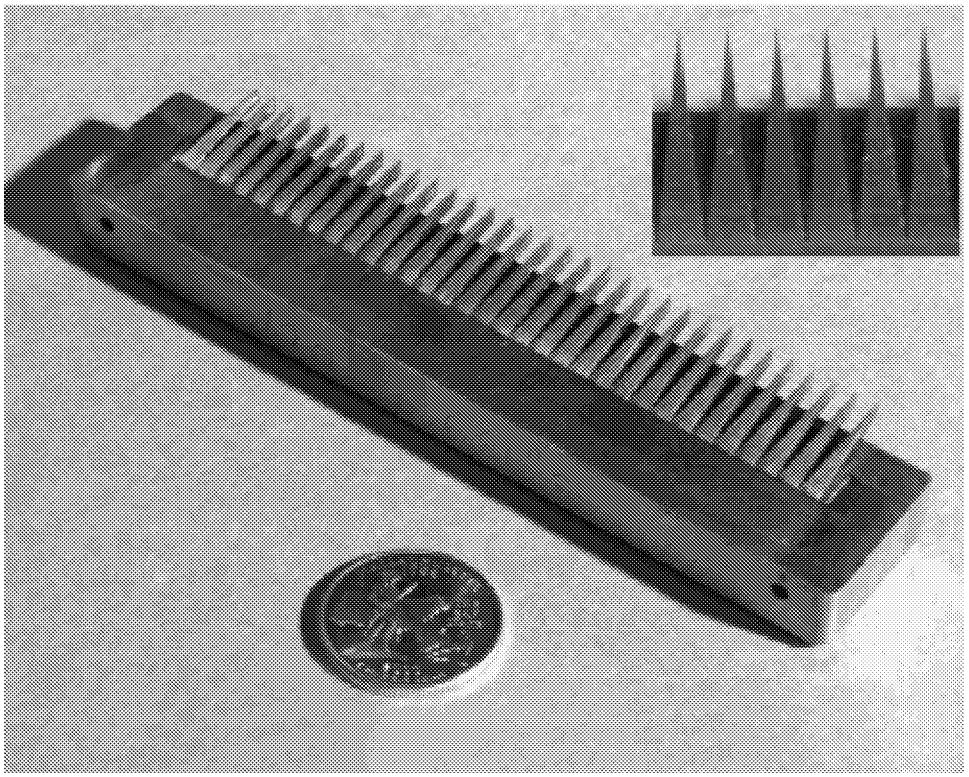

Figure 11b. Photograph of Trip Configuration 2b.

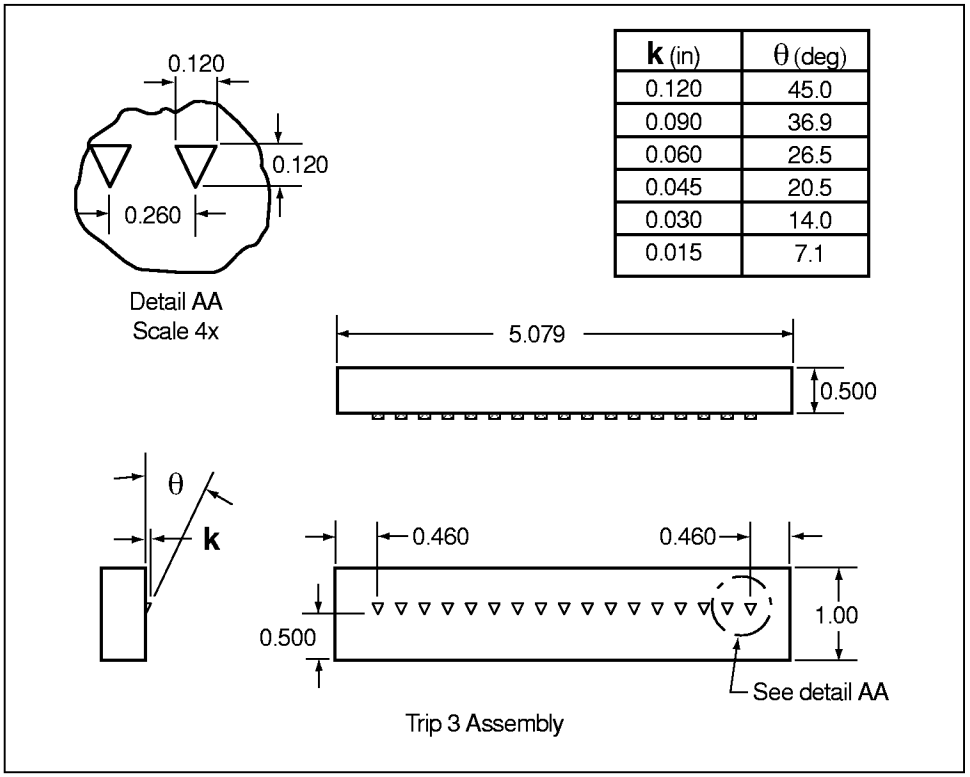

Figure 12a. Detailed sketch of Trip Configuration 3.

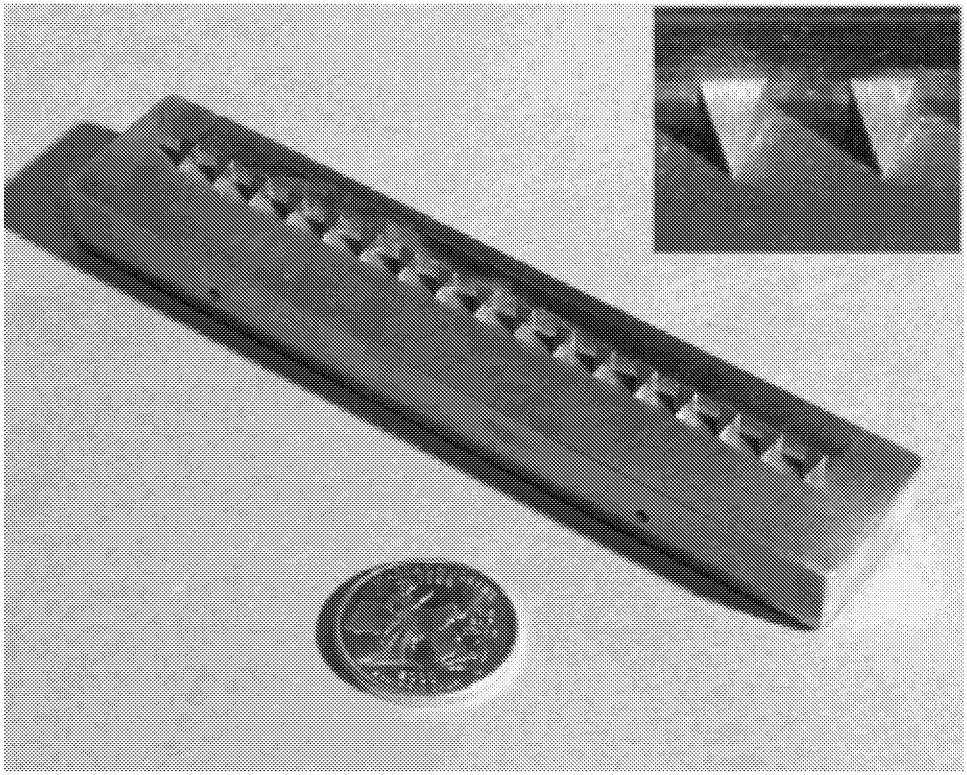

Figure 12b. Photograph of Trip Configuration 3.

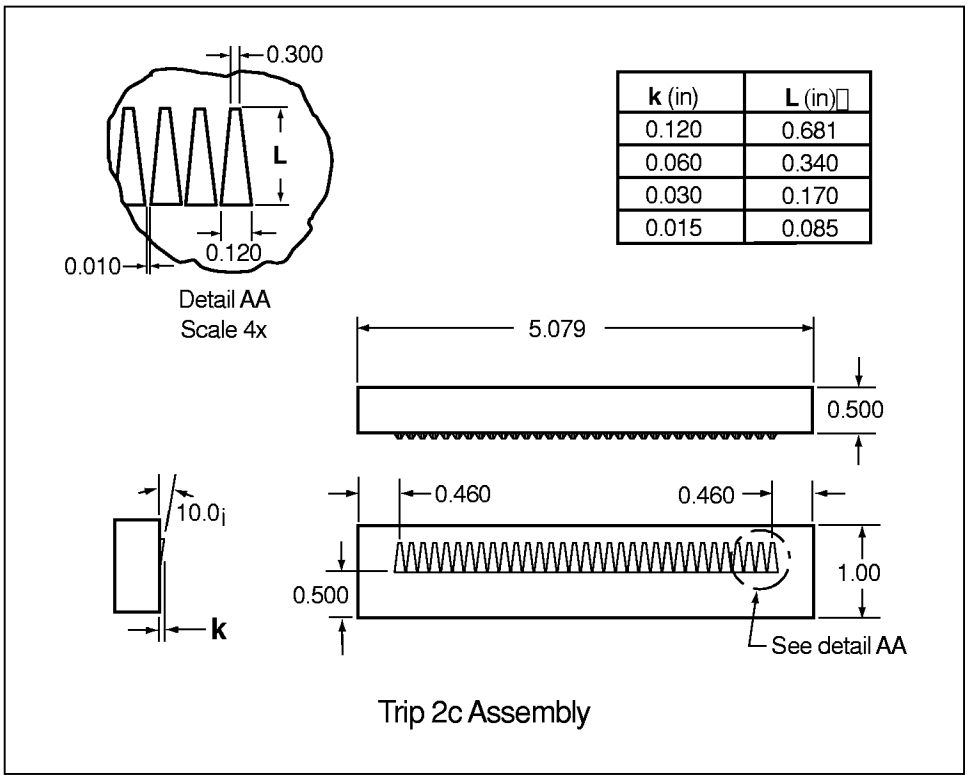

Figure 13a. Detailed sketch of Trip Configuration 2c.

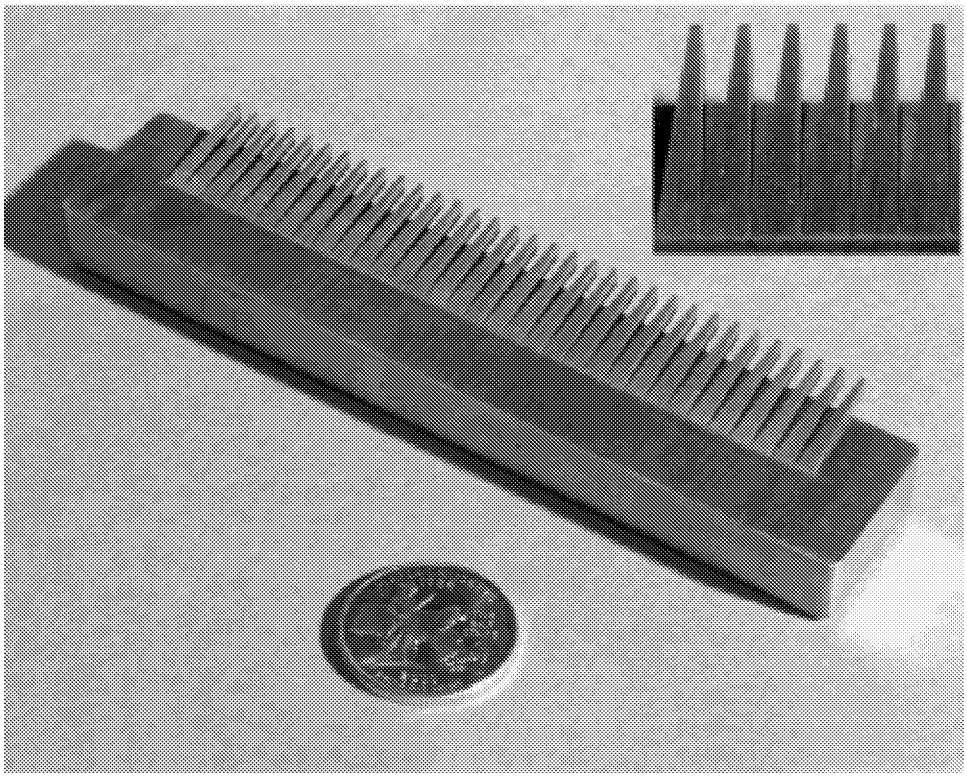

Figure 13b. Photograph of Trip Configuration 3.

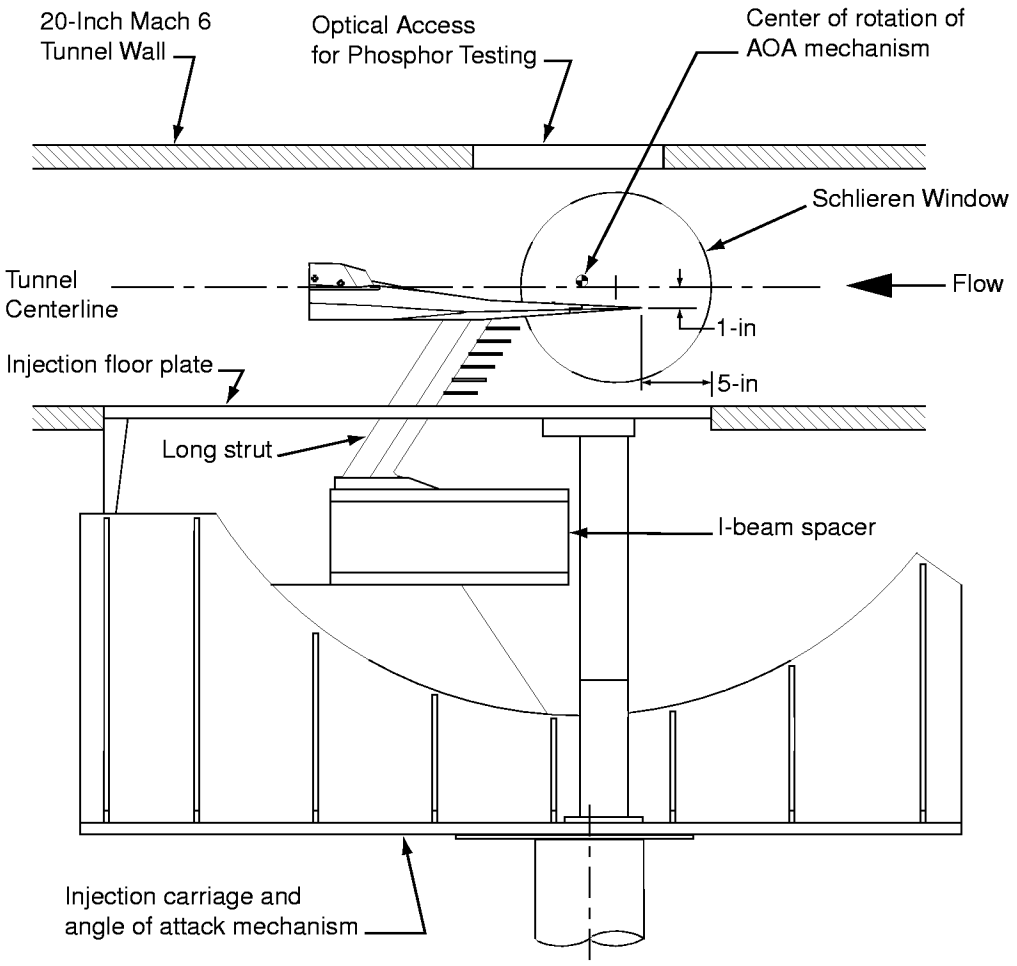

Figure 14. Detailed sketch of model support hardware in the injected position with the long strut and the Hyper-X forebody model at α = 0-deg.

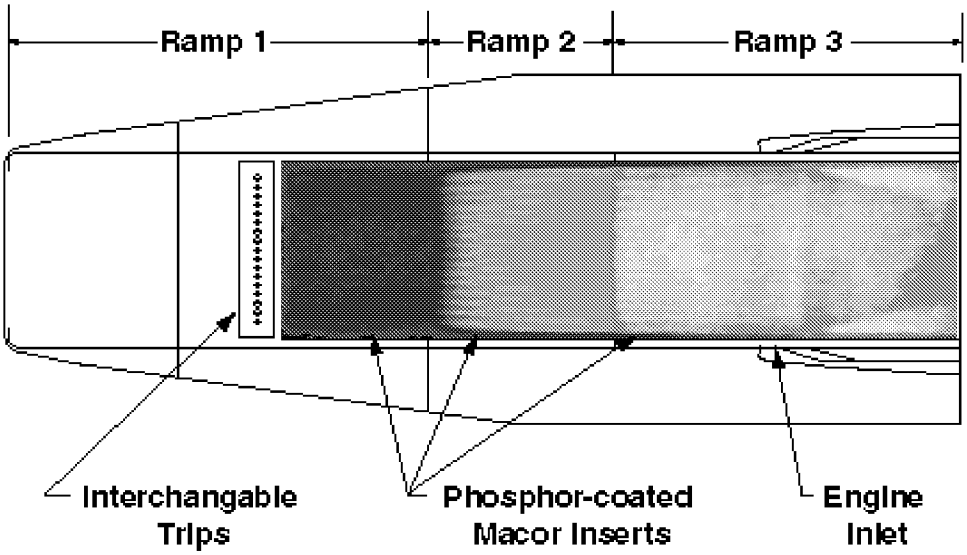

Figure 15. Comparison of phosphor image to model scale.

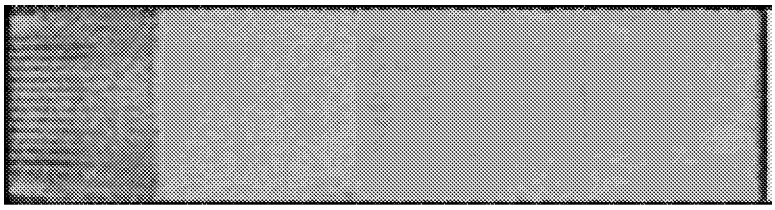

Test 6755 Run 1
α = 2-deg
Re = 2.17 x 10^6/ft
Trip # 1
k = 0.120-in.
Open Cowl

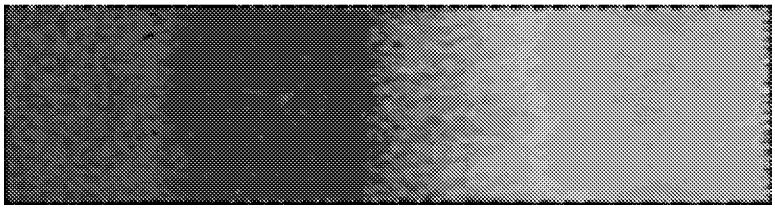

Test 6755 Run 2
α = 2-deg
Re = 2.17 x 10^6/ft
No Trip
Model Baseline
Open Cowl

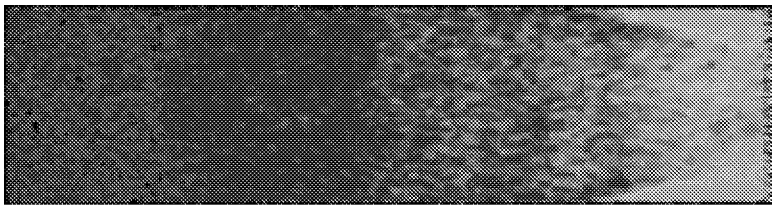

Test 6755 Run 3
α = 2-deg
Re = 1.01 x 10^6/ft
No Trip
Model Baseline
Open Cowl

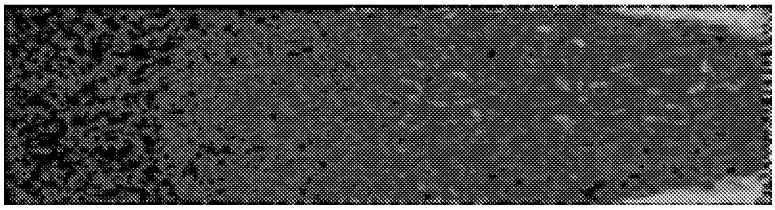

Test 6755 Run 4
α = 2-deg
Re = 0.47 x 10^6/ft
No Trip
Model Baseline
Open Cowl

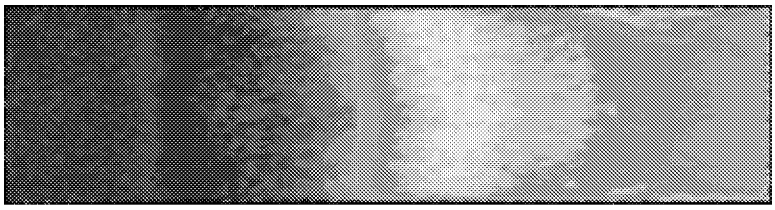

Test 6755 Run 5
α = 2-deg
Re = 4.40 x 10^6/ft
No Trip
Model Baseline
Open Cowl

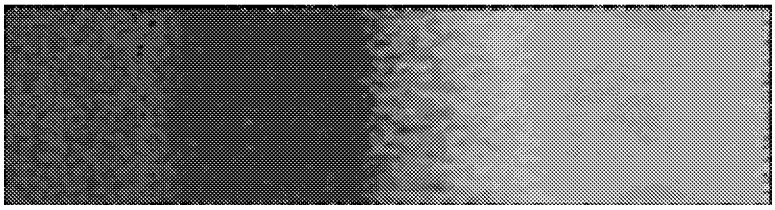

Test 6755 Run 6
α = 2-deg
Re = 2.17 x 10^6/ft
Trip # 1
k = 0.015-in.
Open Cowl

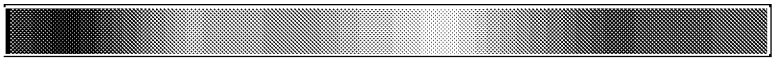

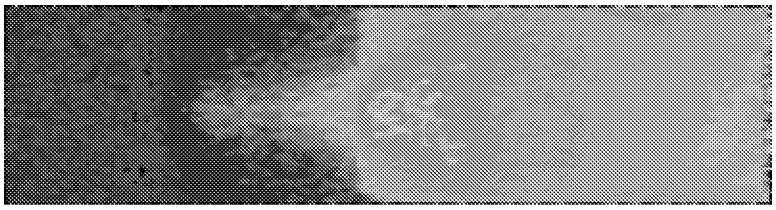

Test 6755 Run 7
α = 2-deg
Re = 2.21 x 10^6/ft
Trip # 1
k = 0.030-in.
Open Cowl

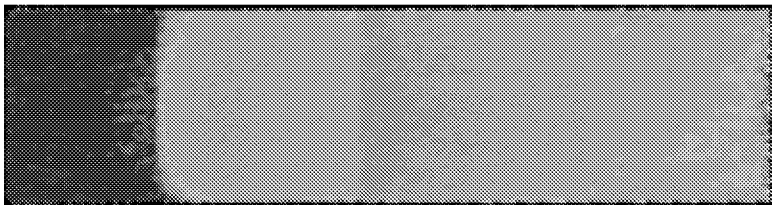

Test 6755 Run 8
α = 2-deg
Re = 2.20 x 10^6/ft
Trip # 1
k = 0.045-in.
Open Cowl

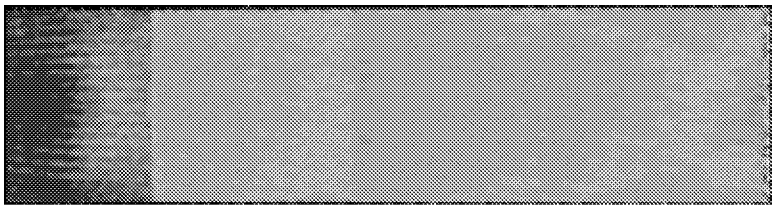

Test 6755 Run 9
α = 2-deg
Re = 2.21 x 10^6/ft
Trip # 1
k = 0.060-in.
Open Cowl

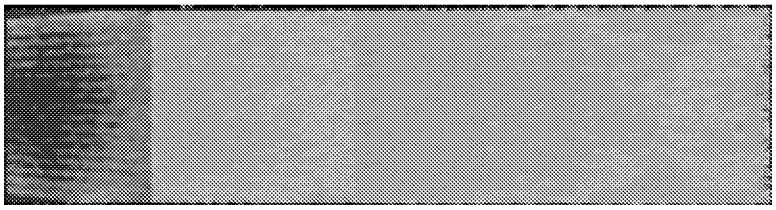

Test 6755 Run 10
α = 2-deg
Re = 2.21 x 10^6/ft
Trip # 1
k = 0.075-in.
Open Cowl

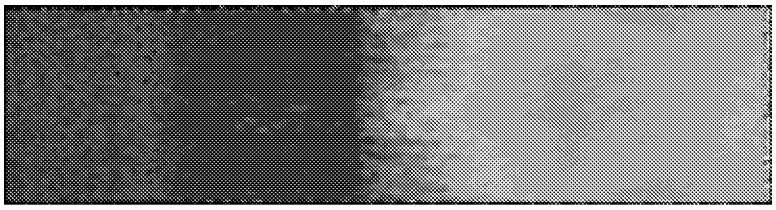

Test 6755 Run 11
α = 2-deg
Re = 2.19 x 10^6/ft
Trip # 1
k = 0.020-in.
Open Cowl

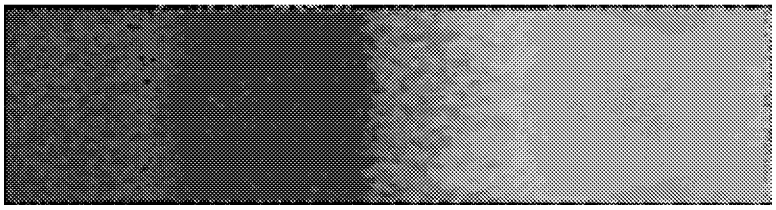

Test 6755 Run 12
α = 2-deg
Re = 2.21 x 10^6/ft
Trip # 2a
k = 0.015-in.
Open Cowl

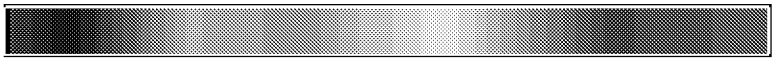

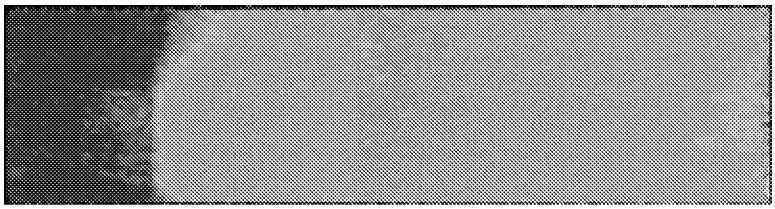

Test 6755 Run 14
α = 2-deg
Re = 2.19 x 10^6/ft
Trip # 2a
k = 0.045-in.
Open Cowl

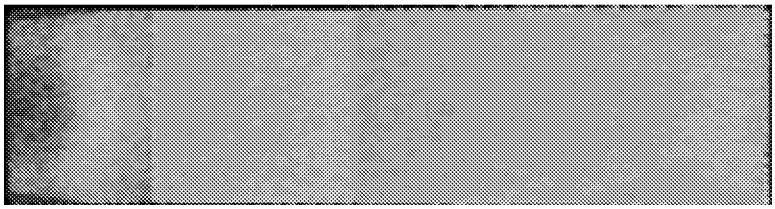

Test 6755 Run 15
α = 2-deg
Re = 2.20 x 10^6/ft
Trip # 2a
k = 0.060-in.
Open Cowl

Test 6755 Run 16
α = 2-deg
Re = 2.20 x 10^6/ft
Trip # 2a
k = 0.030-in.
Open Cowl

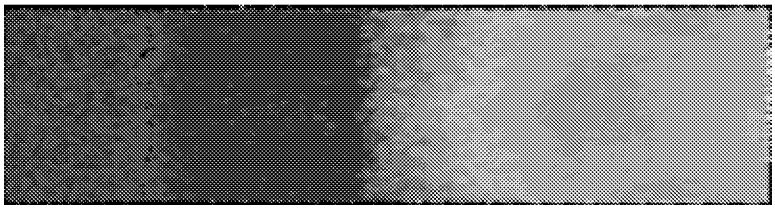

Test 6755 Run 17
α = 2-deg
Re = 2.18 x 10^6/ft
Trip # 2b
k = 0.015-in.
Open Cowl

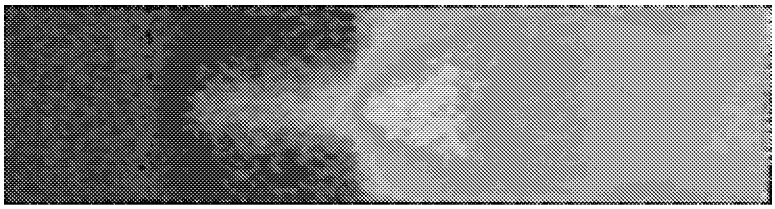

Test 6755 Run 18
α = 2-deg
Re = 2.21 x 10^6/ft
Trip # 2b
k = 0.030-in.
Open Cowl

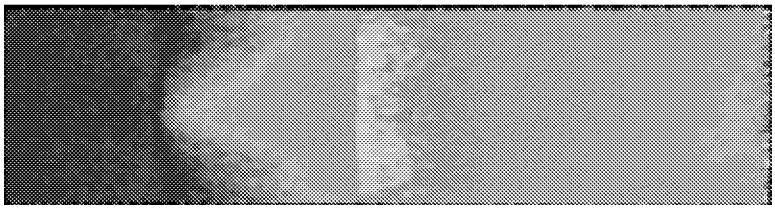

Test 6755 Run 19
α = 2-deg
Re = 2.18 x 10^6/ft
Trip # 2b
k = 0.045-in.
Open Cowl

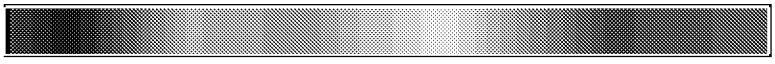

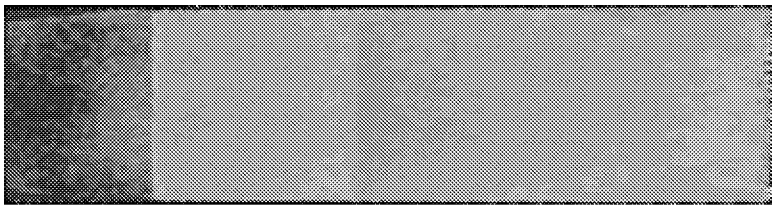

Test 6755 Run 20
α = 2-deg
Re = 2.22 x 10^6/ft
Trip # 2b
k = 0.060-in.
Open Cowl

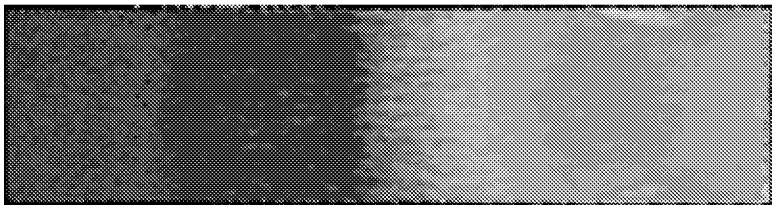

Test 6755 Run 21
α = 2-deg
Re = 2.18 x 10^6/ft
Trip # 3
k = 0.015-in.
Open Cowl

Test 6755 Run 22
α = 2-deg
Re = 2.21 x 10^6/ft
Trip # 3
k = 0.030-in.
Open Cowl

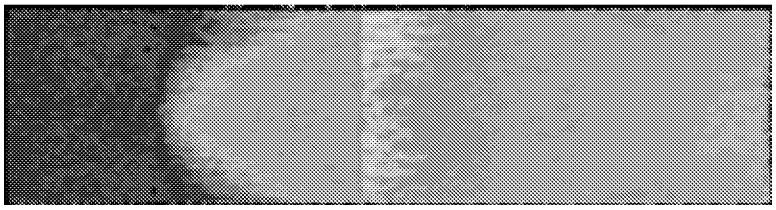

Test 6755 Run 23
α = 2-deg
Re = 2.18 x 10^6/ft
Trip # 3
k = 0.045-in.
Open Cowl

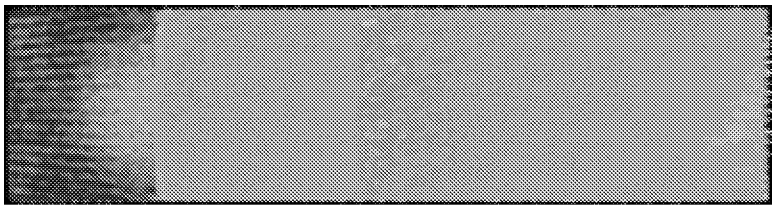

Test 6755 Run 24
α = 2-deg
Re = 2.23 x 10^6/ft
Trip # 3
k = 0.060-in.
Open Cowl

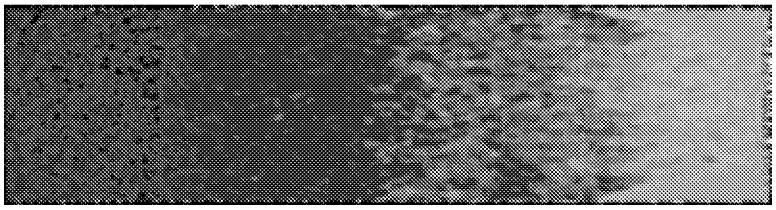

Test 6755 Run 25
α = 2-deg
Re = 1.06 x 10^6/ft
Trip # 1
k = 0.020-in.
Open Cowl

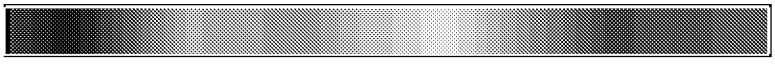

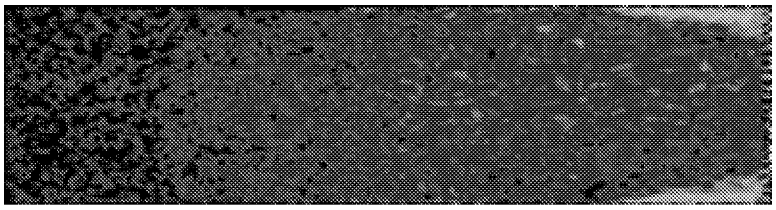

Test 6755 Run 26
α = 2-deg
Re = 1.11 x 10^6/ft
Trip # 1
k = 0.030-in.
Open Cowl

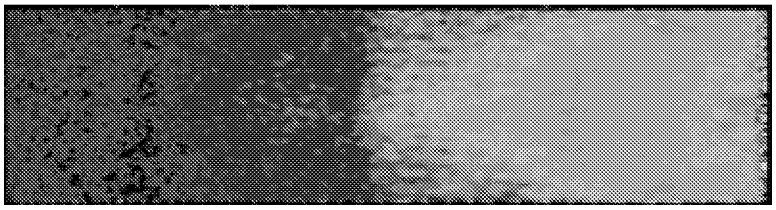

Test 6755 Run 27
α = 2-deg
Re = 1.10 x 10^6/ft
Trip # 1
k = 0.045-in.
Open Cowl

Test 6755 Run 28
α = 2-deg
Re = 1.09 x 10^6/ft
Trip # 1
k = 0.060-in.
Open Cowl

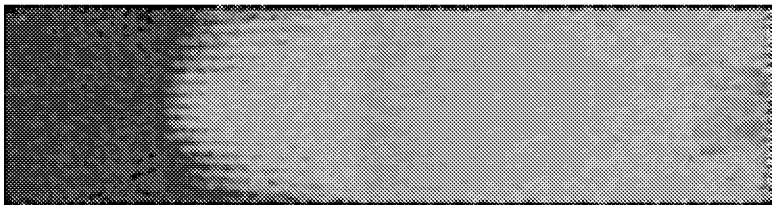

Test 6755 Run 29
α = 2-deg
Re = 1.07 x 10^6/ft
Trip # 3
k = 0.045-in.
Open Cowl

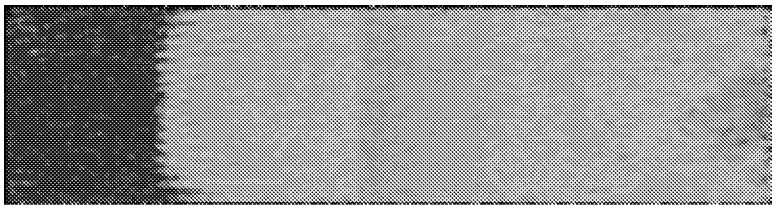

Test 6755 Run 30
α = 2-deg
Re = 1.10 x 10^6/ft
Trip # 1
k = 0.090-in.
Open Cowl

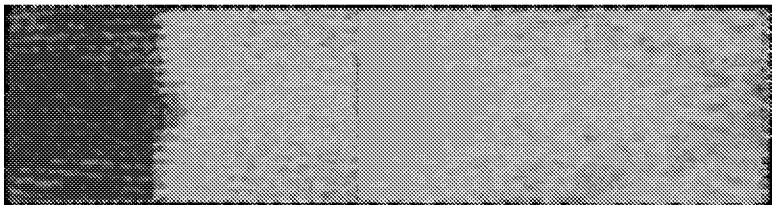

Test 6755 Run 31
α = 2-deg
Re = 1.07 x 10^6/ft
Trip # 1
k = 0.120-in.
Open Cowl

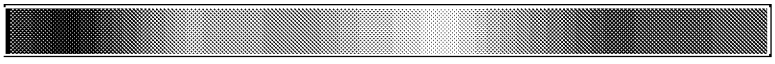

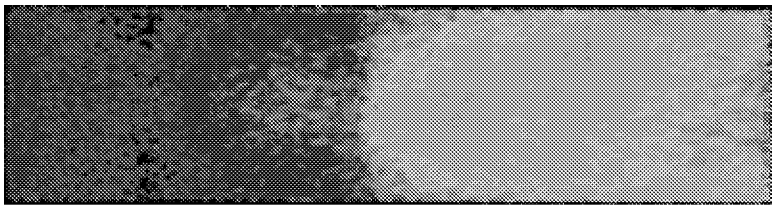

Test 6755 Run 32
α = 2-deg
Re = 1.11 x 10^6/ft
Trip # 2a
k = 0.060-in.
Open Cowl

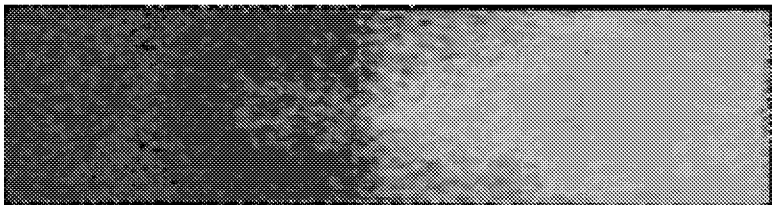

Test 6755 Run 33
α = 2-deg
Re = 1.11 x 10^6/ft
Trip # 2b
k = 0.060-in.
Open Cowl

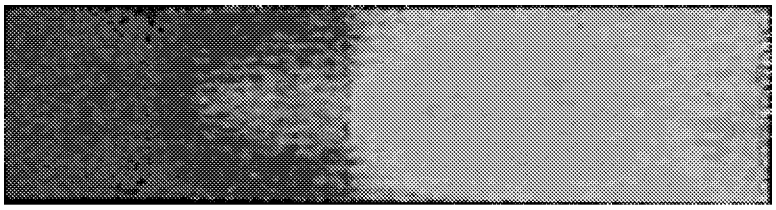

Test 6755 Run 34
α = 2-deg
Re = 1.08 x 10^6/ft
Trip # 3
k = 0.060-in.
Open Cowl

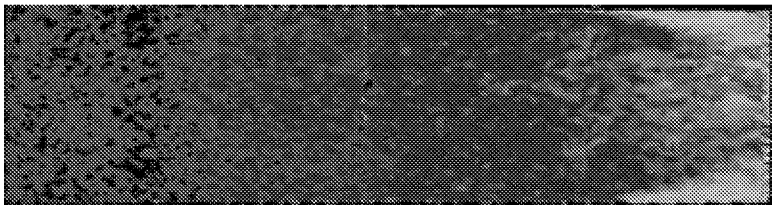

Test 6755 Run 35
α = 0-deg
Re = 1.11 x 10^6/ft
No Trip
Model Baseline
Open Cowl

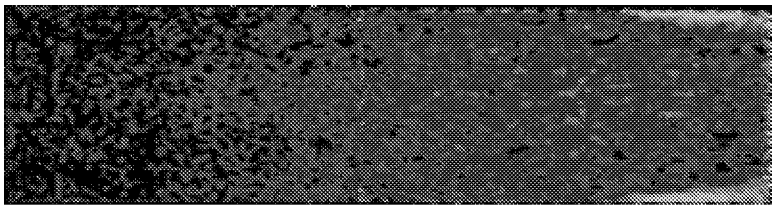

Test 6755 Run 36
α = 0-deg
Re = 0.49 x 106/ft
No Trip
Model Baseline
Open Cowl

Test 6755 Run 37
α = 0-deg
Re = 2.24 x 106/ft
No Trip
Model Baseline
Open Cowl

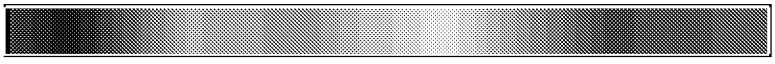

h/h_{ref}

0.00 0.25 0.50 0.75 1.00

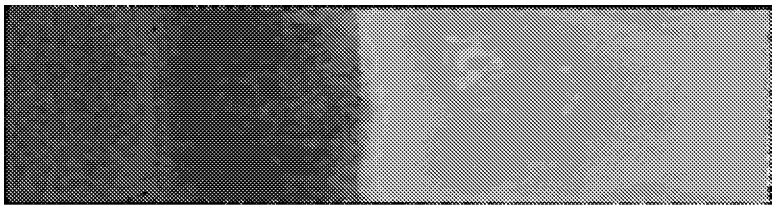

Test 6755 Run 38
α = 0-deg
Re = 4.44 x 106/ft
No Trip
Model Baseline
Open Cowl

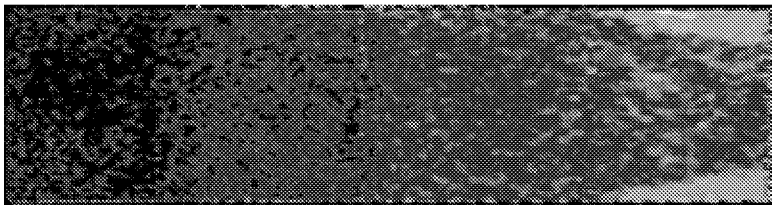

Test 6755 Run 39
α = 4-deg
Re = 0.47 x 106/ft
No Trip
Model Baseline
Open Cowl

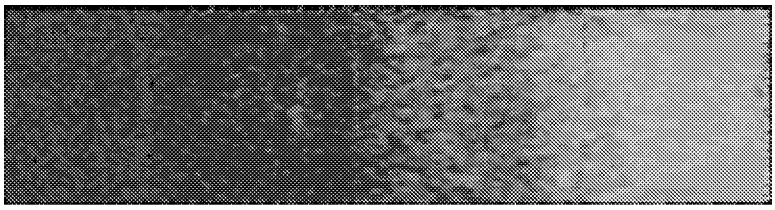

Test 6755 Run 40
α = 4-deg
Re = 1.04 x 10^6/ft
No Trip
Model Baseline
Open Cowl

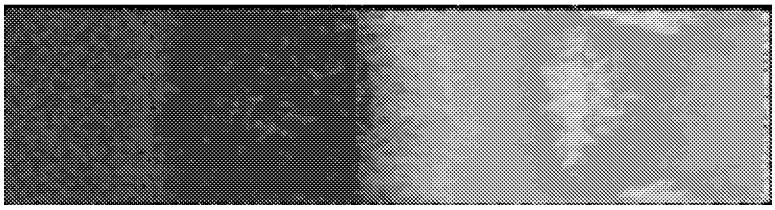

Test 6755 Run 41
α = 4-deg
Re = 2.23 x 10^6/ft
No Trip
Model Baseline
Open Cowl

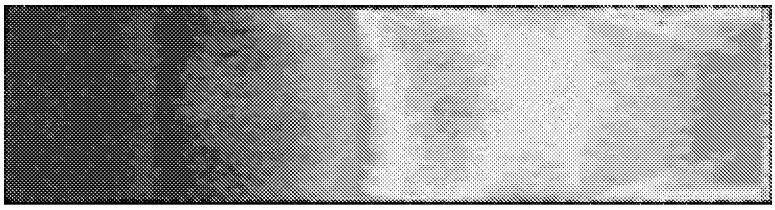

Test 6755 Run 42
α = 4-deg
Re = 4.41 x 10^6/ft
No Trip
Model Baseline
Open Cowl

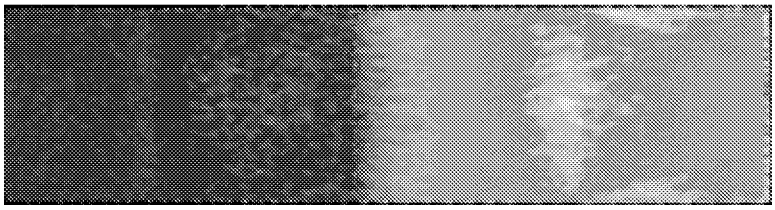

Test 6755 Run 43
α = 4-deg
Re = 2.25 x 10^6/ft
Trip # 1
k = 0.015-in.
Open Cowl

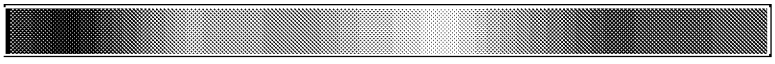

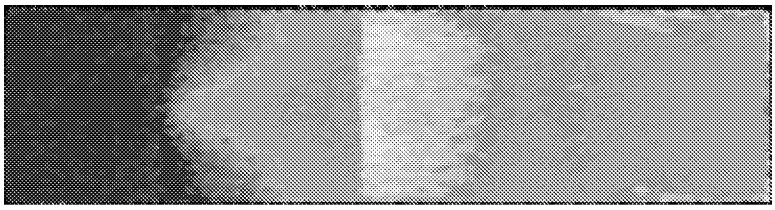

Test 6755 Run 44
α = 4-deg
Re = 2.23 x 10^6/ft
Trip # 1
k = 0.030-in.
Open Cowl

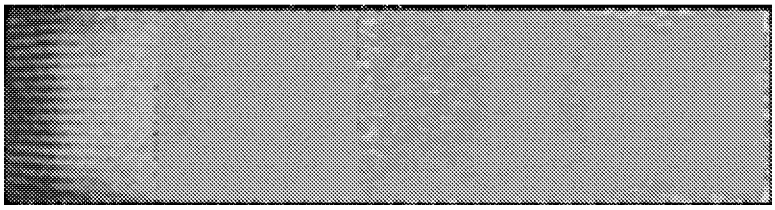

Test 6755 Run 45
α = 4-deg
Re = 2.23 x 10^6/ft
Trip # 1
k = 0.045-in.
Open Cowl

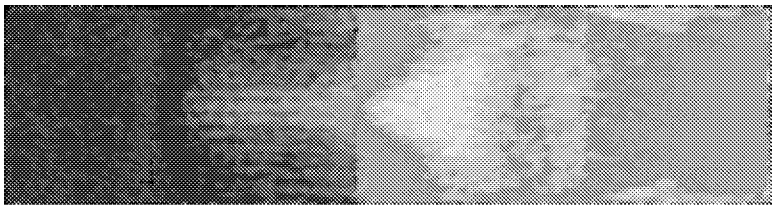

Test 6755 Run 46
α = 4-deg
Re = 2.21 x 10^6/ft
Trip # 1
k = 0.020-in.
Open Cowl

Test 6755 Run 47
α = 4-deg
Re = 2.23 x 10^6/ft
Trip # 2a
k = 0.030-in.
Open Cowl

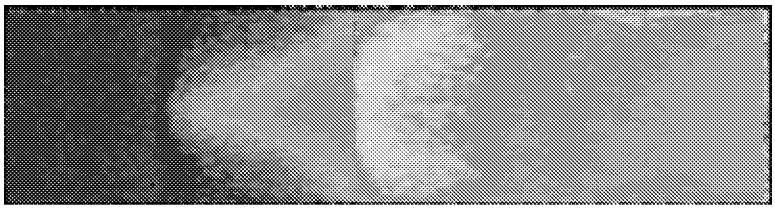

Test 6755 Run 48
α = 4-deg
Re = 2.18 x 10^6/ft
Trip # 2b
k = 0.030-in.
Open Cowl

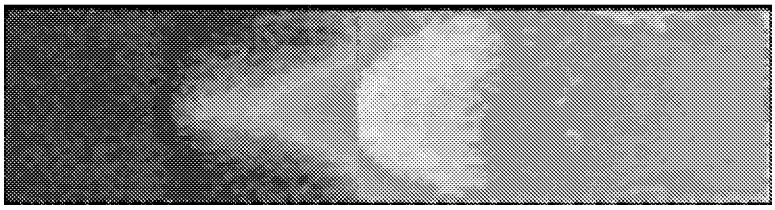

Test 6755 Run 49
α = 4-deg
Re = 2.23 x 10^6/ft
Trip # 2b-backwards
k = 0.030-in.
Open Cowl

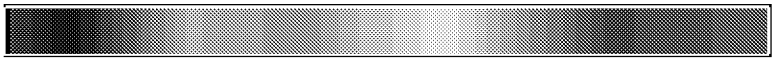

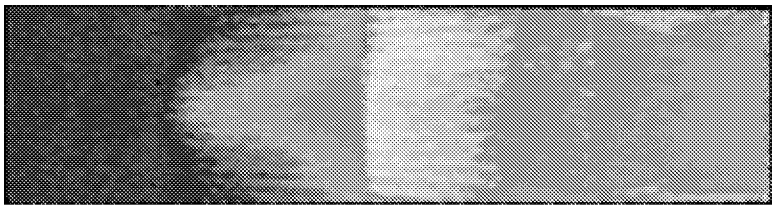

Test 6755 Run 50
α = 4-deg
Re = 2.21 x 10^6/ft
Trip # 3
k = 0.030-in.
Open Cowl

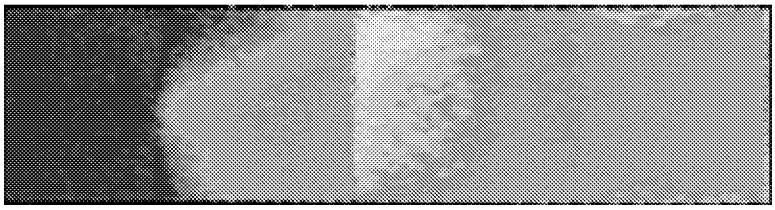

Test 6755 Run 51
α = 4-deg
Re = 2.20 x 10^6/ft
Trip # 2a
k = 0.030-in.
Open Cowl

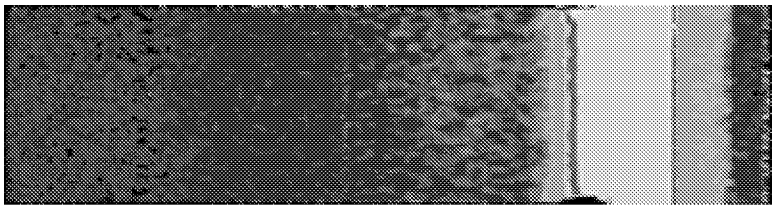

Test 6755 Run 52
α = 2-deg
Re = 1.06 x 10^6/ft
No Trip
Model Baseline
Closed Cowl

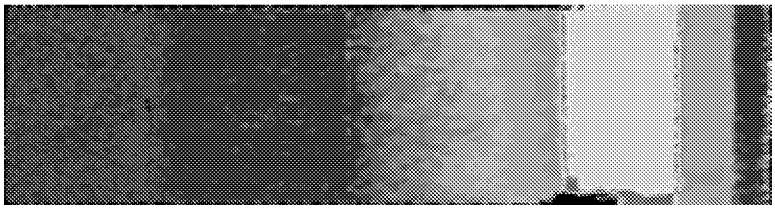

Test 6755 Run 53
α = 2-deg
Re = 2.23 x 10^6/ft
No Trip
Model Baseline
Closed Cowl

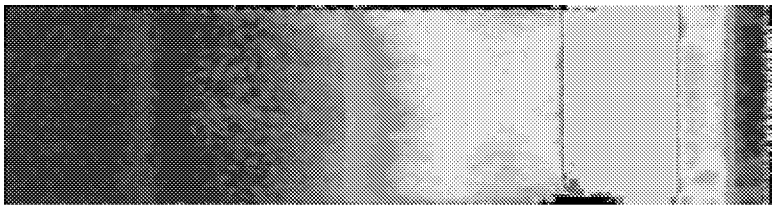

Test 6755 Run 54
α = 2-deg
Re = 4.32 x 10^6/ft
No Trip
Model Baseline
Closed Cowl

Test 6755 Run 55
α = 2-deg
Re = 2.20 x 10^6/ft
Trip # 1
k = 0.030-in.
Closed Cowl

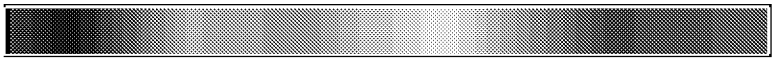

h/h_{ref}

0.00 0.25 0.50 0.75 1.00

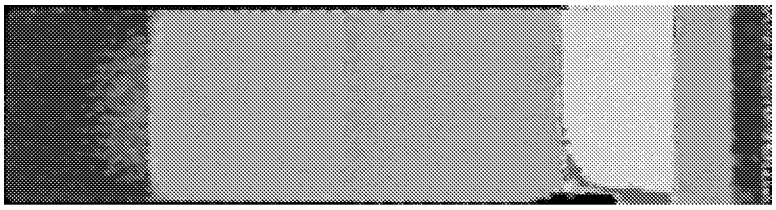

Test 6755 Run 56
α = 2-deg
Re = 2.24 x 10^6/ft
Trip # 1
k = 0.045-in.
Closed Cowl

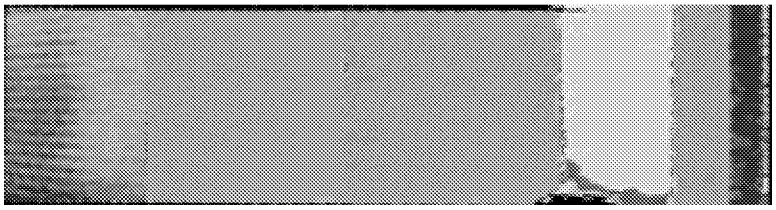

Test 6755 Run 57
α = 2-deg
Re = 2.22 x 10^6/ft
Trip # 1
k = 0.060-in.
Closed Cowl

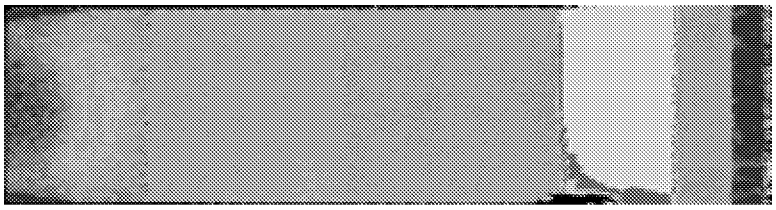

Test 6755 Run 58
α = 2-deg
Re = 2.21 x 10^6/ft
Trip # 2a
k = 0.060-in.
Closed Cowl

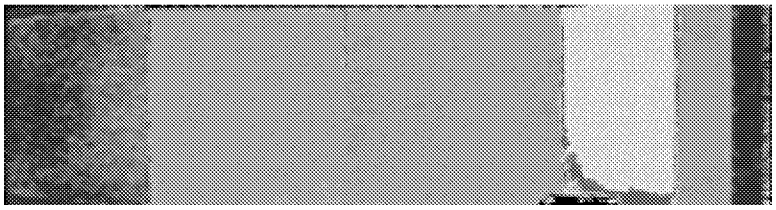

Test 6755 Run 59
α = 2-deg
Re = 2.23 x 10^6/ft
Trip # 2b
k = 0.060-in.
Closed Cowl

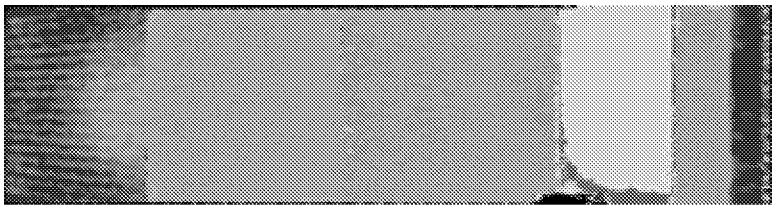

Test 6755 Run 60
α = 2-deg
Re = 2.20 x 10^6/ft
Trip # 3
k = 0.060-in.
Closed Cowl

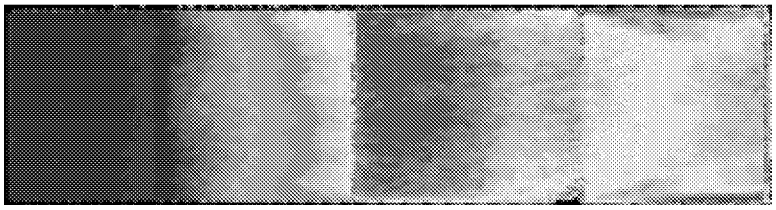

Test 6755 Run 61
α = 2-deg
Re = 6.67 x 10^6/ft
No Trip
Model Baseline
Open Cowl

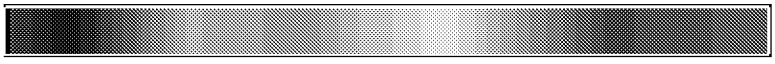

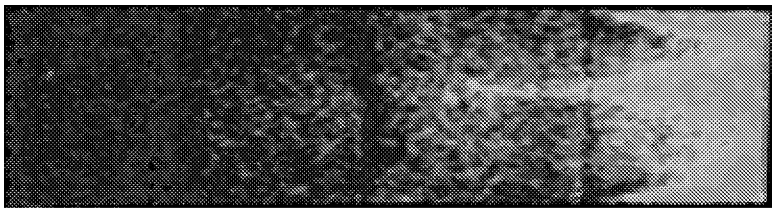

Test 6791 Run 1
α = 2-deg
Re = 1.12 x 10^6/ft
No Trip
Model Baseline
Open Cowl

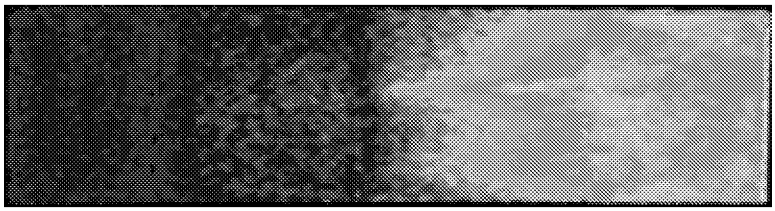

Test 6791 Run 2
α = 2-deg
Re = 2.25 x 10^6/ft
No Trip
Model Baseline
Open Cowl

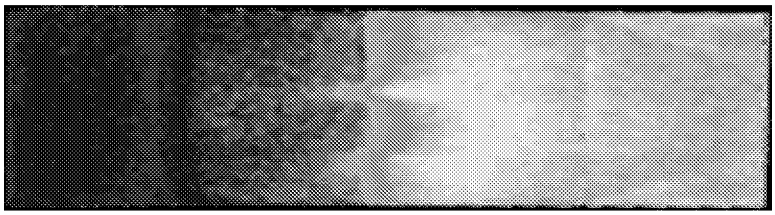

Test 6791 Run 3
α = 2-deg
Re = 4.39 x 10^6/ft
No Trip
Model Baseline
Open Cowl

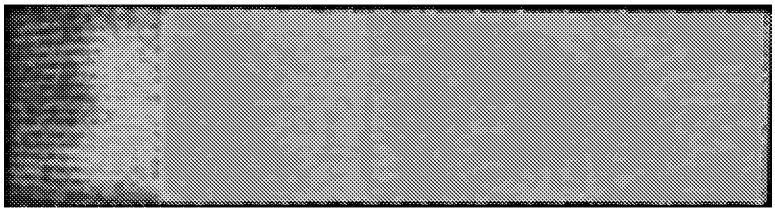

Test 6791 Run 4
α = 2-deg
Re = 2.24 x 10^6/ft
Trip # 1
k = 0.060-in.
Open Cowl

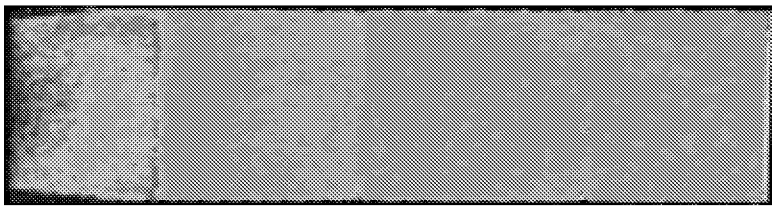

Test 6791 Run 5
α = 2-deg
Re = 2.25 x 10^6/ft
Trip # 2c
k = 0.060-in.
Open Cowl

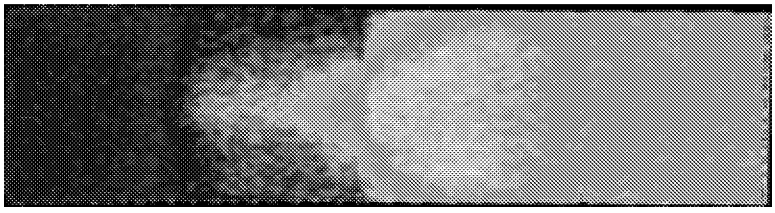

Test 6791 Run 6
α = 2-deg
Re = 2.22 x 10^6/ft
Trip # 2c
k = 0.030-in.
Open Cowl

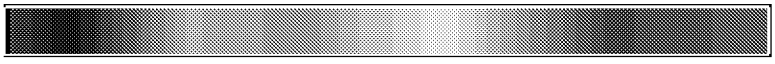

h/h_{ref}

0.00 0.25 0.50 0.75 1.00

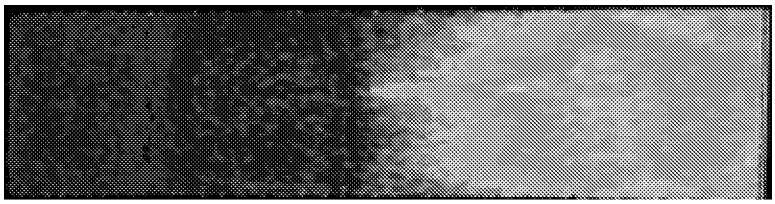

Test 6791 Run 7
α = 2-deg
Re = 2.2 x 10^6/ft
Trip # 2c
k = 0.015-in.
Open Cowl

Test 6791 Run 8
α = 2-deg
Re = 2.2 x 10^6/ft
Trip # 2b
k = 0.030-in.
Open Cowl

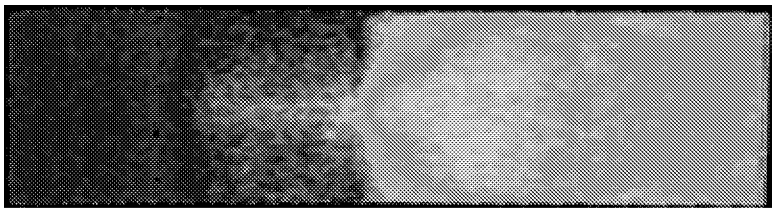

Test 6791 Run 9
α = 2-deg
Re = 2.2 x 10^6/ft
Trip # 1
k = 0.030-in.
Open Cowl

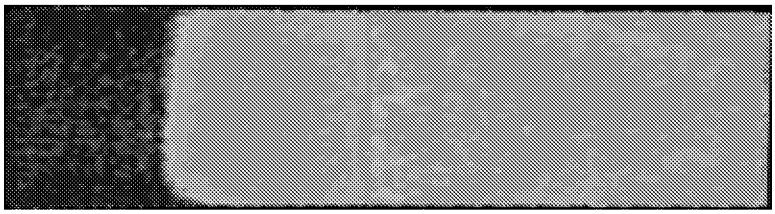

Test 6791 Run 10
α = 2-deg
Re = 2.2 x 10^6/ft
Trip # 1
k = 0.045-in.
Open Cowl

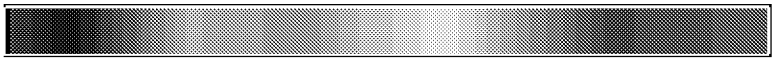

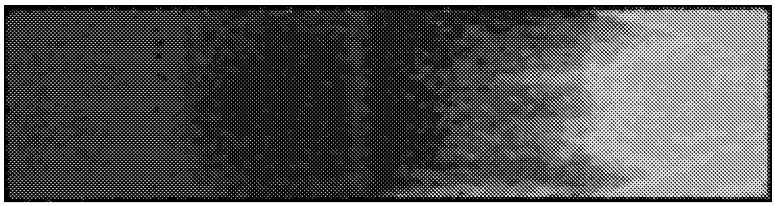

Test 6793 Run 2
α = -0.5-deg
Re = 2.2 x 10^6/ft
No Trip
Model Baseline
Open Cowl

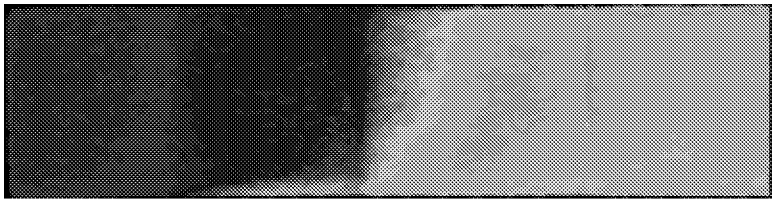

Test 6793 Run 3
α = -0.5-deg
Re = 4.4 x 10^6/ft
No Trip
Model Baseline
Open Cowl

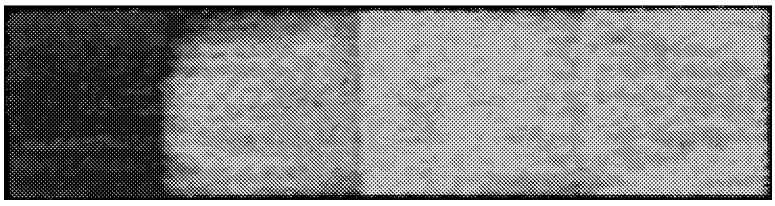

Test 6793 Run 4
α = -0.5-deg
Re = 2.2 x 10^6/ft
#24 Grit
k = 0.038-in.
Open Cowl

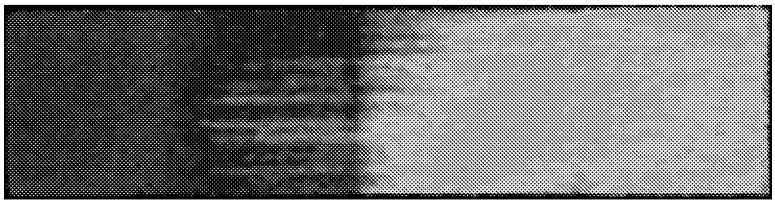

Test 6793 Run 5
α = -0.5-deg
Re = 2.2 x 10^6/ft
#46 Grit
k = 0.024-in.
Open Cowl

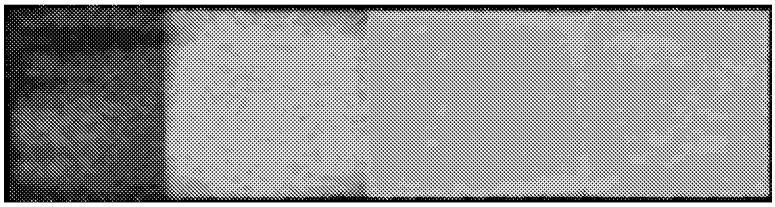

Test 6793 Run 6
α = -0.5-deg
Re = 4.4 x 10^6/ft
#46 Grit
k = 0.024-in.
Open Cowl

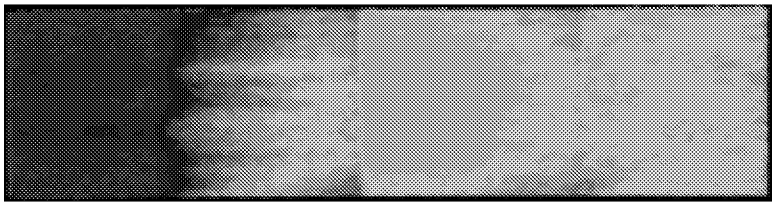

Test 6793 Run 7
α = -0.5-deg
Re = 4.4 x 10^6/ft
#60 Grit
k = 0.017-in.
Open Cowl

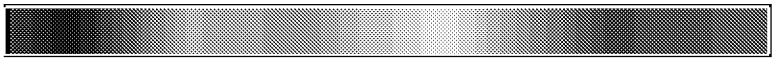

Test 6793 Run 8
α = -0.5-deg
Re = 2.2 x 10^6/ft
#60 Grit
k = 0.017-in.
Open Cowl

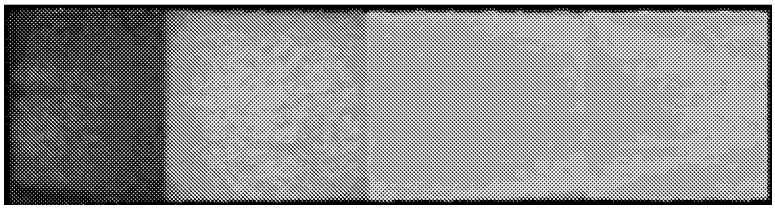

Test 6793 Run 9
α = -0.5-deg
Re = 6.0 x 10^6/ft
#60 Grit
k = 0.017-in.
Open Cowl

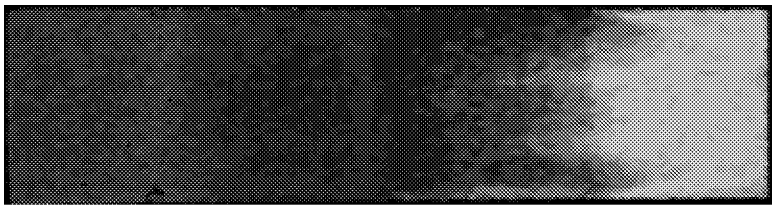

Test 6793 Run 10
α = -0.5-deg
Re = 2.2 x 10^6/ft
2D Kapton strip
k = 0.010-in.
Open Cowl

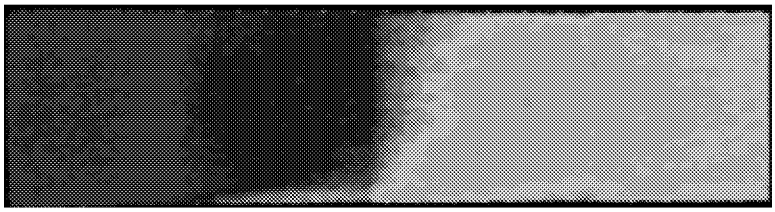

Test 6793 Run 11
α = -0.5-deg
Re = 4.4 x 10^6/ft
2D Kapton strip
k = 0.010-in
Open Cowl

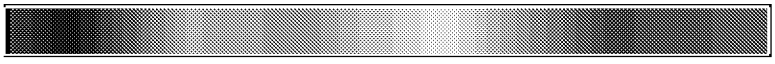

Appendix D

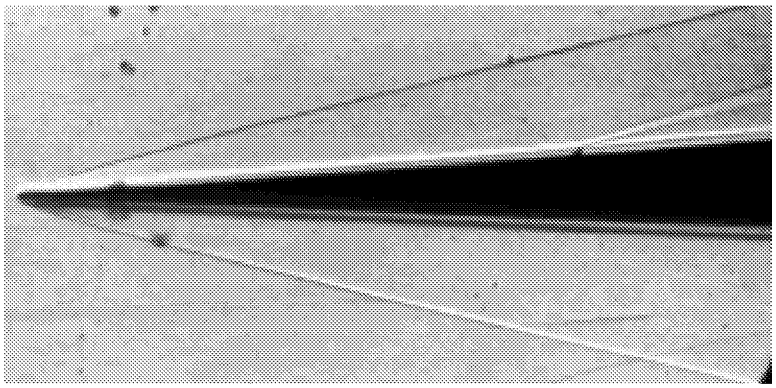

Run 15
α = 2-deg
Re = 2.2 x 10^6/ft
Trip # 2a
k = 0.060-in.

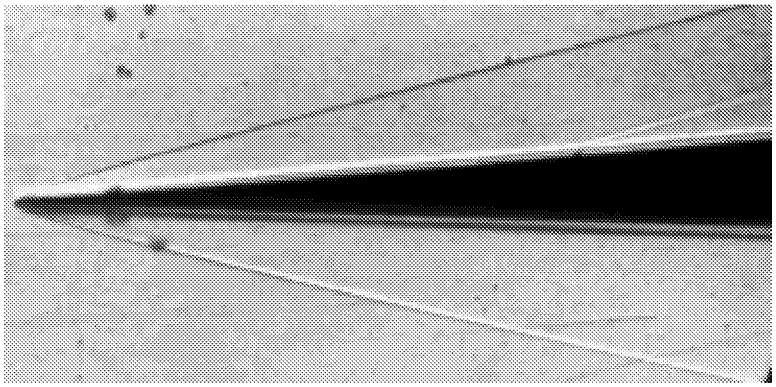

Run 16
α = 2-deg
Re = 2.2 x 10^6/ft
Trip # 2a
k = 0.030-in.

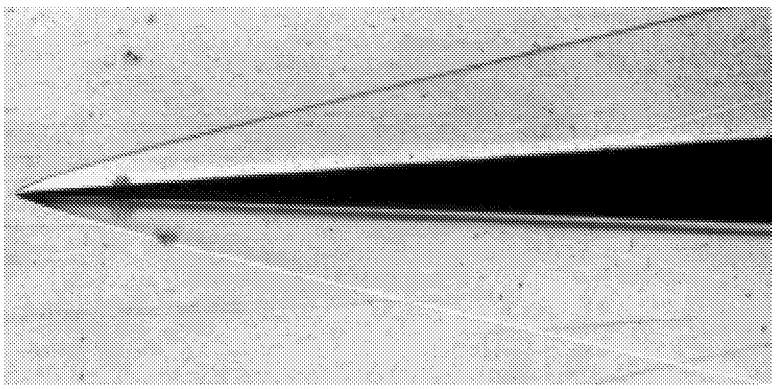

Run 17
α = 2-deg
Re = 2.2 x 10^6/ft
Trip # 2b
k = 0.015-in.

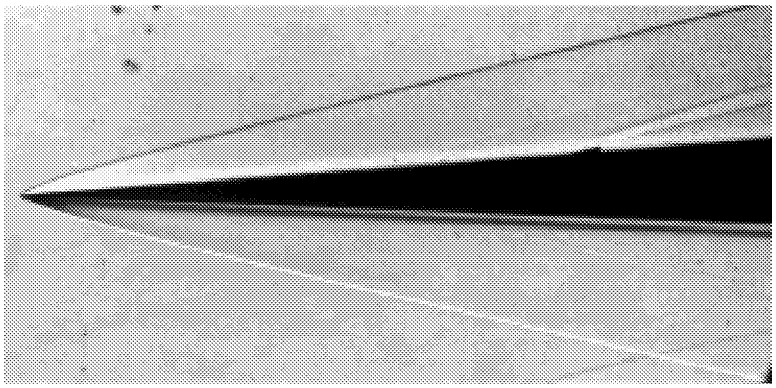

Run 20
α = 2-deg
Re = 2.2 x 10^6/ft
Trip # 2b
k = 0.060-in.

Appendix D

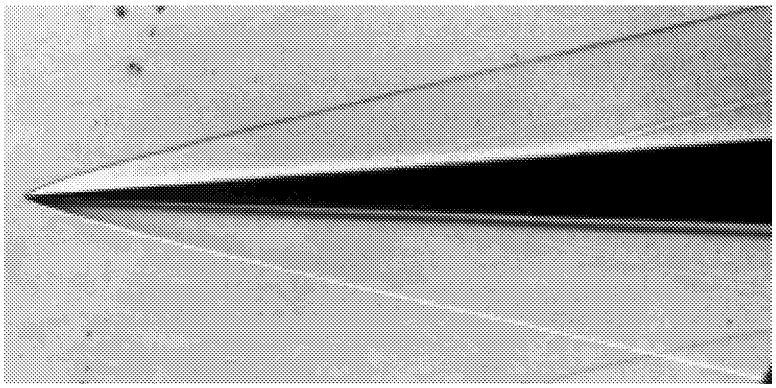

Run 21
α = 2-deg
Re = 2.2 x 10^6/ft
Trip # 3
k = 0.015-in.

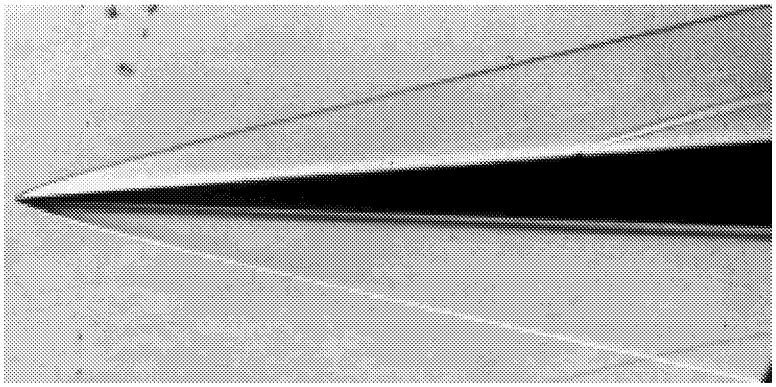

Run 22
α = 2-deg
Re = 2.2 x 10^6/ft
Trip # 3
k = 0.030-in.

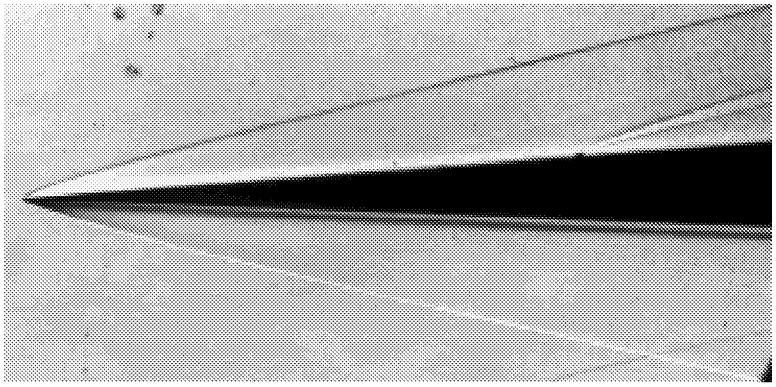

Run 23
α = 2-deg
Re = 2.2 x 10^6/ft
Trip # 3
k = 0.045-in.

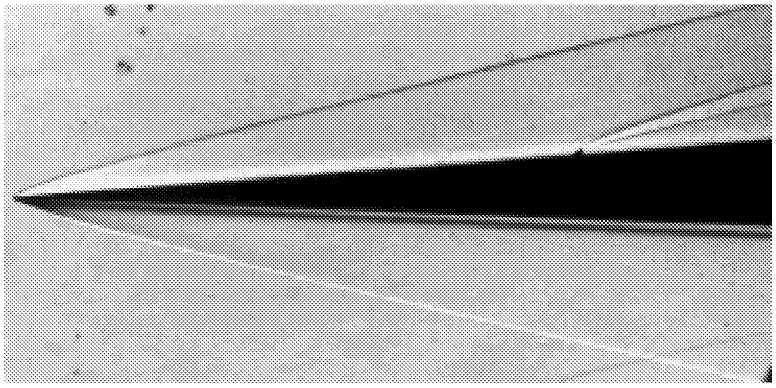

Run 24
α = 2-deg
Re = 2.2 x 10^6/ft
Trip # 3
k = 0.060-in.

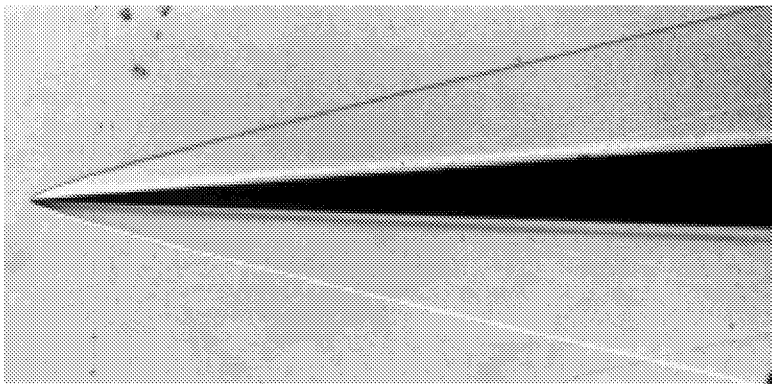

Run 25
α = 2-deg
Re = 1.1 x 10^6/ft
Trip # 1
k = 0.020-in.

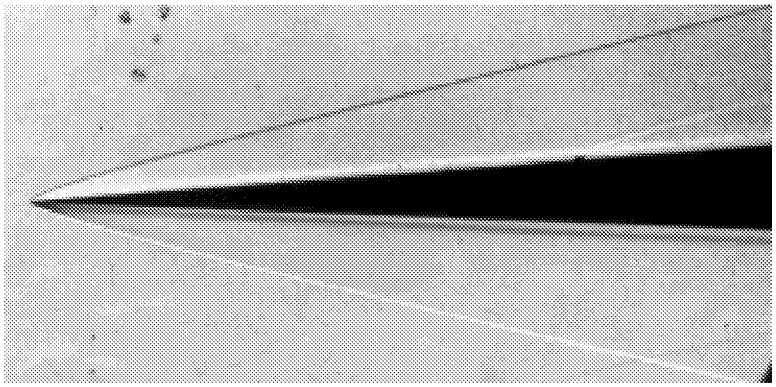

Run 26
α = 2-deg
Re = 1.1 x 10^6/ft
Trip # 1
k = 0.030-in.

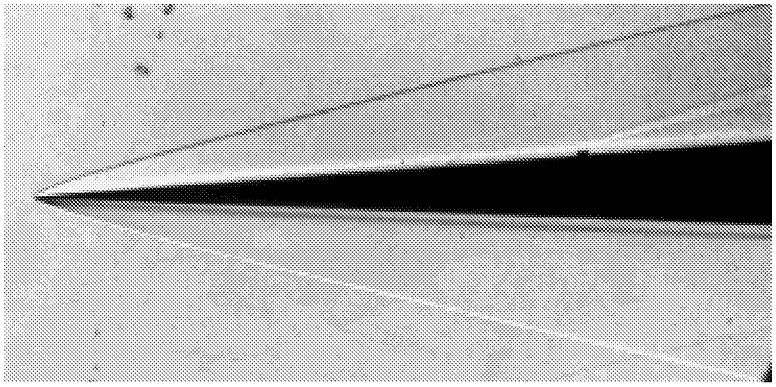

Run 27
α = 2-deg
Re = 1.1 x 10^6/ft
Trip # 1
k = 0.045-in.

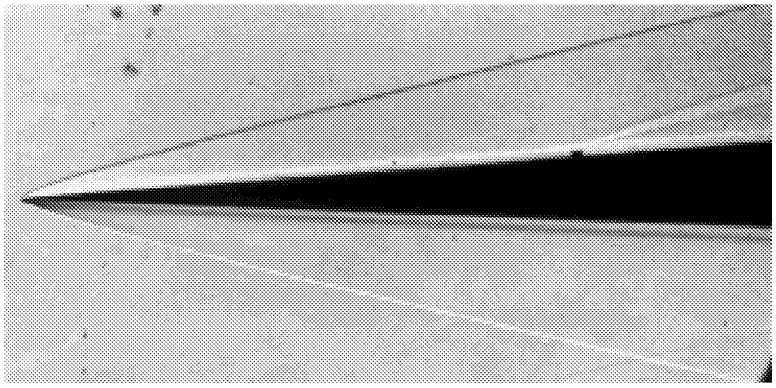

Run 28
α = 2-deg
Re = 1.1 x 10^6/ft
Trip # 1
k = 0.060-in.

Appendix D

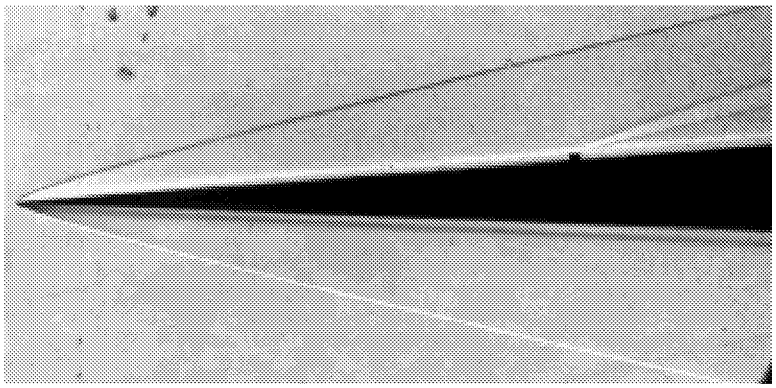

Run 29
α = 2-deg
Re = 1.1 x 10^6/ft
Trip # 1
k = 0.075-in.

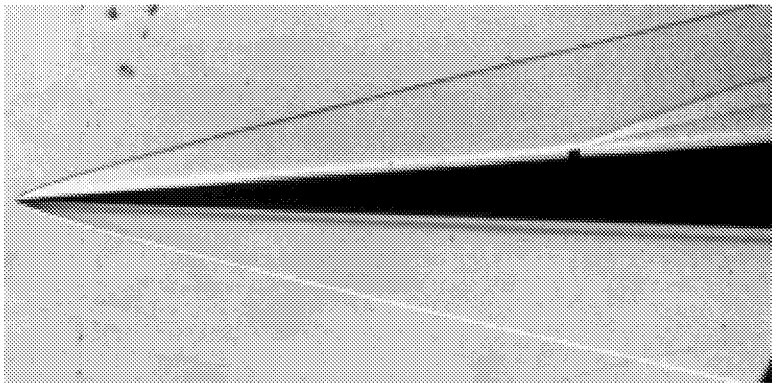

Run 30
α = 2-deg
Re = 1.1 x 10^6/ft
Trip # 1
k = 0.090-in.

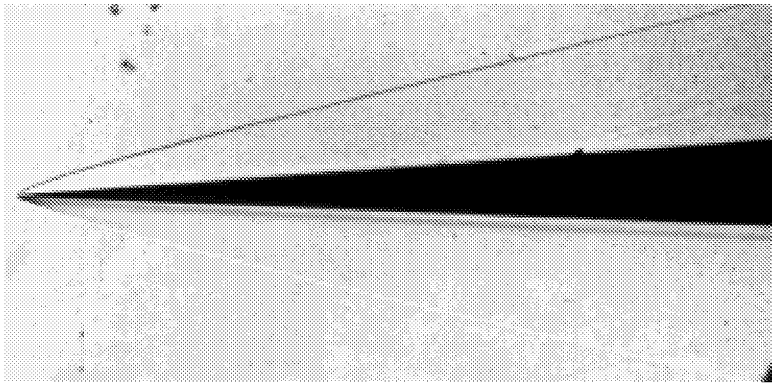

Run 32
α = 2-deg
Re = 1.1 x 10^6/ft
Trip # 2a
k = 0.060-in.

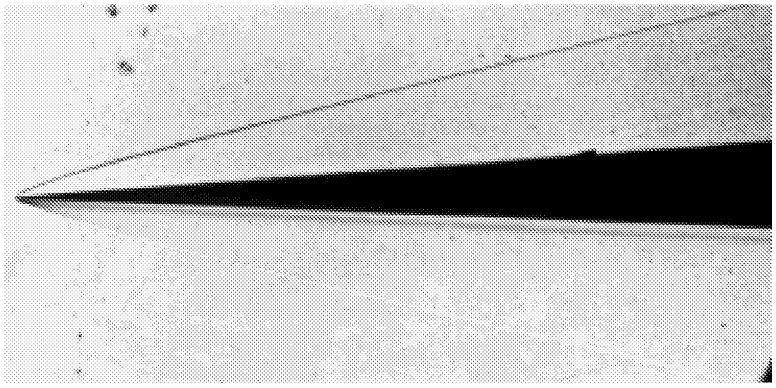

Run 33
α = 2-deg
Re = 1.1 x 10^6/ft
Trip # 2b
k = 0.060-in.

Appendix D

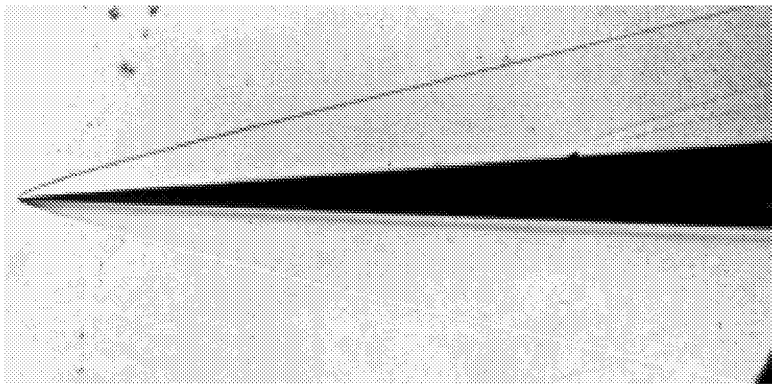

Run 34
α = 2-deg
Re = 1.1 x 10^6/ft
Trip # 3
k = 0.060-in.

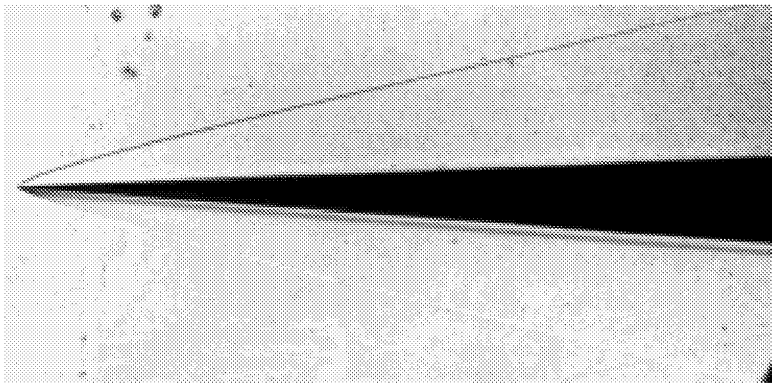

Run 35
α = 0-deg
Re = 1.1 x 10^6/ft
No Trip Baseline

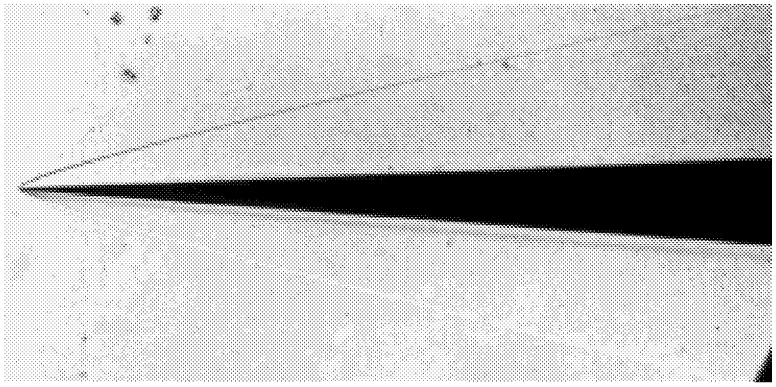

Run 36
α = 0-deg
Re = 0.5 x 10^6/ft
No Trip Baseline

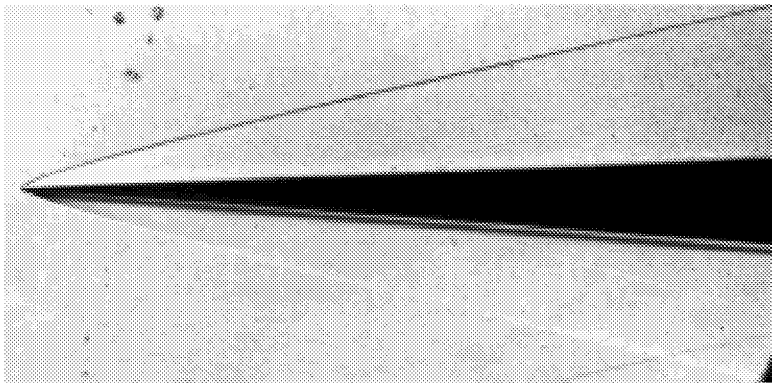

Run 37
α = 0-deg
Re = 2.2 x 10^6/ft
No Trip Baseline

Appendix D

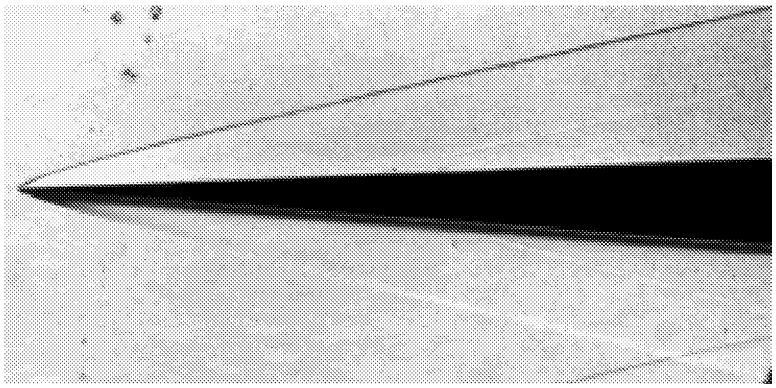

Run 38
α = 0-deg
Re = 4.4x 10^6/ft
No Trip Baseline

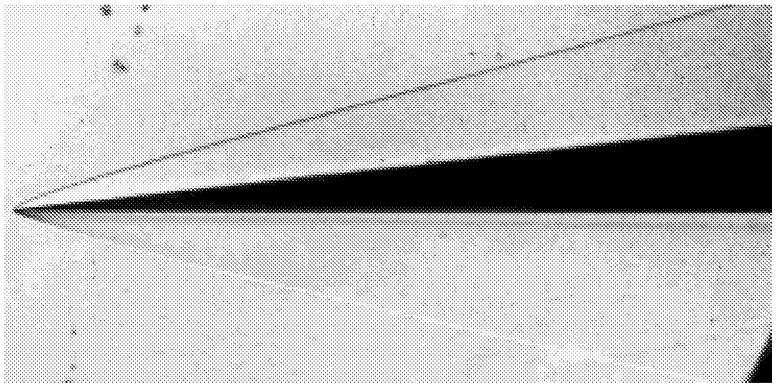

Run 39
α = 4-deg
Re = 0.5 x 10^6/ft
No Trip Baseline

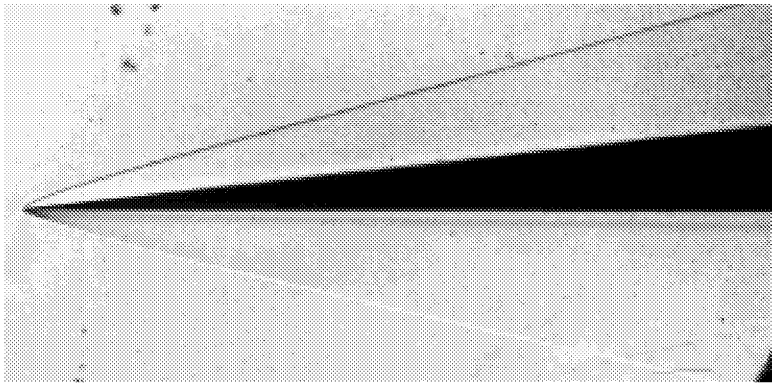

Run 40
α = 4-deg
Re = 1.1 x 10^6/ft
No Trip Baseline

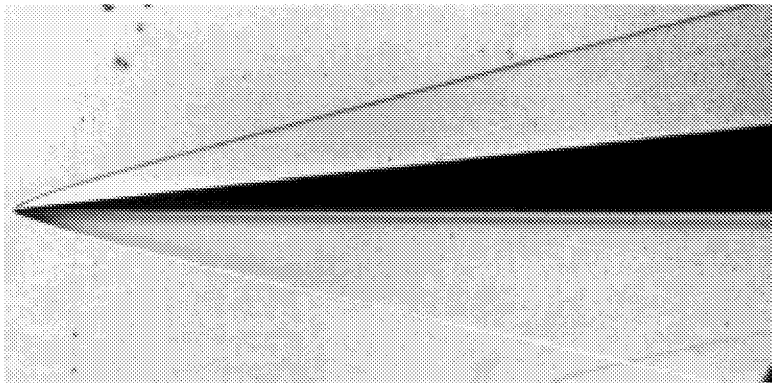

Run 41
α = 4-deg
Re = 2.2 x 10^6/ft
No Trip Baseline

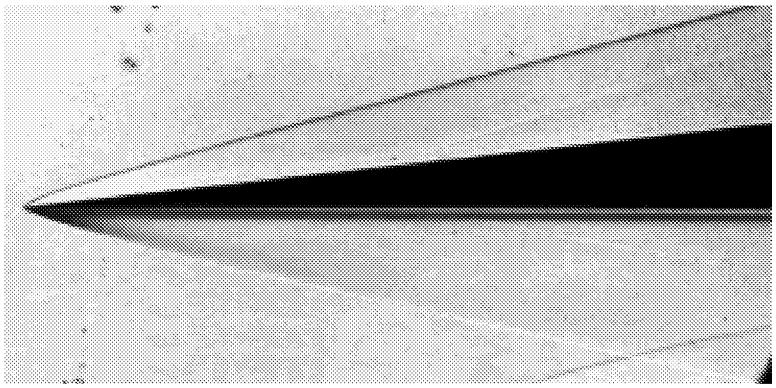

Run 42
α = 4-deg
Re = 4.4 x 10^6/ft
No Trip Baseline

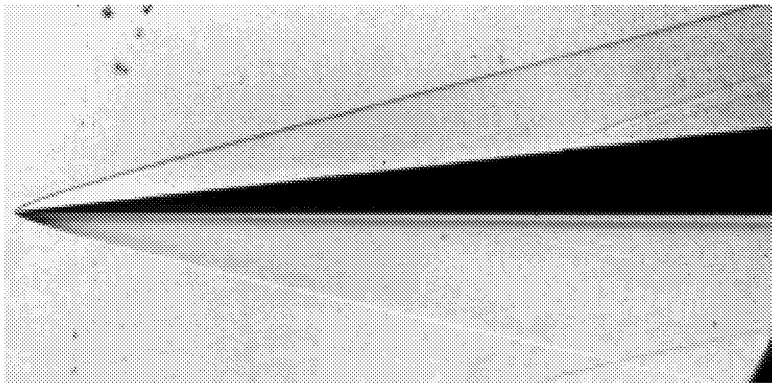

Run 43
α = 4-deg
Re = 2.2 x 10^6/ft
Trip # 1
k = 0.015-in.

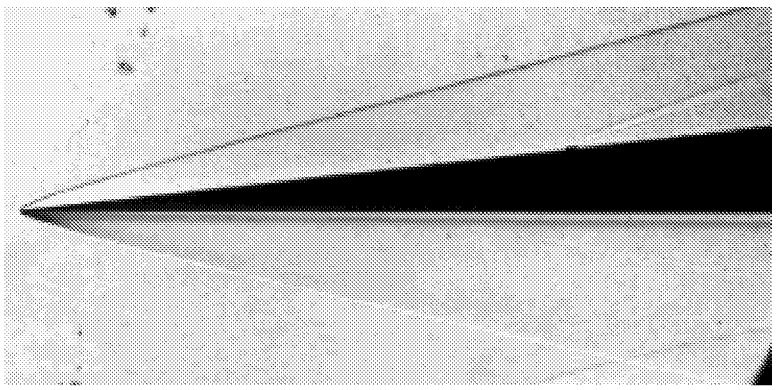

Run 44
α = 4-deg
Re = 2.2 x 10^6/ft
Trip # 1
k = 0.030-in.

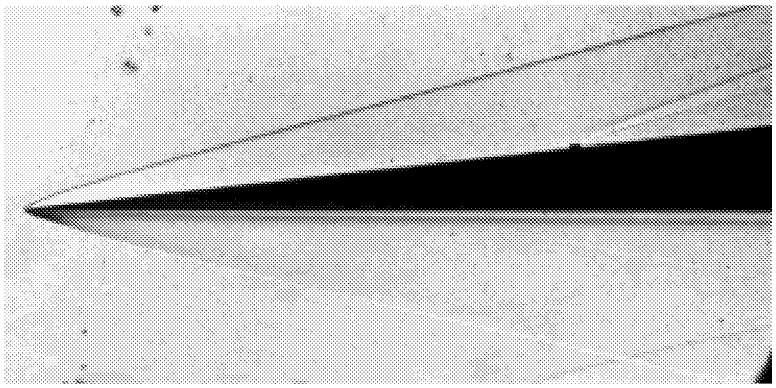

Run 45
α = 4-deg
Re = 2.2 x 10^6/ft
Trip # 1
k = 0.045-in.

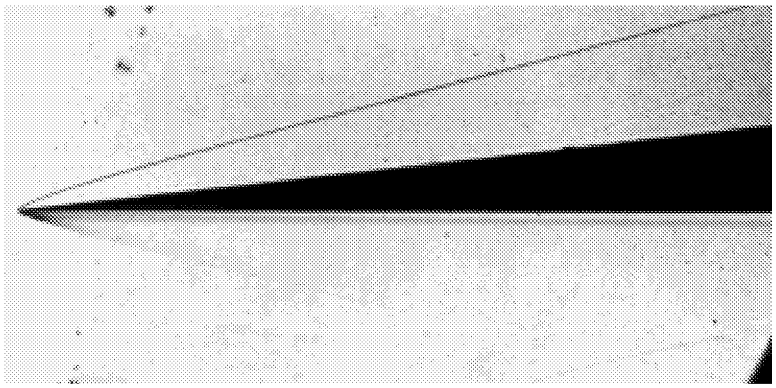

Run 46
α = 4-deg
Re = 2.2 x 10^6/ft
Trip # 1
k = 0.020-in.

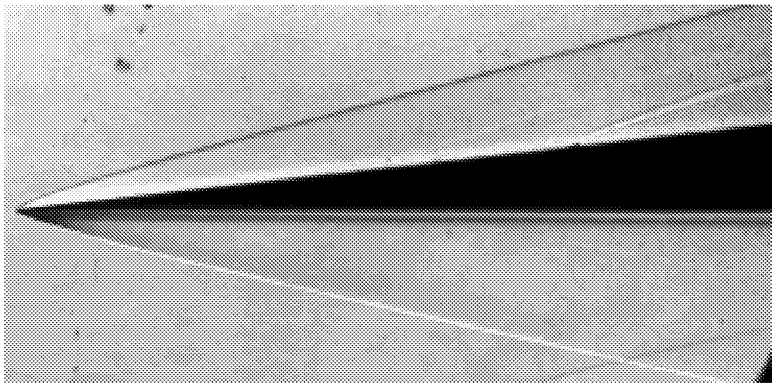

Run 47
α = 4-deg
Re = 2.2 x 10^6/ft
Trip # 2a
k = 0.030-in.

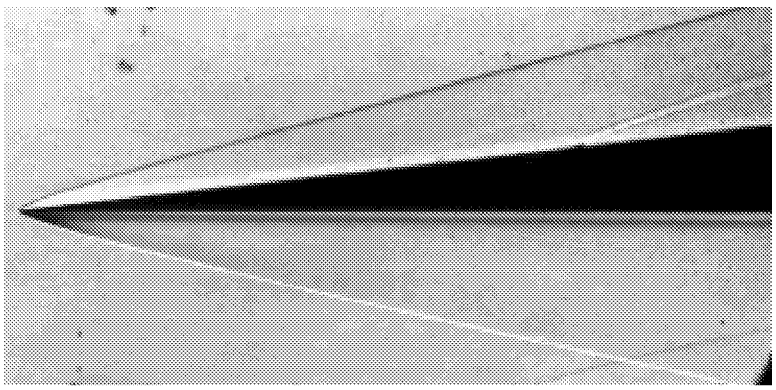

Run 48
α = 4-deg
Re = 2.2 x 10^6/ft
Trip # 2b
k = 0.030-in.

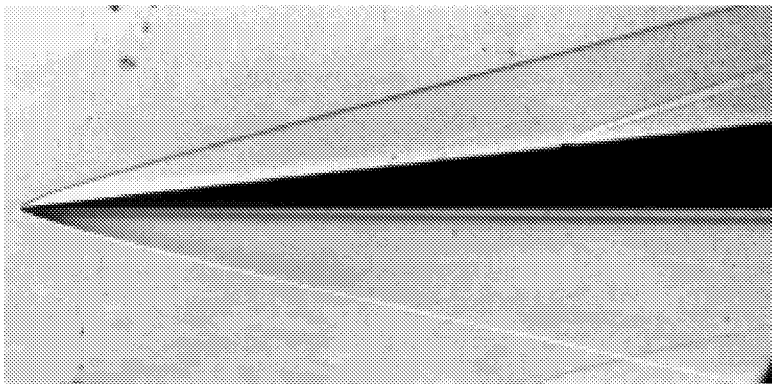

Run 49
α = 4-deg
Re = 2.2 x 10^6/ft
Trip # 2b-backwaeds
k = 0.030-in.

Appendix D

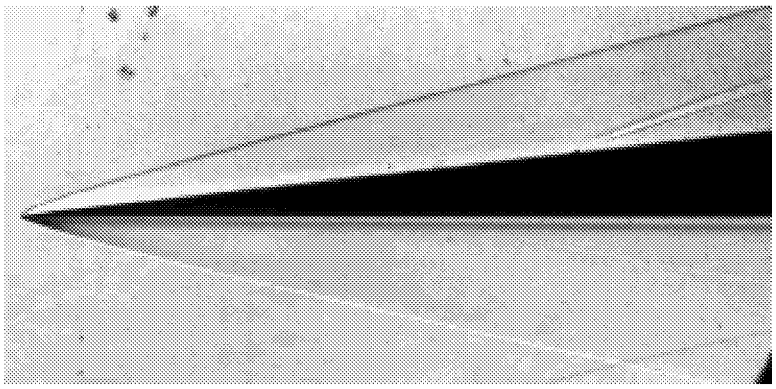

Run 50
α = 4-deg
Re = 2.2 x 10^6/ft
Trip # 3
k = 0.030-in.

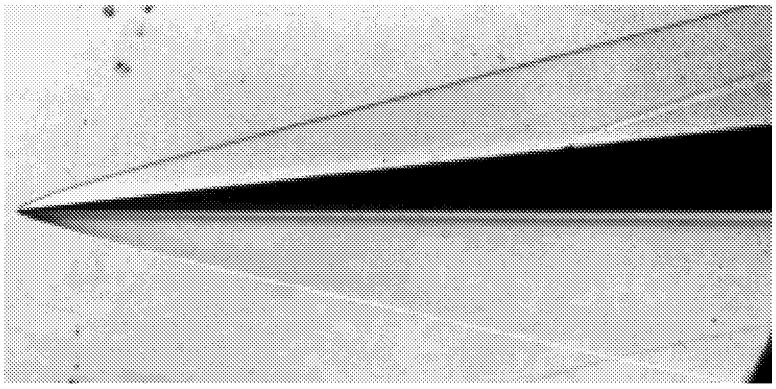

Run 51
α = 4-deg
Re = 2.2 x 10^6/ft
Trip # 2a
k = 0.030-in.

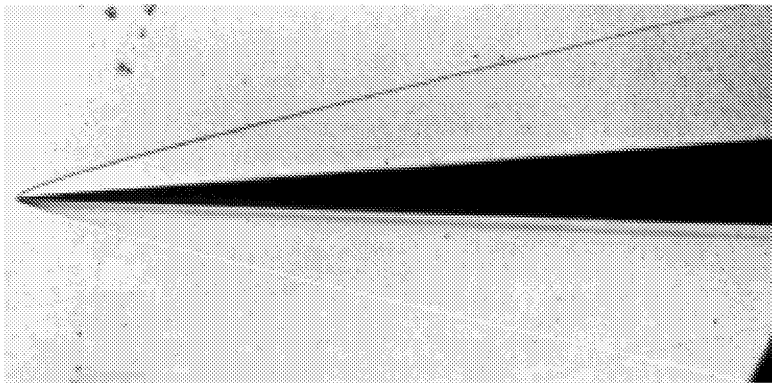

Run 52
α = 2-deg
Re = 1.1 x 10^6/ft
No Trip Baseline

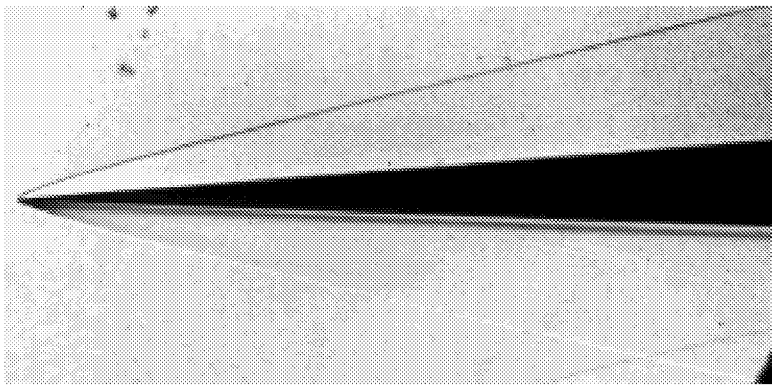

Run 53
α = 2-deg
Re = 2.2 x 10^6/ft
No Trip Baseline

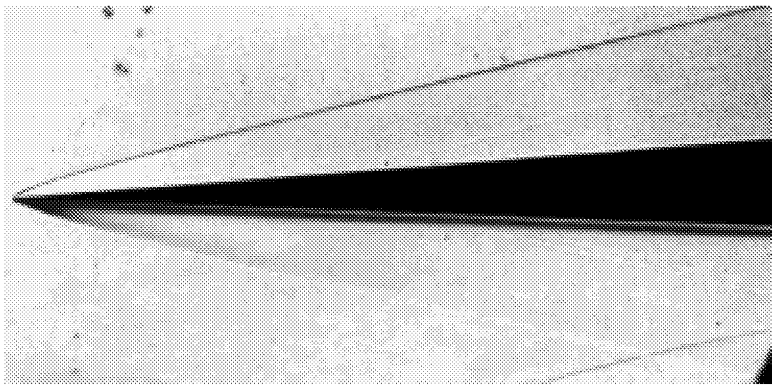

Run 54
α = 2-deg
Re = 4.4 x 10^6/ft
No Trip Baseline

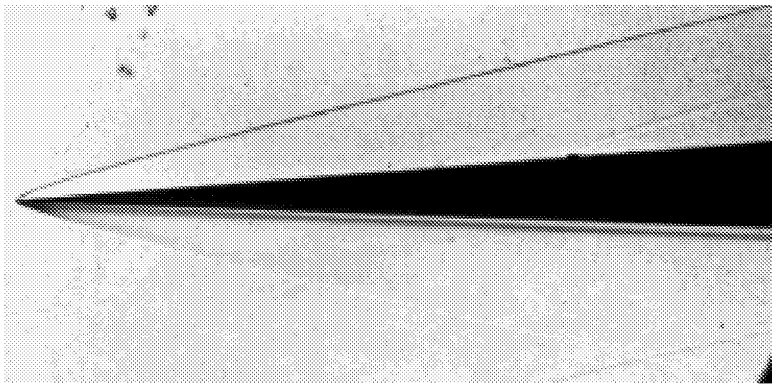

Run 55
α = 2-deg
Re = 2.2 x 10^6/ft
Trip # 1
k = 0.030-in.

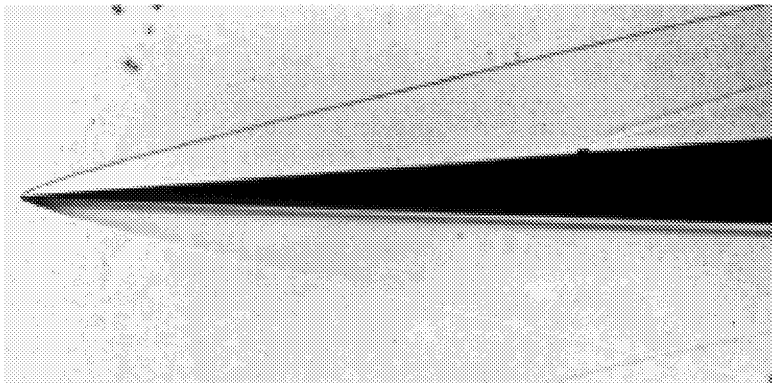

Run 56
α = 2-deg
Re = 2.2 x 10^6/ft
Trip # 1
k = 0.045-in.

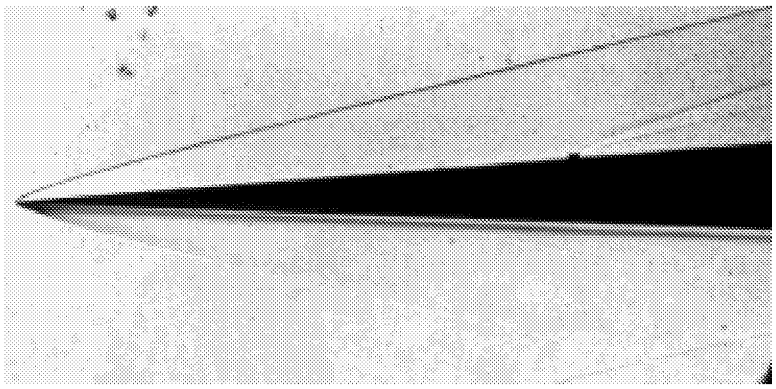

Run 57
α = 2-deg
Re = 2.2 x 10^6/ft
Trip # 1
k = 0.060-in.

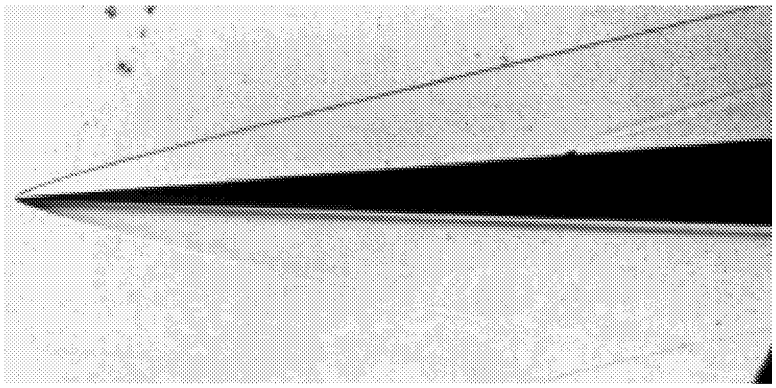

Run 58
α = 2-deg
Re = 2.2 x 10^6/ft
Trip # 2a
k = 0.060-in.

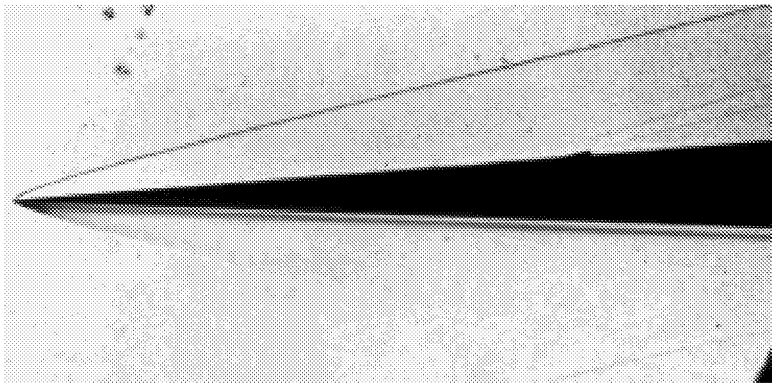

Run 59
α = 2-deg
Re = 2.2 x 10^6/ft
Trip # 2b
k = 0.060-in.

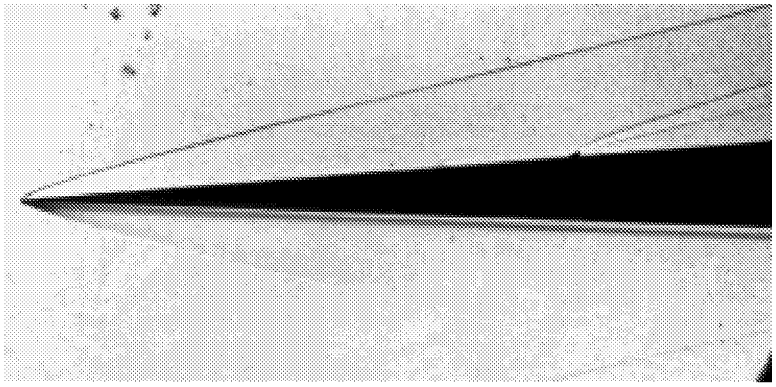

Run 60
α = 2-deg
Re = 2.2 x 10^6/ft
Trip # 3
k = 0.060-in.

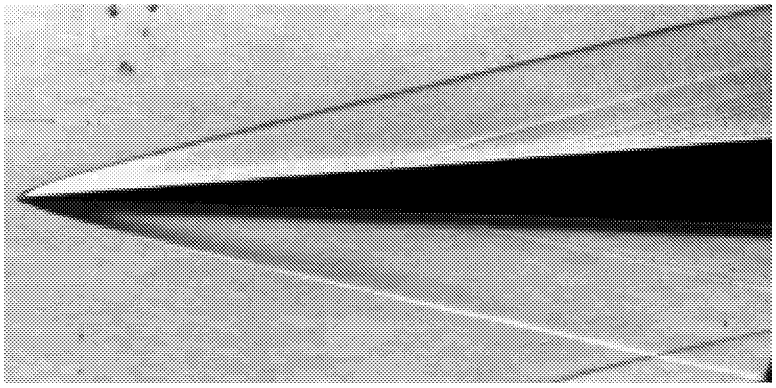

Run 61
α = 2-deg
Re = 6.7 x 10^6/ft
No Trip Baseline

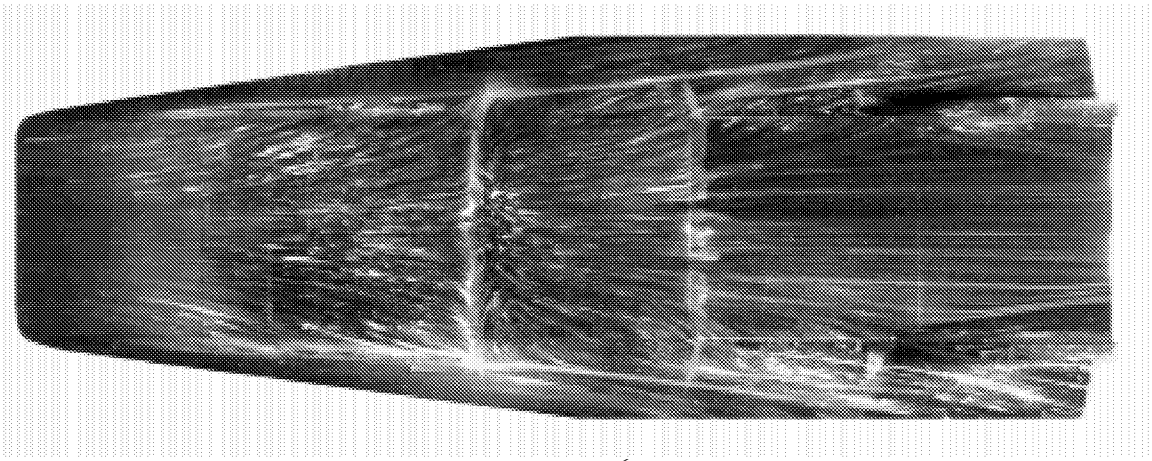

Test 6768 Run 1 α = 2-deg Re = 2.2x10^6/ft No Trip Baseline Open Cowl

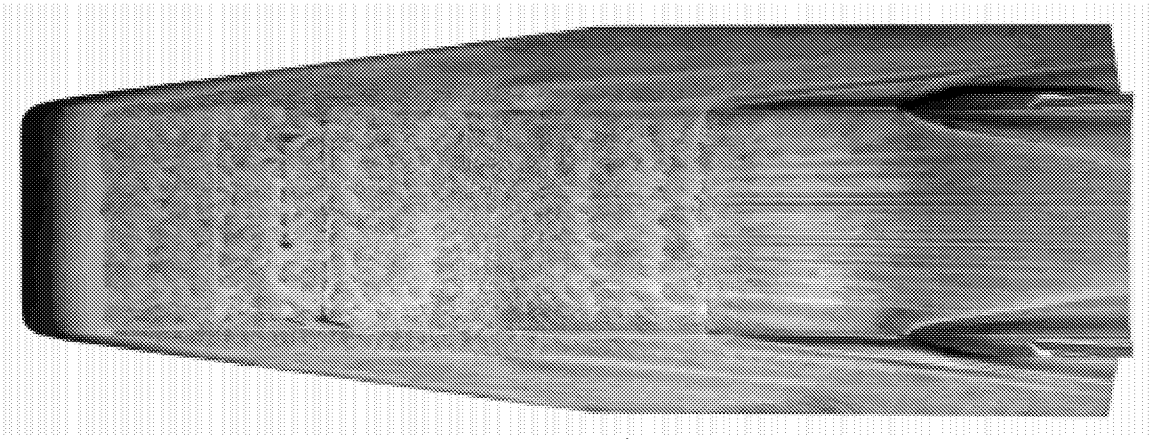

Test 6768 Run 3 α = 2-deg Re = 2.2x10^6/ft No Trip Baseline Open Cowl

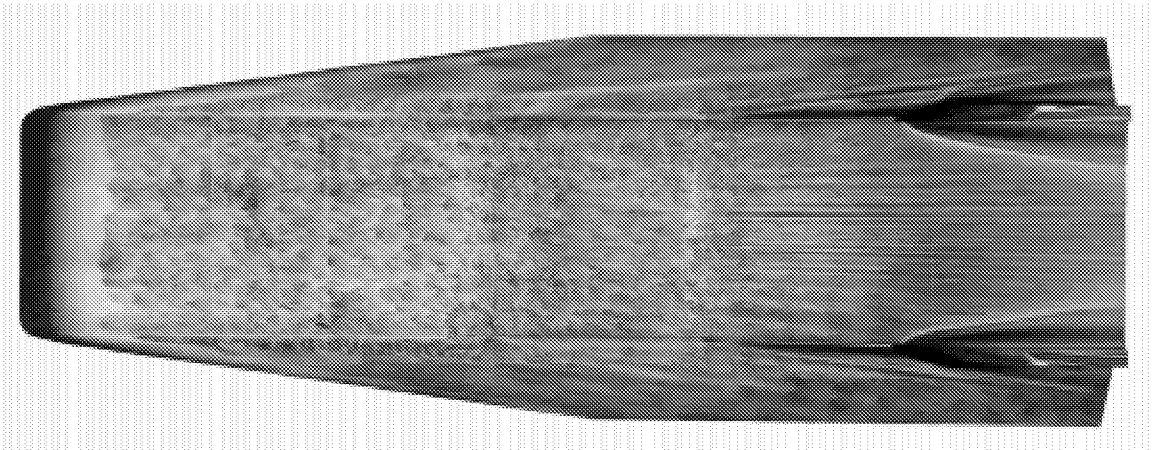

Test 6768 Run 4 α = 2-deg Re = 2.2x10^6/ft No Trip Baseline Open Cowl

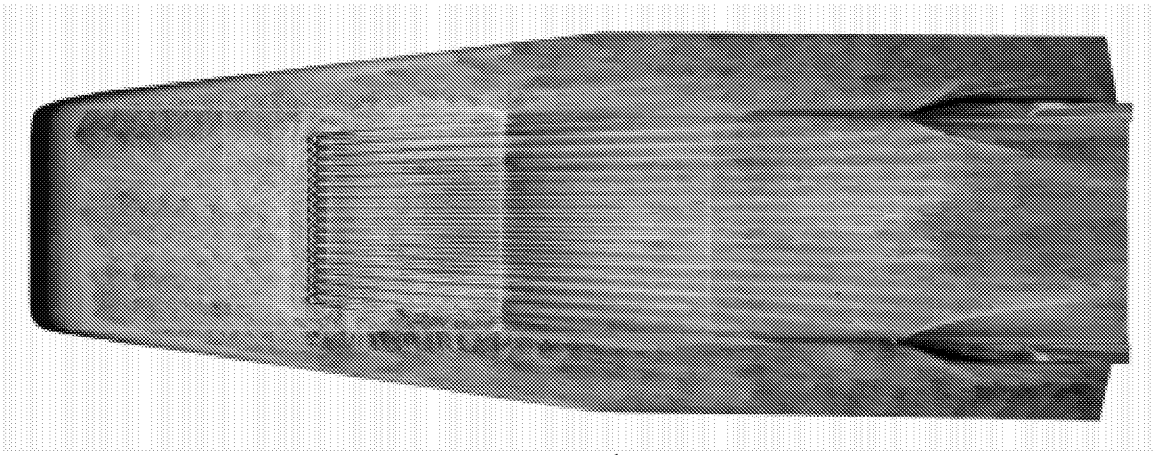

Test 6768 Run 5 α = 2-deg Re = 2.2x10^6/ft Trip 1 k=0.060-in Open Cowl

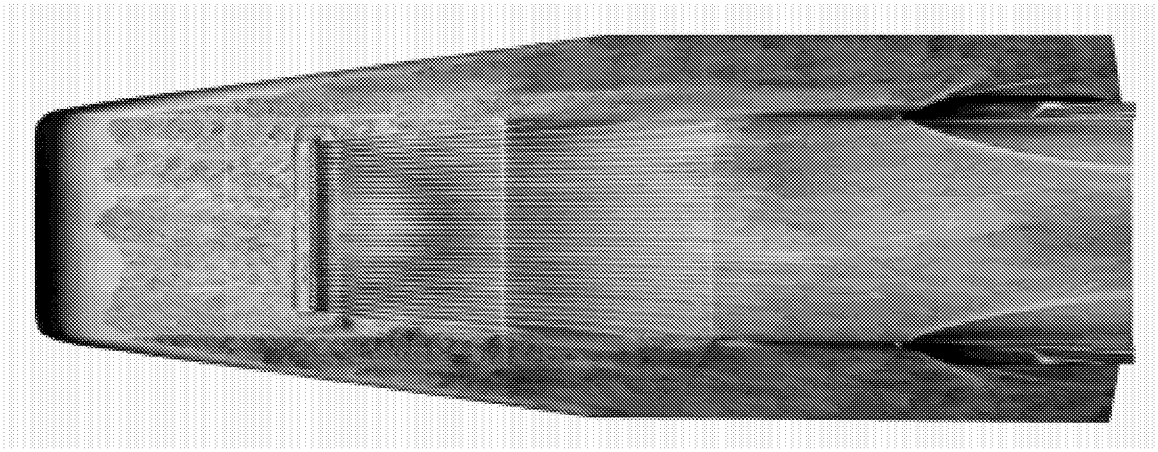

Test 6768 Run 6 α = 2-deg Re = 2.2x10^6/ft Trip 2a k=0.060-in Open Cowl

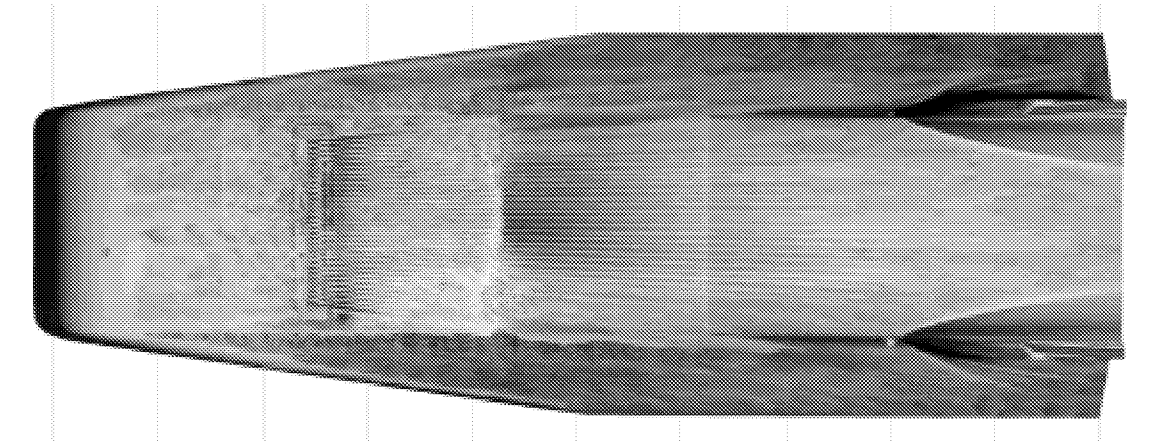

Test 6768 Run 7 α = 2-deg Re = 2.2x10^6/ft Trip 2b k=0.060-in Open Cowl

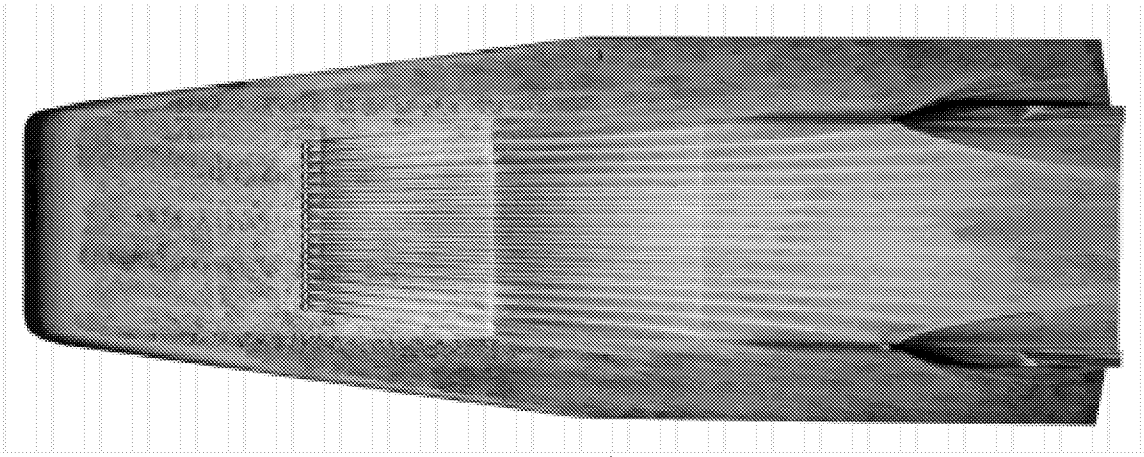

Test 6768 Run 9 α = 2-deg Re = 2.2x10^6/ft Trip 3 k=0.060-in Open Cowl

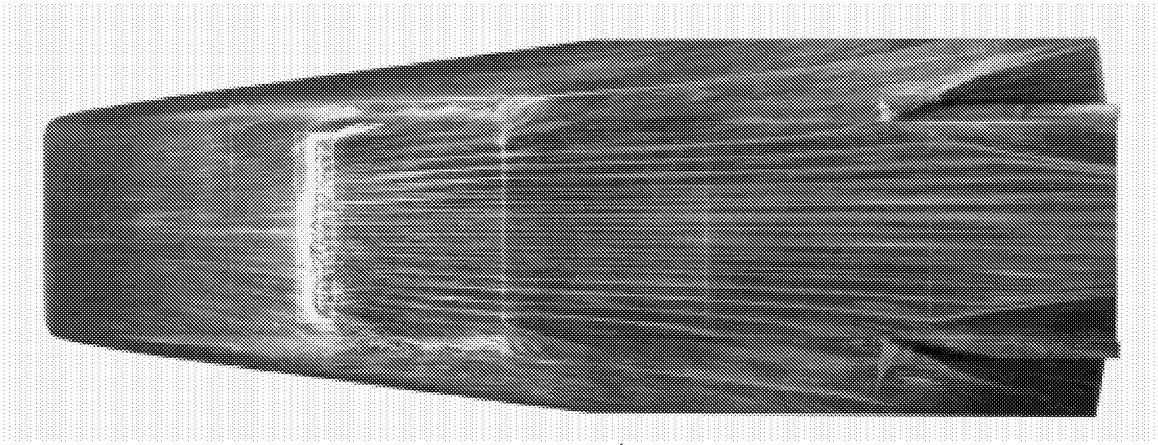

Test 6768 Run 10 α = 2-deg Re = 2.2x10^6/ft Trip 3 k=0.060-in Open Cowl

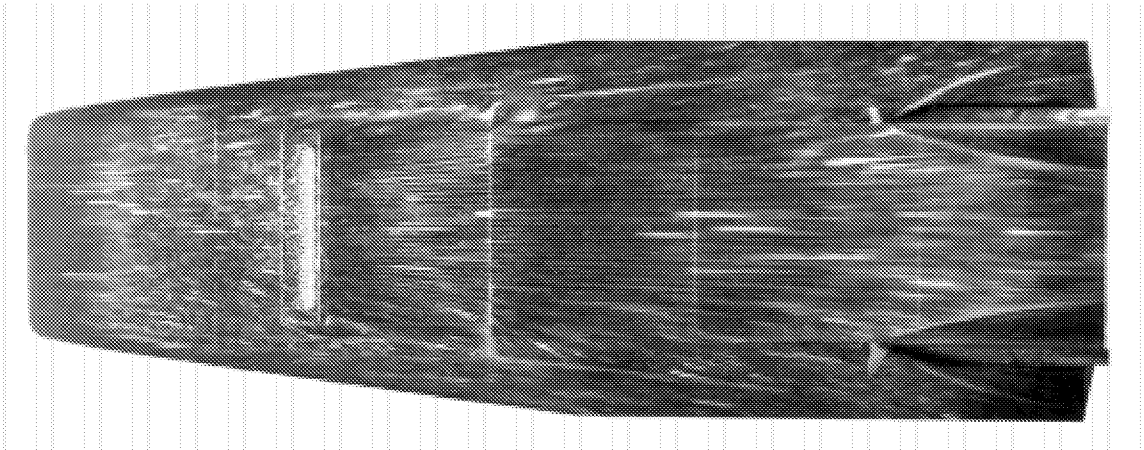

Test 6768 Run 11 α = 2-deg Re = 2.2x10^6/ft Trip 2b k=0.060-in Open Cowl

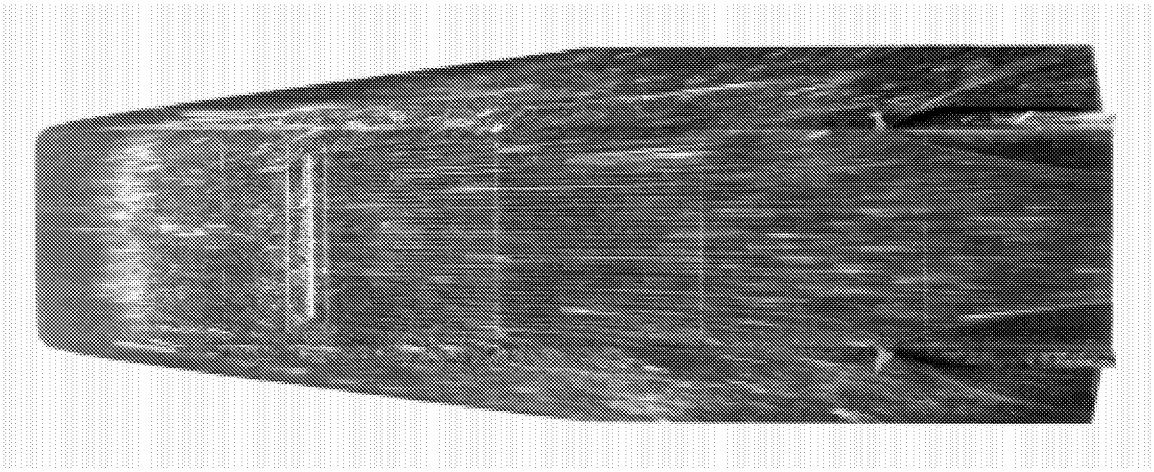

Test 6768 Run 12 α = 2-deg Re = 2.2x10^6/ft Trip 2a k=0.060-in Open Cowl

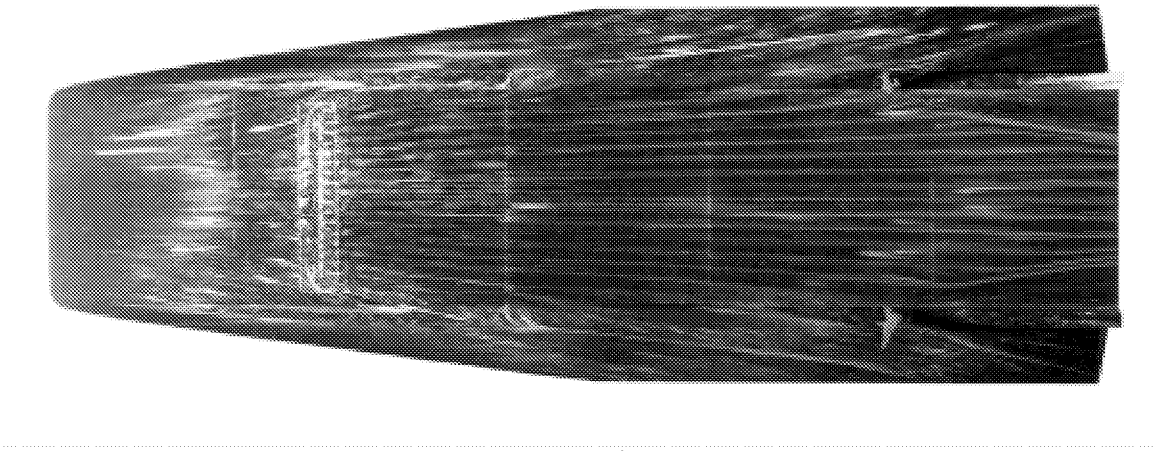

Test 6768 Run 13 α = 2-deg Re = 2.2x10^6/ft Trip 1 k=0.060-in Open Cowl

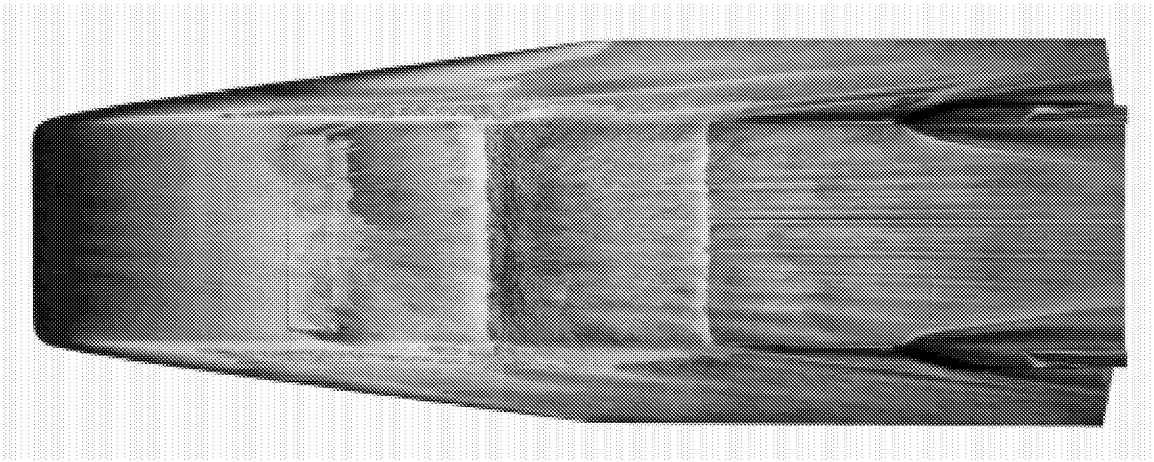

Test 6768 Run 14 α = 2-deg Re = 2.2x10^6/ft No Trip Baseline Open Cowl

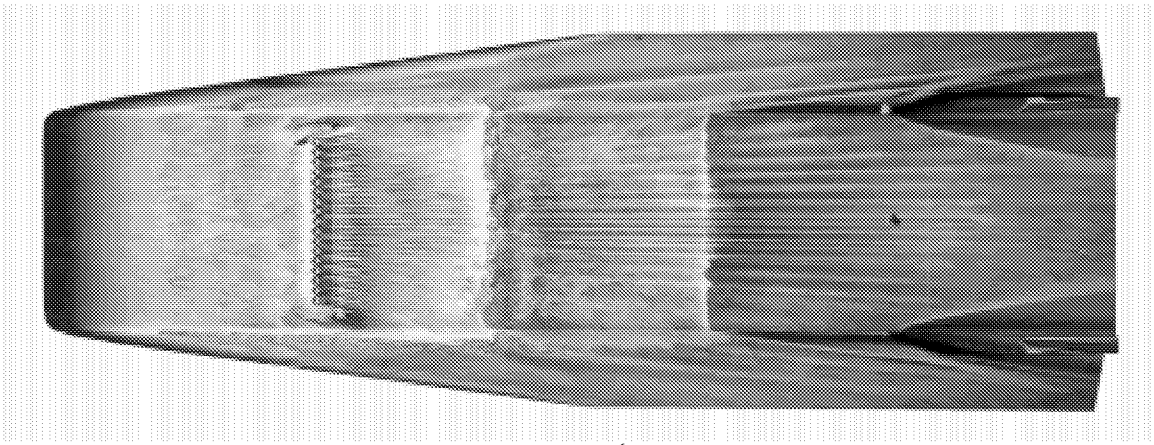

Test 6768 Run 15 α = 2-deg Re = 2.2x10^6/ft Trip 1 k=0.030-in Open Cowl

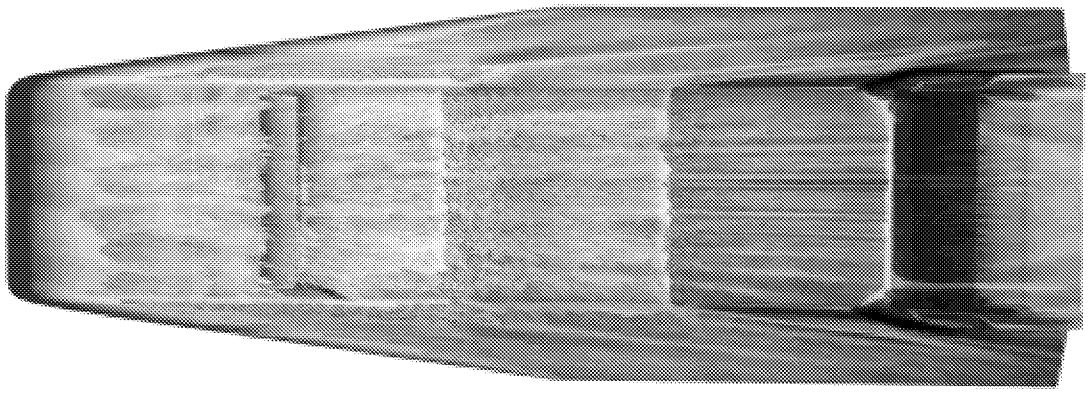

Test 6768 Run 16 α = 2-deg Re = 2.2x10^6/ft No Trip Baseline Closed Cowl

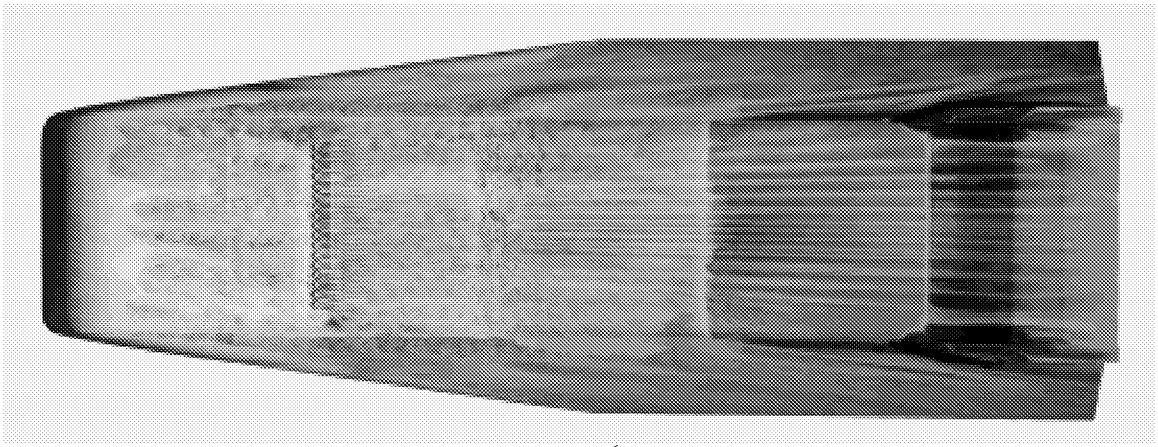

Test 6768 Run 17 α = 2-deg Re = 2.2x10^6/ft Trip 1 k=0.030-in Closed Cowl

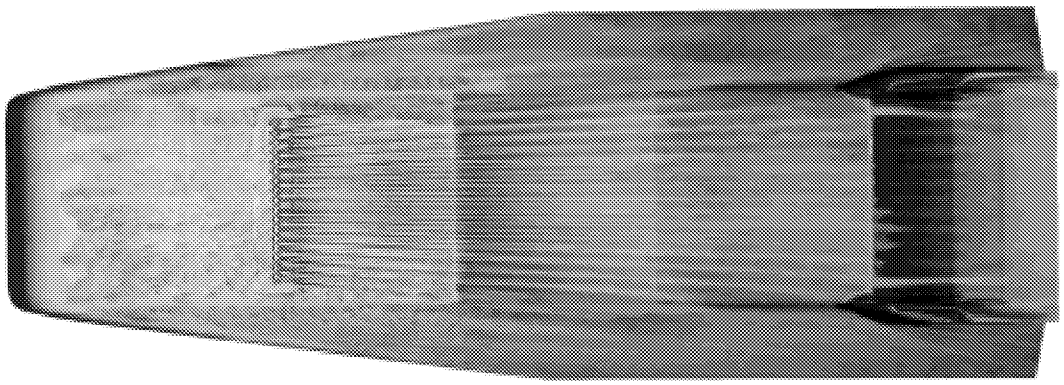

Test 6768 Run 18 α = 2-deg Re = 2.2x10^6/ft Trip 3 k=0.060-in Closed Cowl

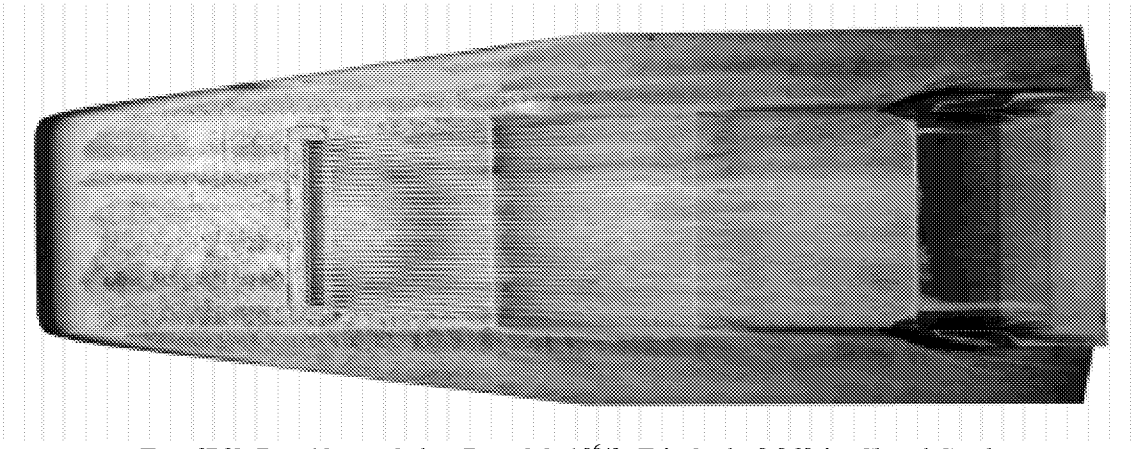

Test 6768 Run 19 α = 2-deg Re = 2.2x10^6/ft Trip 2a k=0.060-in Closed Cowl

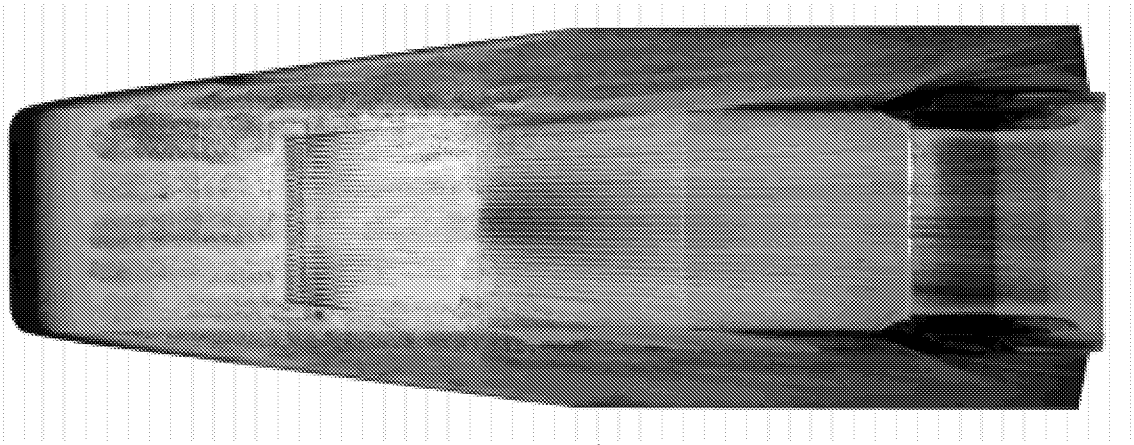

Test 6768 Run 21 α = 2-deg Re = 2.2x10^6/ft Trip 2b k=0.060-in Closed Cowl

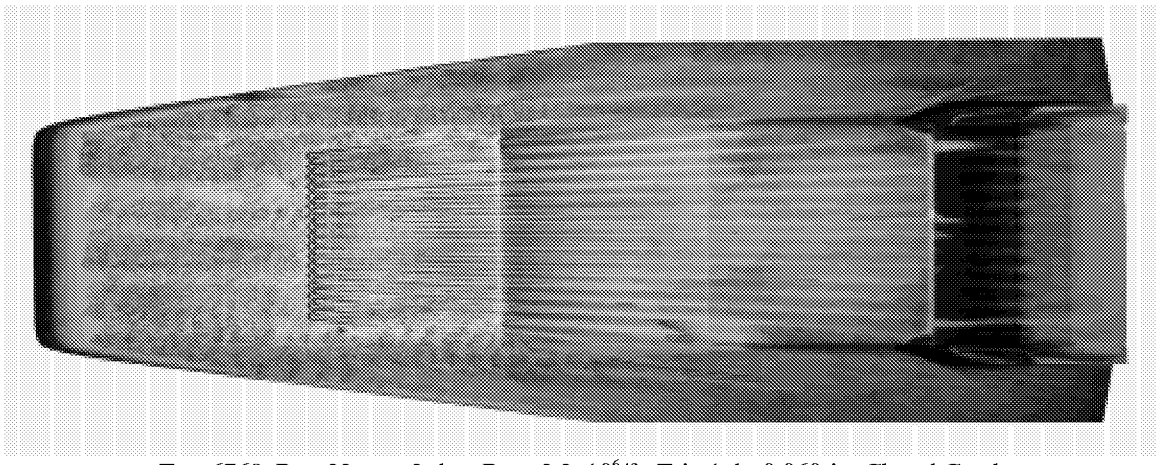

Test 6768 Run 22 α = 2-deg Re = 2.2x10^6/ft Trip 1 k=0.060-in Closed Cowl

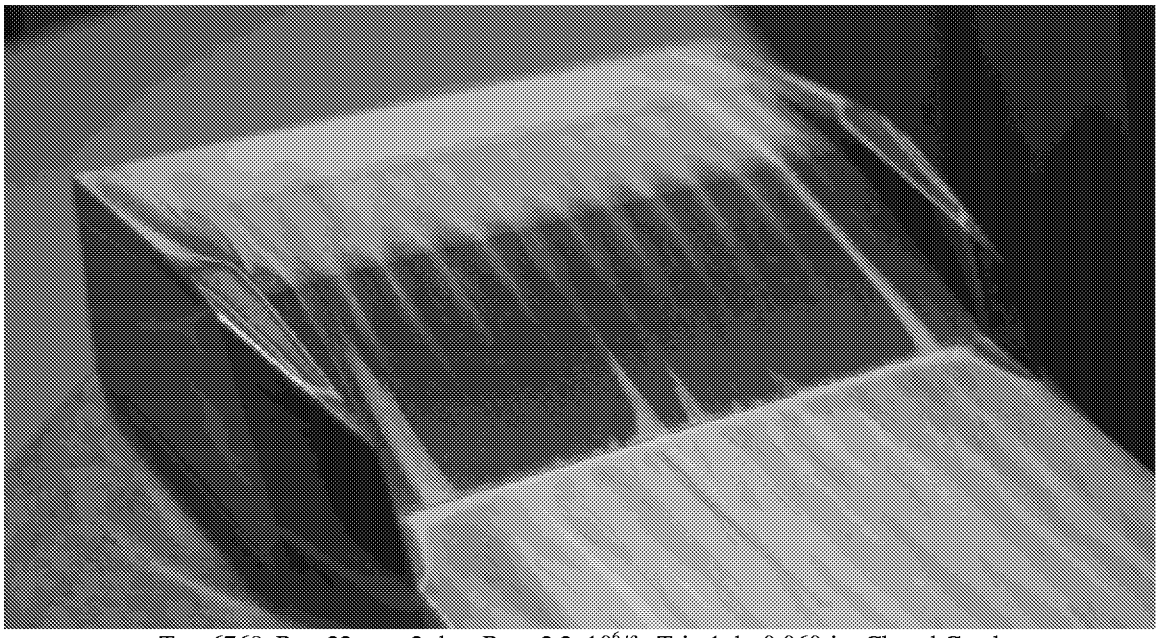

Test 6768 Run 22 α = 2-deg Re = 2.2x10^6/ft Trip 1 k=0.060-in Closed Cowl

REPORT DOCUMENTATION PAGE

Form Approved
OMB No. 0704-0188

1. AGENCY USE ONLY (Leave blank)	2. REPORT DATE	3. REPORT TYPE AND DATES COVERED
	August 2000	Technical Memorandum

4. TITLE AND SUBTITLE
Forced Boundary-Layer Transition on X-43 (Hyper-X) in NASA LaRC 20-Inch Mach 6 Air Tunnel

5. FUNDING NUMBERS
WU 242-80-01-01

6. AUTHOR(S)
Scott A. Berry, Michael DiFulvio, and Matthew K. Kowalkowski

7. PERFORMING ORGANIZATION NAME(S) AND ADDRESS(ES)
NASA Langley Research Center
Hampton, VA 23681-2199

8. PERFORMING ORGANIZATION REPORT NUMBER
L-18016

9. SPONSORING/MONITORING AGENCY NAME(S) AND ADDRESS(ES)
National Aeronautics and Space Administration
Washington, DC 20546-0001

10. SPONSORING/MONITORING AGENCY REPORT NUMBER
NASA/TM-2000-210316

11. SUPPLEMENTARY NOTES

12a. DISTRIBUTION/AVAILABILITY STATEMENT
Unclassified-Unlimited
Subject Category 34 Distribution: Nonstandard
Availability: NASA CASI (301) 621-0390

12b. DISTRIBUTION CODE

13. ABSTRACT (Maximum 200 words)
Aeroheating and boundary layer transition characteristics for the X-43 (Hyper-X) configuration have been experimentally examined in the Langley 20-Inch Mach 6 Air Tunnel. Global surface heat transfer distributions, and surface streamline patterns were measured on a 0.333-scale model of the Hyper-X forebody. Parametric variations include angles-of-attack of 0-deg, 2-deg, and 4-deg; Reynolds numbers based on model length of 1.2 to 15.4 million; and inlet cowl door both open and closed. The effects of discrete roughness elements on the forebody boundary layer, which included variations in trip configuration and height, were investigated. This document is intended to serve as a release of preliminary data to the Hyper-X program; analysis is limited to observations of the experimental trends in order to expedite dissemination.

14. SUBJECT TERMS	15. NUMBER OF PAGES
Boundary-layer transition, hypersonic, roughness	63
	16. PRICE CODE: A04

17. SECURITY CLASSIFICATION OF REPORT	18. SECURITY CLASSIFICATION OF THIS PAGE	19. SECURITY CLASSIFICATION OF ABSTRACT	20. LIMITATION OF ABSTRACT
Unclassified	Unclassified	Unclassified	UL